CONCEPTUAL DESIGN FOR A RE-ENTRANT TYPE FUEL CHANNEL FOR SUPERCRITICAL WATER-COOLED NUCLEAR REACTORS

by

Jeffrey Samuel

A Thesis Submitted in Partial Fulfillment of the Requirements for the Degree of

Master of Applied Science

in

The Faculty of Energy Systems and Nuclear Science

University of Ontario Institute of Technology

April, 2011

© Jeffrey Samuel, 2011

ABSTRACT

Current CANDU-type nuclear reactors use a once-through fuel-channel with an annulus gas insulating it from the moderator. The current reference design for a CANDU-type SuperCritical Water-Cooled Reactor (SCWR) is to eliminate the annulus gap and use a ceramic insert to insulate the coolant from the moderator. While such a design may work, alternative fuel-channel design concepts are under development to explore the optimum efficiency of SCWRs. One such alternative approach is called the Re-Entrant fuel-channel.

The Re-Entrant fuel-channel consists of three tubes, the inner tube (flow tube), pressure tube and an outer tube. The fuel bundles are placed in the inner tube. An annulus is formed between the flow and pressure tubes, through which the primary coolant flows. A ceramic insulator is placed between the pressure tube and the outer tube. The coolant flows through the annulus receiving heat from the inner tube from one end of the channel to another. At the far end, the flow will reverse direction and enter the inner tube, and hence the fuel-string. At the inlet, the temperature is 350°C for a high-pressure coolant (pressure of 25 MPa), which is just below the pseudocritical point. At the outlet, the temperature is about 625ºC at the same pressure (the pressure drop is small and can be neglected). The objective of this work was to design the Re-Entrant channel and to estimate the heat loss to the moderator for the proposed new fuel-channel design.

A numerical model was developed and MATLAB was used to calculate the heat loss from the insulated Re-Entrant fuel-channel along with the temperature profiles and the heat transfer coefficients for a given set of flow, pressure, temperature and power boundary conditions. Thermophysical properties were obtained from NIST REFPROP software. With the results from the numerical model, the design of the Re-Entrant fuel-channel was optimized to improve its efficiency.

ACKNOWLEDGEMENTS

Financial support from the NSERC/NRCan/AECL Generation IV Energy Technologies Program and NSERC Discovery Grants is gratefully acknowledged.

I am deeply grateful to my supervisors, Dr. Harvel and Dr. Pioro, for their support and encouragement in my research and the writing of this thesis. I sincerely appreciate their constant guidance and support during the period of this work and most of all, their patience and understanding.

I would like to thank my colleagues Amjad Farah, Adepoju Adenariwo, Harwinder Thind, Lisa Grande and Graham Richards for their valuable discussions. I'm also indebted to the members of the Nuclear Design Laboratory at UOIT for giving me the perfect working atmosphere and also for their kindness.

I'm especially thankful to my friends Ciandra D'Souza, Krista Nicholson and Donald Draper, for helping me through the difficult times by keeping me sane, and for being a source of inspiration during the course of my research.

Finally, I would like to thank my parents, Naomi and James Richard, for always being a tremendous source of emotional, moral and material support.

TABLE OF CONTENTS

1 INTRODUCTION 1

1.1 Objective 5

2 BACKGROUND AND LITERATURE REVIEW 7

2.1 Generation IV Nuclear Technology 7

2.2 Generation IV Concepts 10

2.2.1 SuperCritical Water-cooled Reactor Concepts 11

2.3 SCW Properties 15

2.4 SCW Correlations 22

2.5 Fuel Channel Design Concepts 27

3 PROPOSED FUEL CHANNEL DESIGN CONCEPT 30

4 NUMERICAL MODEL OF RE-ENTRANT FUEL-CHANNEL 42

4.1 Fundamental Equations 42

4.2 Flow Area, Wetted Perimeter, Hydraulic Diameter 44

4.3 Nodalization 47

4.4 Initial Estimate of Temperature profiles for Hot and Cold Side 47

4.5 Initial Estimate of Temperature of Fuel Sheath 49

4.6 Thermal Resistances 50

4.7 Heat Transferred from Hot Side to Cold Side and Heat Loss to Moderator from Cold Side 53

4.8 Actual Temperature Profile of Cold Side, Hot Side & Fuel Sheath 54

4.9 Surface Temperatures of Tubes 55

4.10 MATLAB code 55

5 HEAT TRANSFER ANALYSIS 57

5.1 Reference Case: No Heat Loss to the Moderator 57

5.2 Heat Loss to the Moderator 71

5.2.1 Non-insulated Re-Entrant channel 71

5.2.2 Porous Yttria Stabilized Zirconia Insulated Re-Entrant Channel 82

5.2.3 Zirconium Dioxide (ZrO_2) Insulated Re-Entrant Channel 86

5.2.4 Heat Loss Comparison 89

5.3 Impact of Non-Uniform Flux Shapes 93

6 CONCLUDING REMARKS 106

7 FUTURE WORK 108

REFERENCES 109

APPENDIX A: NUMERICAL MODEL IN MATLAB 113

APPENDIX B: VERIFICATION OF NUMERICAL MODEL 127

APPENDIX C: IMPACT OF INSULATORS – THERMOPHYSICAL PROPERTIES 128

APPENDIX D: IMPACT OF NON-UNIFORM FLUX SHAPES – THERMOPHYSICAL PROPERTIES 132

APPENDIX E: CONTRIBUTIONS TO KNOWLEDGE 142

LIST OF TABLES

Table 3.1: Parameters of fuel bundle options for the Re-Entrant channel **37**

Table 3.2: Reference case Re-Entrant Channel Dimensions **40**

Table 4.1: Reference case Re-Entrant Channel Parameters **46**

Table 5.1: Heat loss comparison **78**

Table 5.2: Heat loss comparison for insulated Re-Entrant channel **92**

Table 5.3: Heat loss comparison for insulated Re-Entrant channel with different axial power profiles **103**

Table 5.4: Peak sheath temperature and location of peak sheath temperature for insulated Re-Entrant channel with different axial power profiles **104**

Table 5.5: Location of pseudocritical point in the Re-Entrant channel with different axial power profiles **105**

LIST OF FIGURES

Figure 2.1: Nuclear Reactor Technology in Canada **8**

Figure 2.2: Pressure Vessel Type SCWR **13**

Figure 2.3: Pressure Tube Type SCWR **13**

Figure 2.4: T-s diagram for direct cycle SCWR with no-reheat option **14**

Figure 2.5 (a): Specific Heat vs. Temperature of water in the pseudocritical region **16**

Figure 2.5 (b): Density vs. Temperature of water in the pseudocritical region **17**

Figure 2.5 (c): Thermal Conductivity vs. Temperature of water in the pseudocritical region **18**

Figure 2.5 (d): Prandtl Number vs. Temperature of water in the pseudocritical region **19**

Figure 2.5 (e): Dynamic Viscosity vs. Temperature of water in the pseudocritical region **20**

Figure 2.5 (f): Kinematic Viscosity vs. Temperature of water in the pseudocritical region **21**

Figure 2.6: Comparison between SCW correlations when bulk fluid temperature is 350°C and wall temperature is 400°C **26**

Figure 2.7: CANDU type fuel-channel **28**

Figure 2.8: SCWR type fuel-channel concept **28**

Figure 3.1 (a): Horizontal Re-Entrant channel configuration **32**

Figure 3.1 (b): Horizontal Re-Entrant channel configuration **32**

Figure 3.2 (a): Vertical Re-Entrant channel configuration **33**

Figure 3.2 (b): Vertical Re-Entrant channel configuration **33**

Figure 3.3: Proposed New Fuel Channel **34**

Figure 3.4 (a): Fuel length of Re-Entrant channel **35**

Figure 3.4 (b): Entrance Region of Re-Entrant channel **35**

Figure 3.4 (c): Re-Entrant region of Re-Entrant channel **35**

Figure 3.5: Cross-sectional view of Re-Entrant channel **40**

Figure 4.1: Re-Entrant flow-channel showing nodes and initial temperature estimates **48**

Figure 4.2: Thermal Conductivity of porous YSZ **52**

Figure 4.3: Flow chart representing Numerical Model in MATLAB **56**

Figure 5.1: Axial temperature profile along the fuelled channel length for a channel power of 8.5 MW_{th}, inner-tube thickness of 2 mm, inlet temperature of 350°C, mass flow rate of 4.37 kg/s and uniform heat flux **59**

Figure 5.2: Specific heat, thermal conductivity and Prandtl number profiles along the fuel-channel for a channel power of 8.5 MW_{th}, inner-tube thickness of 2 mm, inlet temperature of 350°C, mass flow rate of 4.37 kg/s and uniform heat flux **61**

Figure 5.3: Average specific heat, average Prandtl number, Heat Flux and HTC profiles along the fuel-channel for a channel power of 8.5 MW_{th}, inner-tube thickness of 2 mm, inlet temperature of 350°C, mass flow rate of 4.37 kg/s and uniform heat flux **62**

Figure 5.4: Outer-sheath-temperature profile along the channel length for powers of 8.5 MW_{th} and 5.5 MW_{th}, inner-tube thickness of 2 mm, inlet temperature of 350°C, mass flow rate of 4.37 kg/s and uniform heat flux **64**

Figure 5.5: Outer-sheath temperature profiles with variable flow-tube thickness, inlet temperature of 350°C, mass flow rate of 4.37 kg/s and uniform heat flux **65**

Figure 5.6: Change in temperature across the flow tube for different wall thermal conductivities, inner-tube thickness of 2 mm, inlet temperature of 350°C, mass flow rate of 4.37 kg/s and uniform heat flux **67**

Figure 5.7: Temperature Profile of Outer Sheath Temperature for variable wall thermal conductivity, inner-tube thickness of 2 mm, inlet temperature of 350°C, mass flow rate of 4.37 kg/s and uniform heat flux **68**

Figure 5.8: Axial temperature profile along the fuelled channel length for a channel power of 10 MW_{th}, inner-tube thickness of 2 mm, inlet temperature of 350°C, mass flow rate of 4.37 kg/s and uniform heat flux **70**

Figure 5.9: Temperature profile along the channel length for a channel power of 8.5 MW_{th}, inner-tube thickness of 2 mm, pressure tube thickness of 11 mm, inlet temperature of 350°C, mass flow rate of 4.37 kg/s and uniform heat flux **72**

Figure 5.10: Specific heat, thermal conductivity and Prandtl number profiles along the fuel-channel for a channel power of 8.5 MW, inner-tube thickness of 2 mm, pressure tube thickness of 11 mm, inlet temperature of 350°C, mass flow rate of 4.37 kg/s and uniform heat flux **74**

Figure 5.11: Average specific heat, average Prandtl number and HTC profiles along the fuel-channel for a channel power of 8.5 MW, inner-tube thickness of 2 mm, pressure tube thickness of 11 mm, inlet temperature of 350°C, mass flow rate of 4.37 kg/s and uniform heat flux **75**

Figure 5.12: Temperature gradients along the radial distance from center for a non insulated Re-Entrant channel **76**

Figure 5.13: Heat loss to the moderator when pressure tube thickness is varied for a channel power of 8.5 MW_{th}, inner-tube thickness of 2 mm, inlet temperature of 350°C, mass flow rate of 4.37 kg/s and uniform heat flux **80**

Figure 5.14: Change in temperature across the pressure tube when thermal conductivity is varied for a channel power of 8.5 MW_{th}, inner-tube thickness of 2 mm, pressure tube thickness of 11 mm, inlet temperature of 350°C, mass flow rate of 4.37 kg/s and uniform heat flux **81**

Figure 5.15: Temperature profile along the Porous YSZ insulated channel length for a channel power of 8.5 MW_{th}, inner-tube thickness of 2 mm, pressure tube thickness of 11 mm, inlet temperature of 350°C, mass flow rate of 4.37 kg/s and uniform heat flux **84**

Figure 5.16: Temperature gradients along the radial distance from center for a Porous YSZ insulated Re-Entrant channel for a channel power of 8.5 MW_{th}, inner-tube thickness of 2 mm, pressure tube thickness of 11 mm, insulation thickness of 7 mm, inlet temperature of 350°C, mass flow rate of 4.37 kg/s and uniform heat flux **85**

Figure 5.17: Temperature profile along the ZrO_2 insulated channel length for a channel power of 8.5 MW_{th}, inner-tube thickness of 2 mm, pressure tube thickness of 11 mm, insulation thickness of 7 mm, inlet temperature of 350°C, mass flow rate of 4.37 kg/s and uniform heat flux **87**

Figure 5.18: Temperature gradients along the radial distance from center for a ZrO_2 insulated Re-Entrant channel for a channel power of 8.5 MW_{th}, inner-tube thickness of 2 mm, pressure tube thickness of 11 mm, insulation thickness of 7 mm, inlet temperature of 350°C, mass flow rate of 4.37 kg/s and uniform heat flux **88**

Figure 5.19: Heat loss to Moderator for cold side of Re-Entrant channel for variable Porous YSZ insulation thickness and variable solid ZrO_2 insulation thickness assuming mixed type heat loss to the moderator **90**

Figure 5.20: Heat loss to Moderator for cold side of Re-Entrant channel for variable Porous YSZ insulation thickness and variable solid ZrO_2 insulation thickness assuming free convection heat loss to the moderator **91**

Figure 5.21: Axial Power Profiles **95**

Figure 5.22: Case 1 (Uniform Power Profile): Temperature profiles along the 7 mm thick Porous YSZ insulated fuel-channel for a total channel power of 8.5 MW_{th}, inner-tube thickness of 2 mm, pressure tube thickness of 11 mm, inlet temperature of 350°C and mass flow rate of 4.37 kg/s **96**

Figure 5.23: Case 2 (Typical Nominal Power Profile): Temperature profiles along the 7 mm thick Porous YSZ insulated fuel-channel for a total channel power of 8.5 MW_{th}, inner-tube thickness of 2 mm, pressure tube thickness of 11 mm, inlet temperature of 350°C and mass flow rate of 4.37 kg/s **97**

Figure 5.24: Case 3 (Peaked Shape Power Profile): Temperature profiles along the 7 mm thick Porous YSZ insulated fuel-channel for a total channel power of 8.5 MW_{th}, inner-tube thickness of 2 mm, pressure tube thickness of 11 mm, inlet temperature of 350°C and mass flow rate of 4.37 kg/s **98**

Figure 5.25: Case 4 (Upstream-skewed Power Profile): Temperature profiles along the 7 mm thick Porous YSZ insulated fuel-channel for a total channel power of 8.5 MW_{th}, inner-tube thickness of 2 mm, pressure tube thickness of 11 mm, inlet temperature of 350°C and mass flow rate of 4.37 kg/s **99**

Figure 5.26: Case 5 (Downstream-skewed Power Profile): Temperature profiles along the 7 mm thick Porous YSZ insulated fuel-channel for a total channel power of 8.5 MW_{th}, inner-tube thickness of 2 mm, pressure tube thickness of 11 mm, inlet temperature of 350°C and mass flow rate of 4.37 kg/s **100**

Figure 5.27: Case 6 (Variable Power Profile): Temperature profiles along the 7 mm thick Porous YSZ insulated fuel-channel for a total channel power of 8.5 MW_{th}, inner-tube thickness of 2 mm, pressure tube thickness of 11 mm, inlet temperature of 350°C and mass flow rate of 4.37 kg/s **101**

Figure B.1: Comparison of coolant temperature for a total channel power of 8.5 MW_{th}, mass flow rate of 4.37 kg/s, uniform heat flux and no heat loss to the moderator **127**

Figure C 1(a): Specific heat, thermal conductivity and Prandtl number profiles along a YSZ insulated fuel-channel for a channel power of 8.5 MW_{th}, inner-tube thickness of 2 mm, pressure tube thickness of 11 mm, inlet temperature of 350°C, mass flow rate of 4.37 kg/s and uniform heat flux **128**

Figure C 1(b): Average specific heat, average Prandtl number and HTC profiles along a YSZ insulated fuel-channel for a channel power of 8.5 MW_{th}, inner-tube thickness of 2 mm, pressure tube thickness of 11 mm, inlet temperature of 350°C, mass flow rate of 4.37 kg/s and uniform heat flux **129**

Figure C 2 (a): Specific heat, thermal conductivity and Prandtl number profiles along a ZrO_2 insulated channel for a channel power of 8.5 MW_{th}, inner-tube thickness of 2 mm, pressure tube thickness of 11 mm, insulation thickness of 7 mm, inlet temperature of 350°C, mass flow rate of 4.37 kg/s and uniform heat flux **130**

Figure C 2(b): Average specific heat, average Prandtl number and HTC profiles along a ZrO_2 insulated channel for a channel power of 8.5 MW_{th}, inner-tube thickness of 2 mm, pressure tube thickness of 11 mm, insulation thickness of 7 mm, inlet temperature of 350°C, mass flow rate of 4.37 kg/s and uniform heat flux **131**

Figure D.1 (a): Case 2 - Specific heat, Prandtl number and thermal conductivity profiles along a 7 mm thick Porous YSZ insulated channel for a total channel power of 8.5 MW_{th}, inner-tube thickness of 2 mm, pressure tube thickness of 11 mm, inlet temperature of 350°C and mass flow rate of 4.37 kg/s **132**

Figure D.1 (b): Case 2 - Average specific heat, average Prandtl number and HTC profiles along a 7 mm thick Porous YSZ insulated channel for a total channel power of 8.5 MW, inner-tube thickness of 2 mm, pressure tube thickness of 11 mm, inlet temperature of 350°C and mass flow rate of 4.37 kg/s **133**

Figure D.2 (a): Case 3 - Specific heat, Prandtl number and thermal conductivity profiles along a 7 mm thick Porous YSZ insulated channel for a total channel power of 8.5 MW_{th}, inner-tube thickness of 2 mm, pressure tube thickness of 11 mm, inlet temperature of 350°C and mass flow rate of 4.37 kg/s **134**

Figure D.2 (b): Case 3 - Average specific heat, average Prandtl number and HTC profiles along a 7 mm thick Porous YSZ insulated channel for a total channel power of 8.5 MW_{th}, inner-tube thickness of 2 mm, pressure tube thickness of 11 mm, inlet temperature of 350°C and mass flow rate of 4.37 kg/s **135**

Figure D.3 (a): Case 4 - Specific heat, Prandtl number and thermal conductivity profiles along a 7 mm thick Porous YSZ insulated channel for a total channel power of 8.5 MW_{th}, inner-tube thickness of 2 mm, pressure tube thickness of 11 mm, inlet temperature of 350°C and mass flow rate of 4.37 kg/s **136**

Figure D.3 (b): Case 4 - Average specific heat, average Prandtl number and HTC profiles along a 7 mm thick Porous YSZ insulated channel for a total channel power of 8.5 MW_{th}, inner-tube thickness of 2 mm, pressure tube thickness of 11 mm, inlet temperature of 350°C and mass flow rate of 4.37 kg/s **137**

Figure D.4 (a): Case 5 - Specific heat, Prandtl number and thermal conductivity profiles along a 7 mm thick Porous YSZ insulated channel for a total channel power of 8.5 MW_{th}, inner-tube thickness of 2 mm, pressure tube thickness of 11 mm, inlet temperature of 350°C and mass flow rate of 4.37 kg/s **138**

Figure D.4 (b): Case 5 - Average specific heat, average Prandtl number and HTC profiles along a 7 mm thick Porous YSZ insulated channel for a total channel power of 8.5 MW_{th}, inner-tube thickness of 2 mm, pressure tube thickness of 11 mm, inlet temperature of 350°C and mass flow rate of 4.37 kg/s **139**

Figure D.5 (a): Case 6 - Specific heat, Prandtl number and thermal conductivity profiles along a 7 mm thick Porous YSZ insulated channel for a total channel power of 8.5 MW_{th}, inner-tube thickness of 2 mm, pressure tube thickness of 11 mm, inlet temperature of 350°C and mass flow rate of 4.37 kg/s **140**

Figure D.5 (b): Case 6 - Average specific heat, average Prandtl number and HTC profiles along a 7 mm thick Porous YSZ insulated channel for a total channel power of 8.5 MW_{th}, inner-tube thickness of 2 mm, pressure tube thickness of 11 mm, inlet temperature of 350°C and mass flow rate of 4.37 kg/s **141**

NOMENCLATURE

A	area, m^2
$\overline{C_p}$	average specific heat, $\frac{J}{kg \cdot K}$, $\left(\frac{H_w - H_b}{T_w - T_b}\right)$
D	diameter, m
g	gravity, $\frac{m}{s^2}$
G	mass flux, $\frac{kg}{m^2 \cdot s}$
H	enthalpy, $\frac{J}{kg}$
h	heat transfer coefficient, $\frac{W}{m^2 \cdot K}$
k	thermal conductivity, $\frac{W}{m \cdot K}$
L	length, m
$\dot{m}$	mass-flow rate, $\frac{kg}{s}$
P	perimeter, m
R	thermal resistance, $\frac{K}{W}$
q	heat transfer rate, W
$\dot{Q}$	total heat transfer rate, W
T	temperature, $°C$
u	fluid velocity in x-direction, $\frac{m}{s}$
v	fluid velocity in y-direction, $\frac{m}{s}$
x	axial location, m

Greek Letters

α	thermal diffusivity, $\frac{m^2}{s}$
β	expansion coefficient, $\frac{1}{K}$
δ	thickness, mm
μ	dynamic viscosity, $Pa \cdot s$
ν	viscosity, $Pa \cdot s$
ρ	density, $\frac{kg}{m^3}$

Dimensionless numbers

Nu	Nusselt number $\left(\frac{HTC \cdot D_{hy}}{k}\right)$
Pr	Prandtl number $\left(\frac{\mu \cdot c_p}{k}\right)$
$\overline{\mathbf{Pr}}$	average Prandtl number $\left(\frac{\mu \cdot \bar{C}_p}{k}\right)$
Ra	Rayleigh number $\left(\frac{g \cdot \beta \cdot (T_w - T_b) \cdot D^3 \cdot \mathbf{Pr}}{\nu^3}\right)$
Re	Reynolds number $\left(\frac{G \cdot D_{hy}}{\mu}\right)$

Subscripts and Superscripts

A	annulus
b	bulk

B	bundles
c	cross section
CE	centre element
cr	critical
cs	cold side
E	fuel element
f	flow
forced	forced convection
free	free convection
fs	fuel sheath
FT	flow tube
hs	hot side
hy	hydraulic
i	inner
IT	inner tube
max	maximum
mod	moderator
n	node
o	outer
os	outer sheath
p	perimeter
pc	pseudocritical
PT	pressure tube
r	radius
total	total (free and forced) convection

w	wall
wet	wetted
x	axial length along fuel-channel

Acronyms

ACR	Advanced CANDU Reactor
CANDU	CANada Deuterium Uranium
FT	Flow Tube
GFR	Gas-cooled Fast Reactor
GIF	Generation IV International Forum
IT	Inner Tube
HEC	High Efficiency Channel
HTC	Heat Transfer Coefficient
LFR	Lead-cooled Fast Reactor
MATLAB	MATrix LABoratory
MSR	Molten Salt Reactor
Mtoe	Million tonnes of oil equivalent
NIST	National Institute of Standards and Technology
OT	Outer Tube
PT	Pressure Tube
PV	Pressure Vessel
REC	Re-Entrant Channel
REFPROP	REFerence fluid thermodynamic and transport PROPerties
SC	SuperCritical

SCW	SuperCritical Water
SCWR	SuperCritical Water-cooled Reactor
SFR	Sodium-cooled Fast Reactor
SS-304	Stainless Steel 304
VHTR	Very-High Temperature Reactor
YSZ	Yttria Stabilized Zirconia

CHAPTER 1

INTRODUCTION

Energy sources available today include fossil fuels, nuclear, hydroelectric, gas, wind, solar, refuse-based and biomass technologies. While the overall energy demand in developed countries has levelled-out in recent decades, the growth in energy demand of developing countries is increasing the pressure on energy resources worldwide. This growth is projected to increase as the world's population grows from the present level of 6 billion to 8 billion in 2025, and as the people in developing nations aspire to have a higher standard of living. Energy demand is derived from three major sectors, namely, domestic and commercial, industry and agriculture, and transport. There is a significant demand for energy in the form of electricity for the first two sectors. Electricity generation presently uses about 40% of the world's energy supply [**1**]. The future total energy growth worldwide is projected to average 1.7% per year to 2030. The demand is expected to reach 191,895 TWh in 2030 as compared to 119,789 TWh in 2002. While the demand in 2002 corresponds to 10,300 million tonnes of oil equivalent (Mtoe), the future demand corresponds to 16,500 Mtoe, where Mtoe is the amount of energy released by burning one million tonnes of crude oil. World electricity demand is projected to rise from 16,000 TWh/year in 2002 to 31,600 TWh/year in 2030, at an average rate of 2.5% per year [**2**]. Thus, electricity demand is growing much faster than overall energy demand.

While demand for oil continues to rise, available resources are declining and consumption is twice the rate of discovery of new oil resources. Most natural gas reserves are located in geopolitically uncertain areas and, hence transport becomes a major problem. Furthermore, natural gas production is likely to approach its peak in the next couple of decades in many countries. Renewable sources of energy cannot meet the extent of the future demand as the intermittent nature of these sources cannot be controlled to provide either continuous base-load power or peak-load power when it is needed. Coal resources are abundant worldwide and coal is economically attractive to

use in large scale, but it is a significant contributor to greenhouse gas emissions among all fossil fuels and has significant health related effects[**1**]. Nuclear power on the other hand is comparatively cleaner. Presently, there are about 440 nuclear power reactors operating in 30 countries worldwide, producing 16% of the world's electricity. 15% of Canada's electricity is generated from nuclear power while over 50% of the electricity generated in the province of Ontario is from nuclear power [**3**]. Assuming the current market share is maintained, the electricity growth translates to 2496 TWh of nuclear power over 28 years. This corresponds to an increase of 89 TWh of nuclear power each year. As traditional fossil fuel power plants are phased out to reduce greenhouse gas emissions, nuclear energy is the only non-greenhouse gas emitting power source that can effectively replace the fossil fuel generated electrical power in sufficient quantity and satisfy increasing global demand.

First generation nuclear reactors were built in the 1950s in Canada. Generation II and Generation III CANada Deuterium Uranium (CANDU) nuclear reactors are currently being used for energy production. In the CANDU design, fission reactions heat the heavy water coolant, which is heavy water in current CANDU reactors, to produce steam which is then used to generate electricity from a turbine generator system. Generation III+ CANDU reactors (e.g. ACR-1000) are currently being developed which would use light-water as the coolant. Research is looking ahead into the next generation, or Generation IV nuclear reactors, which are expected to be more efficient and cheaper to build than current reactor designs

An international effort established the Generation IV International Forum (GIF) in 2001 to indentify and select nuclear energy systems for further development. Argentina, Brazil, Canada, France, Japan, the Republic of Korea, the Republic of South Africa, the United Kingdom, and the United States signed the GIF charter in 2001 while Switzerland, Euratom, the People's Republic of China, and the Russian Federation signed the charter later on. Six different reactor systems were selected, namely, Gas-cooled Fast Reactors (GFRs), Lead-cooled Fast Reactors (LFRs), Molten Salt-cooled Reactors (MSRs), Sodium-cooled Fast Reactor (SFRs), SuperCritical Water-cooled Reactors (SCWRs), and

Very High-Temperature gas-cooled Reactors (VHTRs). Of these types, the SCWR is Canada's premier choice for Generation IV Reactor technology with some materials related research on VHTRs.

SuperCritical Water-cooled nuclear Reactors use light water as the coolant and operate at supercritical pressures and temperatures, that is, pressures and temperatures above the critical point of water. The critical pressure of water is 22.064 MPa and the critical temperature is 373.95°C [**4**]. At the end of the 1950s and 1960s, research was conducted to investigate the possibility of using supercritical fluids in nuclear reactors and several nuclear reactor design concepts using supercritical water were developed in the United States and the former USSR. This idea was abandoned, likely due to material constraints [**5**]. SCWRs have re-emerged as a viable option for Generation IV nuclear reactors now that there is more experience with fossil-based SuperCritical Water (SCW) plants and advanced materials have been developed for use in SCW environments. The main advantages of SCWRs are:

1) an increase in thermal efficiency of nuclear power plants from 30 – 35 % to 45 – 50 % which corresponds to current thermal (fossil fuel type) power plants;
2) an expected decrease in capital and operational costs, hence reduction in electrical-energy costs;
3) a simplified flow circuit with the elimination of steam dryers, steam heat separators etc. (for direct cycle version); and
4) the ability to facilitate steam based technologies such as desalination, thermochemical hydrogen production, or district heating due to higher temperature.

There are two types of SCWRs currently being developed: (i) Pressure Vessel type SCWR, and (ii) Pressure Tube type SCWR. The latter has been chosen by Canada and Russia as their SCWR design concept. While current CANDU-6 reactors operate at a coolant pressure range of 9.9 – 11.2 MPa, and current PWRs operate at a coolant pressure range of 10 – 16 MPa, SCWRs will operate at about 25 MPa. The inlet and outlet design

temperatures for the CANDU-SCWR is expected to be 350°C and 625°C respectively [**6**].

Supercritical water has unique properties such as a liquid-like density and a gas like viscosity [**7**]. There are significant changes in thermophysical properties such as specific heat, density, viscosity, and thermal conductivity of supercritical water within ±25°C from the pseudocritical temperature [**8**]. The density, viscosity, and thermal conductivity drastically decrease with increasing temperature through the pseudocritical region while the specific heat increases and then decreases in this region.

The current CANDU fuel-channel design cannot be used for the SCWR as the higher pressures in the SCWR fuel-channel will cause the pressure tube to rupture. Thus, a new fuel-channel design needs to be developed. The current SCWR channel-type design concept uses a ceramic liner, to reduce heat losses to the moderator, with a perforated metal insert to protect the ceramic liner from fuel bundles [**9**]. While such a design may work, alternative design concepts are under development to explore the optimum efficiency of a SCWR channel-type reactor.

An alternative design being considered is the Re-Entrant fuel-channel (REC) which consists of three tubes: the inner tube (flow tube), the pressure tube, and an outer tube. The fuel bundles, similar to those of the current CANDU reactors, are placed in the inner tube. The flow and pressure tubes form an annulus through which flows the primary coolant. At the far end, the flow will reverse direction and enter the inner tube, and hence the fuel string. The coolant exits the channel from the inner tube. Insulation options such as ceramic and carbon dioxide gas can be used in the gap between the pressure tube and the outer tube. As the coolant enters the channel below the pseudocritical temperature and exits the channel well above the pseudocritical temperature, it passes through the pseudocritical region along the heated length of the fuel-channel [**5**].

The location of the pseudocritical point is one of the main reasons for developing the REC. As deteriorated heat transfer occurs around the pseudocritical point and as there

are also significant material chemistry issues in the pseudocritical region, the occurrence of the pseudocritical point in the annulus of the REC, if possible, may address some of these concerns. Another reason for developing the REC is that the coolant can act as a preheater in the annulus and can reduce heat losses. There are also concerns with the use of the ceramic insulator and perforated liner as unproven technology in supercritical water. An advantage of having the ceramic insulator outside the pressure tube in the REC design is that the ceramic will never come in contact with the coolant, hence avoiding the problem of creating ceramic particles that could enter the primary heat transport system. An advantage of using carbon dioxide gas in the ceramic insulating region in the REC is that it helps in detecting a leak in the pressure tube by analyzing the moisture content in the gas. A disadvantage of the REC is that it may lead to an increased complexity in the end fitting design [**9**].

The pseudocritical region also affects various thermophysical properties of the coolant which impacts the temperature profiles of the coolant and of the outer sheath. The pseudocritical point can either occur in the inner tube or in the annulus of the REC. Thus, it is important to know the location of the pseudocritical point in the channel. This can be done by developing a numerical model of the REC and by modelling the heat transfer across the fuel-channel.

1.1 Objective

Therefore, the primary objective of this thesis is to develop a design concept of an alternative SCWR Fuel Channel concept called the Re- Entrant Fuel Channel and to assess the thermal hydraulic behaviour of the channel. Additional objectives of the work are as follows:

1. Calculate temperature profiles of the coolant, flow tube, pressure tube, outer tube and outer sheath along the length of the fuel-channel to determine the effect of the pseudocritical point on the temperature profiles, and to verify that the outer sheath temperature is below the sheath temperature limit;

2. Calculate the total heat loss from the Re-Entrant Fuel Channel to the moderator and to evaluate the efficiency of the REC;
3. Optimize the design of the channel by performing various sensitivity analyses; and to
4. Compare the total heat loss and efficiency with the existing SCWR channel-type design concept.

Chapter 2 of this thesis will describe the literature review with particular focus on SCWR type reactors, supercritical fluid properties, and the general thermal hydraulic behaviour of supercritical water. Chapter 3 will discuss the methodology and the proposed design options for the REC. The numerical model of the REC is described in Chapter 4. Using the numerical model, a heat transfer analysis was conducted considering no heat loss to the moderator, heat losses to the moderator with different insulators, the impact of non-uniform heat flux shapes, and the impact of boundary conditions. The results of the heat transfer analysis are discussed in detail in Chapter 5. The design of the REC can thus be optimized considering variable power, flow, and initial conditions. Concluding remarks and future work are described in Chapters 6 and 7.

CHAPTER 2

BACKGROUND AND LITERATURE REVIEW

2.1 Generation IV Nuclear Technology

Figure 2.1 shows the advancement of nuclear reactor technology in Canada since the 1950s, when nuclear power was first used for commercial production of electricity.. Nuclear Power Demonstration (NPD), a small scale prototype CANDU type reactor and Douglas Point, a larger prototype, commenced operation in 1962 and 1967 respectively. These reactors are referred to Generation I nuclear reactors and they established the technological base necessary for larger commercial CANDU units.

CANDU 6 reactors are Generation II reactors. The first commercial CANDU unit came into operation in 1971 in Pickering, Ontario [**10**]. CANDU type reactors use heavy water (D_2O) as their coolant and moderator, operate at a pressure of approximately 10 MPa and have inlet and outlet temperatures of approximately 260°C and 310°C respectively [**11**].

The CANDU 3 and CANDU 9 were Generation III reactor concepts which were designed, but never built. The Enhanced CANDU 6 (EC6) is part of the Generation III reactors which is currently being developed by AECL. It retains the basic features of the CANDU 6 design, but incorporates newer technologies that enhance safety, operation, and performance [**12**]. The Advanced CANDU reactor (ACR) is a Generation III+ reactor that is also currently being developed by AECL. The ACR is a light-water cooled and heavy-water moderated reactor [**13**,**14**].

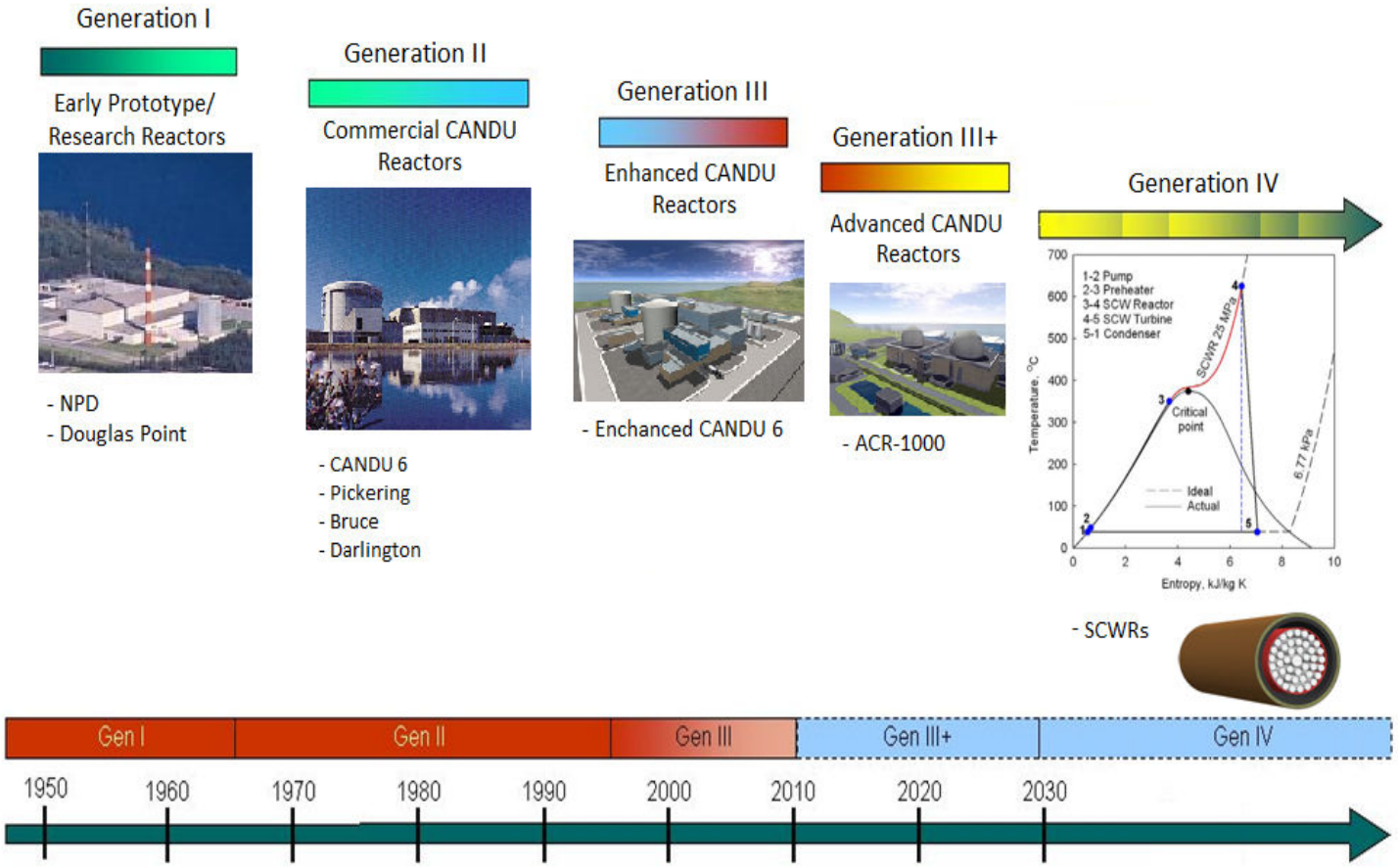

Figure 2.1: Nuclear Reactor Technology in Canada [12,13,,14]

The Generation IV International Forum (GIF) was established in 2001 to select and develop the next generation of nuclear energy systems known as Generation IV. Canada, Argentina, Brazil, France, Japan, the Republic of Korea, the Republic of South Africa, the United Kingdom, and the United States signed the GIF in 2001. Switzerland joined the forum in 2002, Euratom in 2003 and Russia joined in 2006 along with China.

The main requirements for Generation IV reactors as established by the GIF are enhancements in sustainability, safety and reliability, economical viability, proliferation resistance and physical protection [**15**]. These requirements are listed below:

- Sustainability – The Generation IV nuclear energy systems will provide sustainable energy generation that meets clean air objectives and provides long-term availability of systems and effective fuel utilization for worldwide energy production. The Generation IV nuclear energy systems will minimize and manage their nuclear waste and notably reduce the long-tem stewardship burden, thereby improving protection for the public health and environment.

- Economics – Generation IV nuclear energy systems will have a clear life-cycle cost advantage over other energy sources and will have a level of financial risk comparable to other energy projects.

- Safety and Reliability – Generation IV nuclear energy systems operations will excel in safety and reliability. These systems will have a very low likelihood and degree of reactor-core damage and will eliminate the need for offsite emergency response.

- Proliferation Resistance and Physical Protection – Generation IV nuclear energy systems will offer enhanced security for nuclear materials and facilities against acts of terrorism.

Generation IV nuclear energy systems are intended to meet the above requirements in order to provide a sustainable development of nuclear energy.

2.2 Generation IV Concepts

The GIF panel selected six reactor systems for further development from 100 concepts. A brief description of these systems is shown below:

- Very-High Temperature Reactors (VHTRs) – The VHTR is a helium-gas cooled, graphite moderated and thermal neutron spectrum reactor. The reference parameters are a coolant inlet and outlet temperatures of approximately 500°C and 1000°C respectively, an operating pressure of 9 MPa and reactor thermal power of 600 MW. The VHTR will be mainly used for the cogeneration of electricity and hydrogen as well as other process heat applications [**16**].

- Sodium-cooled Fast Reactors (SFR) – Liquid sodium is used as the reactor coolant in this type of fast neutron spectrum reactor whose outlet temperatures ranges from 530°C to 500°C. The SFR is designed for efficient management of high-level wastes such as plutonium and other actinides. Three reactor sizes are being designed, large (600 to 1500 MW) loop-type reactor, intermediate (300 to 600 MW) pool-type reactor and small (50 to 150 MW) modular-type reactor [**16**,**17**].

- Gas-cooled Fast Reactors (GFRs) – GFRs use a direct Brayton cycle gas turbine for electricity and hydrogen production with high efficiency. The 1200 MW reference reactor has a fast neutron spectrum, an inlet temperature of 485°C, outlet temperature of 850°C and an operating pressure of 7 MPa [**16**,**18**].

- Lead-cooled Fast Reactors (LFRs) – LFRs use molten lead or lead-bismuth as an inert coolant and have a fast neutron spectrum. The main purpose of LFRs is

electricity and hydrogen production along with actinide management. LFRs have an inlet temperature of 400 – 420°C and an outlet temperature of 480 – 570°C [**19**].

- Molten Salt Reactors (MSRs) – MSRs have a thermal neutron spectrum and use molten salts such as sodium fluoride salt as their coolant. The coolant outlet temperature of MSRs can range up to 800°C and the reference thermal power is 1,000 MW [**16**,**20**]

- SuperCritical Water-cooled Reactors–SCWRs use Super-critical water as their coolant and operate above the thermodynamic critical point of water to increase efficiency. Both thermal neutron and fast neutron spectra are being considered for this type of reactor. SCWRs operate at 25 MPa and have an outlet temperature of up to 625°C. There are two different types of SCWRs, Pressure Vessel (PV) type SCWR and Pressure Tube (PT) type SCWR [**16**,**21**].

VHTRs and SCWRs are Canada's choice for Generation IV reactors. Extensive research is currently being conducted to develop these two reactor concepts.

2.2.1 SuperCritical Water-cooled Reactor Concepts

As previously mentioned, there are two different types of SCWRs that are currently being developed worldwide. The PV type reactor as seen in Figure 2.2, is a large reactor pressure vessel which has a wall thickness of 0.5 m to contain the reactor core. This type of reactor is analogous to conventional Light Water Reactors and is being developed by the United States.

The PT reactor, which can be seen in Figure 2.3, is analogous to conventional Heavy Water Reactors and is designed to be more flexible with respect to flow, flux and density changes compared to PV reactors. The PT reactor concept is being developed in Canada

and Russia by Atomic Energy of Canada Limited (AECL) and the Research and Development Institute of Power Engineering (RDIPE and NIKIET) respectively [**8**].

The separation between the moderator and the coolant in the PT SCWR concept allows for significant enhancement in safety. While SCW is the coolant, various moderator options are currently being considered.

Three thermodynamic cycle options are being considered for SCWRs. They include the direct, indirect, and dual cycle options. SC "steam" from the reactor is directly fed to a SC turbine in the direct cycle. This eliminates the need for steam generators which results in the highest cycle efficiency among the three cycles. The indirect and dual cycles use heat exchangers to transfer heat from the reactor to the turbine. Two types of heat exchangers are being considered: SC water to SC water and SC water to superheated steam. The maximum temperature of the secondary loop is lower due to heat transfer through the heat exchangers, hence lowering the efficiency of the cycle [**22**]. The above mentioned three options are further divided into various re-heat options. A direct cycle SCWR with no-re-heat option has been chosen for this analysis and the T-s diagram is shown in Figure 2.4. Saturated water enters the pump (Point 1), which compresses the fluid to the supercritical operating pressure. The water is then pre-heated (Point 2 → Point 3), before it enters the fuel-channel. The coolant continues to be heated as it flows through the fuel-channel (Point 3 → Point 4). The SC "steam" outlet from the reactor, which is at pressure of 25 MPa and temperature of 625°C, is then expanded in the SCW turbine (Point 4 → Point 5) to a sub-atmospheric pressure of 6.77 kPa. The steam is condensed inside a condenser and enters the pump (Point 5 → Point 1), thus completing the thermodynamic cycle [**23**].

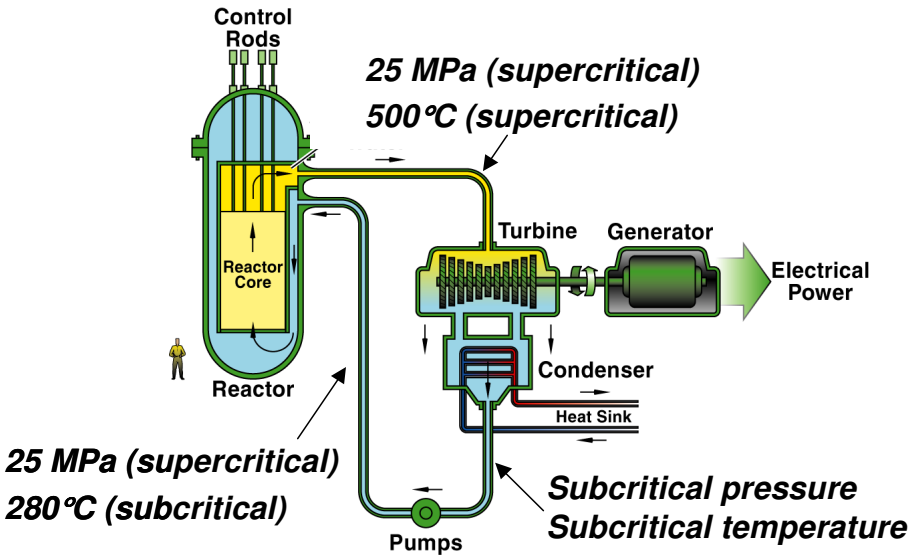

Figure 2.2: Pressure Vessel Type SCWR [5]

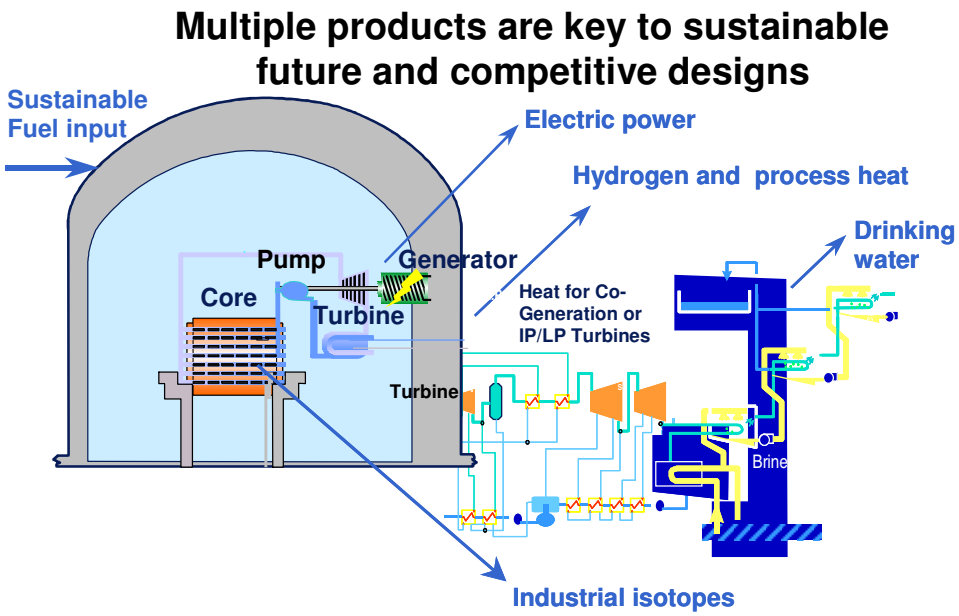

Figure 2.3: Pressure Tube Type SCWR [5]

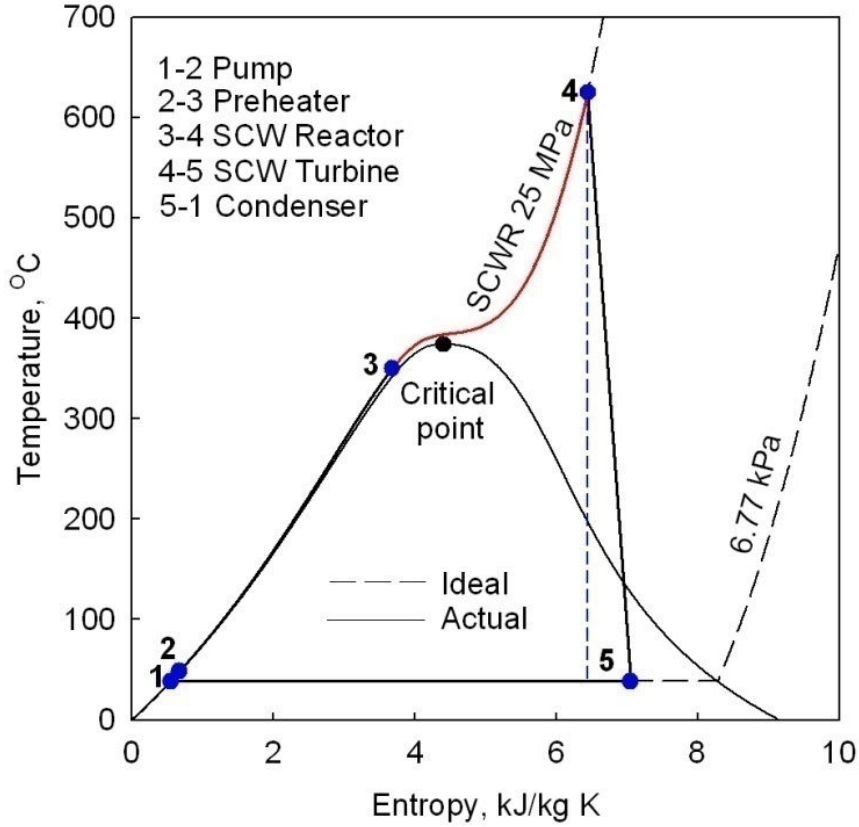

Figure 2.4: T-s diagram for direct cycle SCWR with no-reheat option [23]

The main advantage of SCWRs is an increase in thermal efficiency of Nuclear Power Plants from 30 – 35 % to 45 – 50 % which corresponds to current thermal power plants. SCWRs operate on a direct cycle where the coolant is the reactor is used in the turbines, thus eliminating the need for steam dryers, steam heat separators etc., which would lead to a simplified flow circuit and lower capital and operational costs [**5**]. SCWRs also have the ability to facilitate steam based technologies such as desalination, thermochemical hydrogen production and district heating [**24**].

Supercritical water has unique thermophysical properties and these properties are discussed in the following section.

2.3 SCW Properties

The thermophysical properties of supercritical water undergo significant changes within the critical and pseudocritical regions. The critical point occurs when the distinction between the liquid and vapour phases disappears and is characterized by T_{cr} and P_{cr}. The critical pressure for water is 22.064 MPa and the critical temperature of water is 373.95°C [**4**]. The pseudocritical point is a point at a pressure above the critical pressure and at a temperature corresponding to the maximum specific heat for this particular pressure [**5**].

Since SCWRs will operate at a pressure of 25 MPa, the pseudocritical temperature can be identified by the peak in the specific heat curve shown in Figure 2.5 (a). From Figure 2.5 (a), the pseudocritical temperature corresponds to 384.9°C.

Thermophysical properties such as density, thermal conductivity, dynamic viscosity, kinematic viscosity, and Prandtl number undergo significant changes in the pseudocritical region. These changes can be seen in Figure 2.5 (b-f) (Figures constructed using values extracted from NIST REFPROP at 1°C intervals).

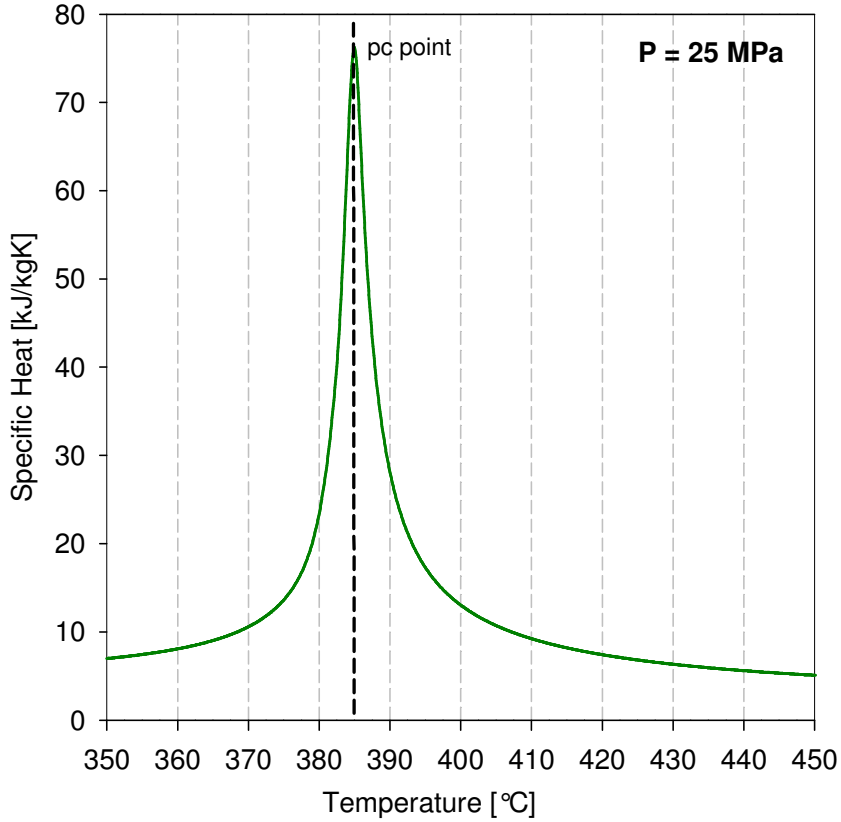

Figure 2.5 (a): Specific Heat vs. Temperature of water in the pseudocritical region at 25 MPa

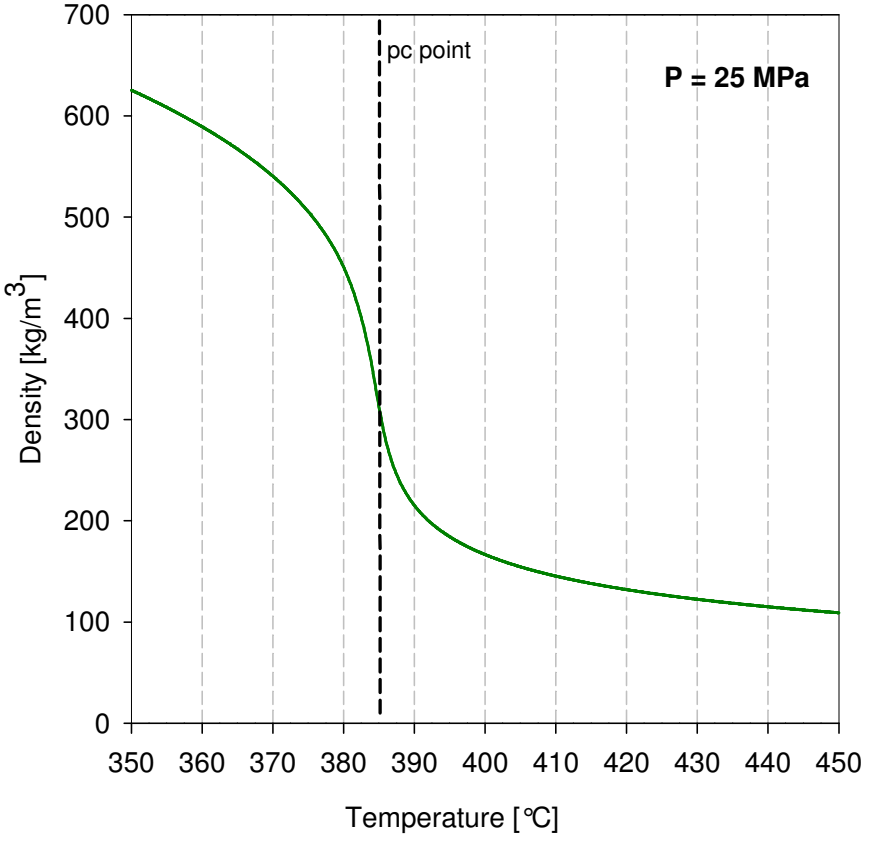

Figure 2.5 (b): Density vs. Temperature of water in the pseudocritical region at 25 MPa

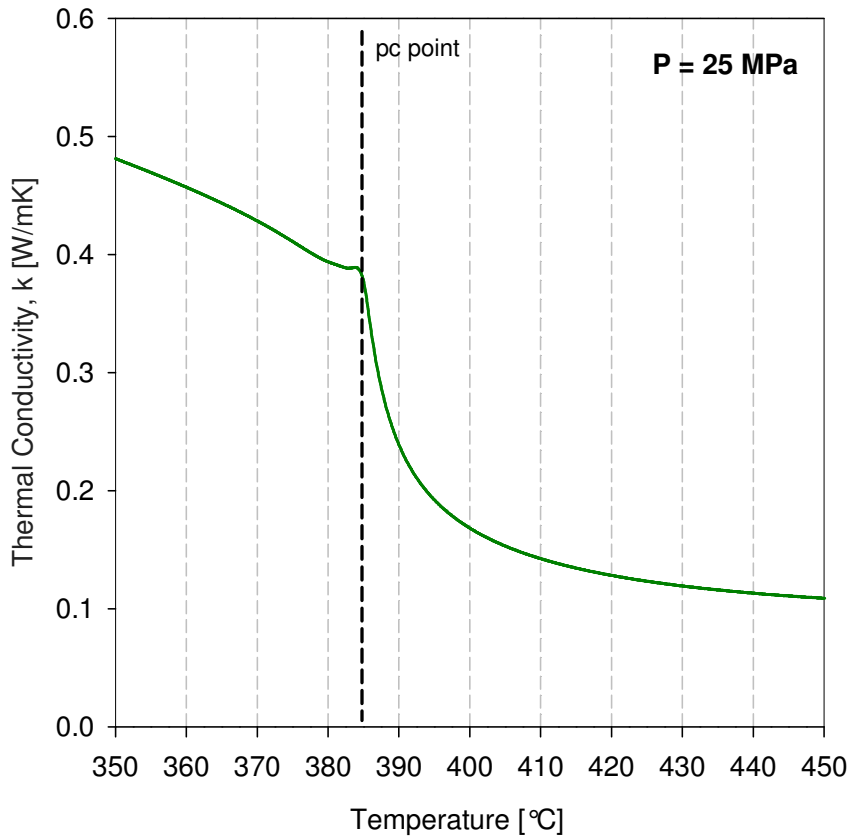

Figure 2.5 (c): Thermal Conductivity vs. Temperature of water in the pseudocritical region at 25 MPa

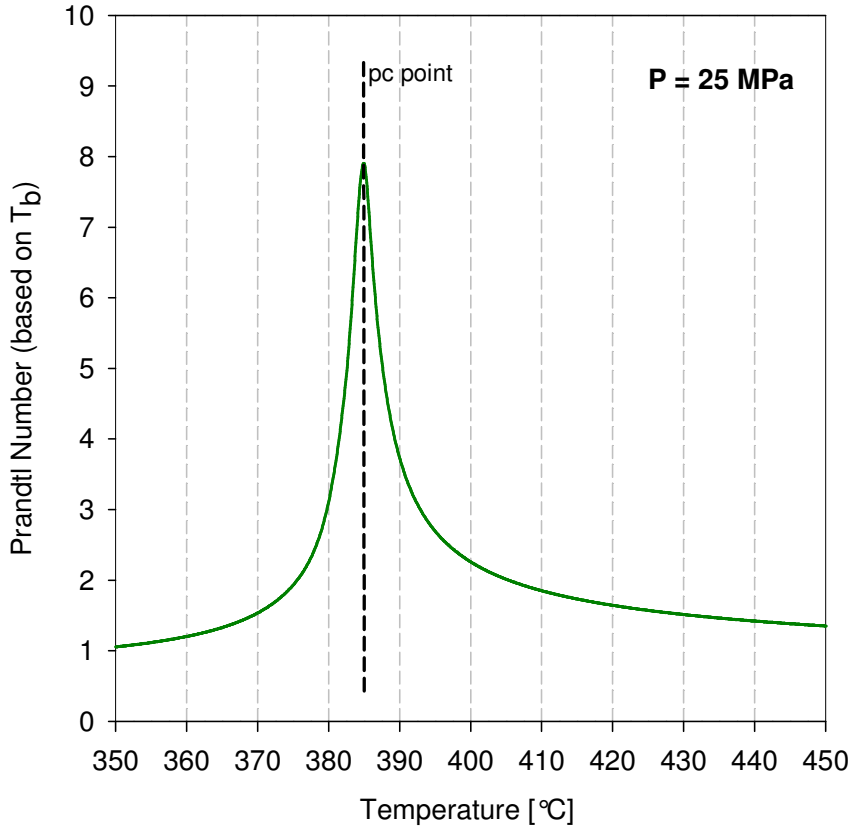

Figure 2.5 (d): Prandtl Number vs. Temperature of water in the pseudocritical region at 25 MPa

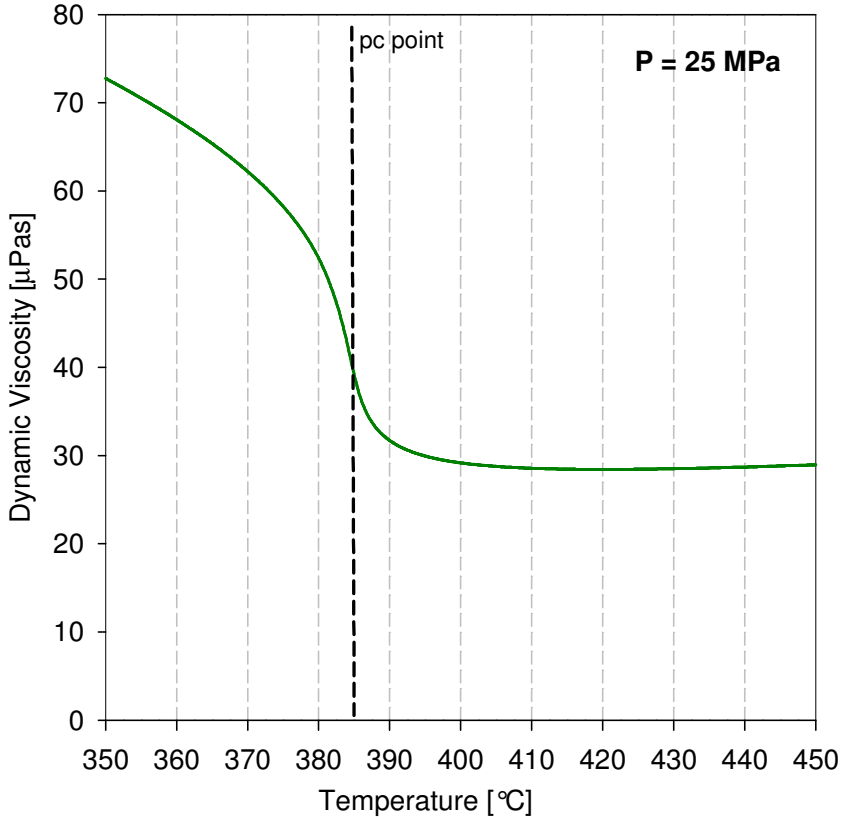

Figure 2.5 (e): Dynamic Viscosity vs. Temperature of water in the pseudocritical region at 25 MPa

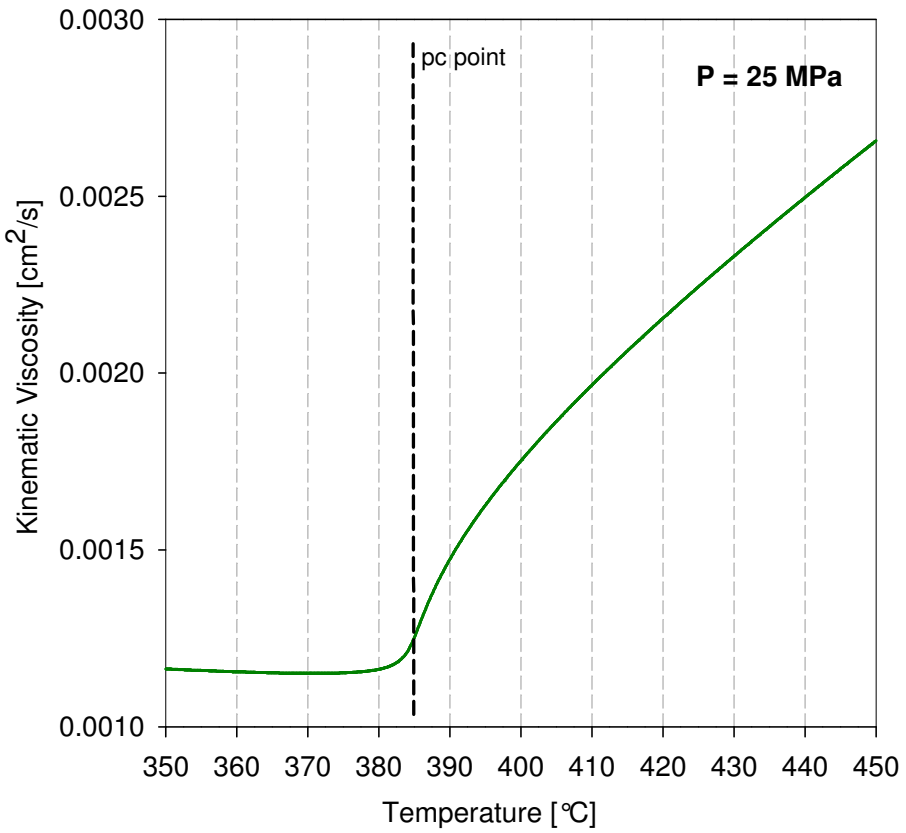

Figure 2.5 (f): Kinematic Viscosity vs. Temperature of water in the pseudocritical region at 25 MPa

The most significant changes occur within ±25°C of the pseudocritical temperature. Properties such as density and dynamic viscosity undergo a significant drop in this region while there in an increase in the kinematic viscosity. Thermal conductivity and Prandtl number peak at the pseudocritical point, albeit the peak in the thermal conductivity is relatively small. As the inlet temperature for a SCWR is 350°C and the outlet temperature is 625°C, the coolant would pass through the pseudocritical region before reaching the channel outlet [**5**]

Various correlations have been developed to calculate the heat transfer characteristics of supercritical water as shown in the following section.

2.4 SCW Correlations

Dyadyakin and Popov developed a correlation for supercritical water heat transfer for fuel bundles [**25**].

$$\mathbf{Nu}_x = 0.0021\,\mathbf{Re}_x^{0.8}\,\overline{\mathbf{Pr}}_x^{0.7}\left(\frac{\rho_w}{\rho_b}\right)_x^{0.45}\left(\frac{\mu_b}{\mu_{in}}\right)_x^{0.2}\left(\frac{\rho_b}{\rho_{in}}\right)_x^{0.1}\left(1+2.5\frac{D_{hy}}{x}\right) \tag{2.1}$$

where x is the axial location along the heated length in metres and D_{hy} is the hydraulic diameter. A tight-lattice, 7 element, helically finned, water-cooled bundle cooled with water was used to develop the correlation. As heat transfer correlations for bundles are generally very sensitive to bundle design because of the effect of different bundle components , and the experiments appear to be for a mobile-type reactor, this correlation cannot be applied to SCWRs [**8**].

The Dittus-Boelter correlation shown in Equation (2.2) is the most widely used heat transfer correlation at subcritical pressures for forced convection. The use of this correlation as shown in Equation (2.2) was proposed by McAdams for forced convective heat transfer in turbulent flows at subcritical pressures [**26**].

$$\mathbf{Nu}_b = 0.0243\, \mathbf{Re}_b^{0.8} \mathbf{Pr}_b^{0.4} \tag{2.2}$$

Equation (2.2) was later used at supercritical conditions. According to Schnurr et al., Equation (2.2) showed good agreement with experimental data for supercritical water flowing inside circular tubes at a pressure of 31 MPa. It was also noted that the equation might produce unrealistic results within some flow conditions near the critical and pseudocritical points but this equation was used as a base for other supercritical heat transfer correlations [**27**].

The original Dittus-Boelter correlation shown above is used in the following form for reference purposes [**28**]:

$$\mathbf{Nu}_b = 0.023\, \mathbf{Re}_b^{0.8} \mathbf{Pr}_b^{0.4} \tag{2.3}$$

Bishop et al. conducted experiments with supercritical water flowing upward inside tubes and annuli for the following range of operating parameters: pressure: 22.8 – 27.6 MPa, bulk fluid temperature: 282 – 527°C, mass flux: 651 – 3662 kg/m^{2}s and heat flux : 0.31 – 3.46 MW/m^2. Their data for heat transfer were generalized using the following correlation:

$$\mathbf{Nu}_b = 0.0069\, \mathbf{Re}_b^{0.9}\, \overline{\mathbf{Pr}}_b^{0.66} \left(\frac{\rho_w}{\rho_b}\right)_x^{0.43} \left(1 + 2.4\frac{D}{x}\right) \tag{2.4}$$

where x is the axial location along the heated length, ρ_w is the density of the fluid at the wall temperature, ρ_b is the density of the fluid at bulk temperature and the last term accounts for entrance-region effects [**29**].

The Bishop et al. correlation is often used without the entrance-region term and is hence written as:

$$\mathbf{Nu}_b = 0.0069\, \mathbf{Re}_b^{0.9}\, \overline{\mathbf{Pr}}_b^{0.66} \left(\frac{\rho_w}{\rho_b}\right)_x^{0.43} \tag{2.5}$$

Swenson et al. investigated heat transfer coefficients in smooth tubes and found that conventional correlations do not work well as they use bulk fluid temperature to calculate thermophysical properties. The Swenson et al. correlation was developed using a pressure range of 22.8 – 41.4 MPa, bulk fluid temperature of 75 – 576°C and mass flux of 542 – 2150 kg/m^{3}s. The correlation uses the wall temperature to calculate thermophysical properties and is shown in Equation (2.6) [**30**].

$$\mathbf{Nu}_w = 0.00459\, \mathbf{Re}_w^{0.923}\, \overline{\mathbf{Pr}}_w^{0.613} \left(\frac{\rho_w}{\rho_b}\right)^{0.231} \tag{2.6}$$

Mokry et al. modified the existing correlations for SCW to obtain a new correlation for forced-convective heat transfer in a vertical bare tube as seen in Equation (2.7) [**8**]:

$$\mathbf{Nu}_b = 0.0061\, \mathbf{Re}_b^{0.904}\, \overline{\mathbf{Pr}}_b^{0.684} \left(\frac{\rho_w}{\rho_b}\right)_x^{0.564} \tag{2.7}$$

Zahlan et al. compared many empirical correlations using a dataset provided by Kirillov et al. from the Institute of Physics and Power Engineering (Obninsk, Russia) and concluded that the Mokry et al. correlation is currently the best known correlation for heat transfer in SCW [**31**,**32**].

A comparison of the previously mentioned correlations is shown in Figure 2.6. The bulk fluid temperature was assumed to be 350°C and the wall temperature was assumed to be 400°C. From the figure, it can be seen that the Mokry et al. correlation is the most conservative of the four correlations shown. Thus, the Mokry et al. correlation will be used for a conservative analysis in this work. The heat transfer calculations should be modified as new heat transfer correlations for SCW are published.

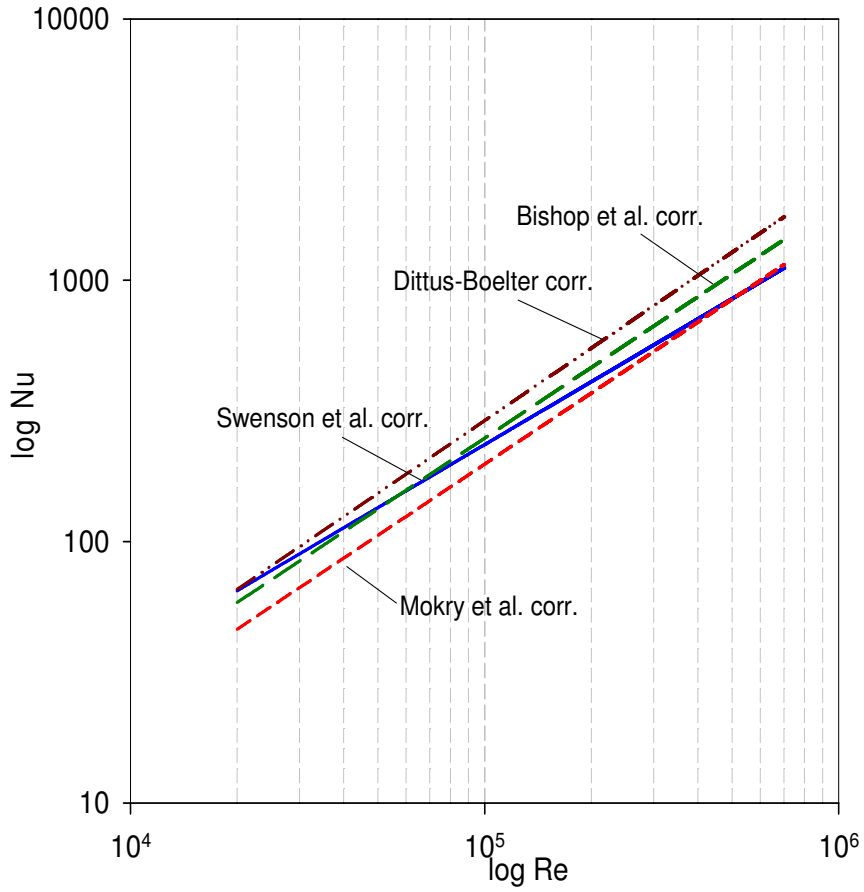

Figure 2.6: Comparison between SCW correlations when bulk fluid temperature is 350°C and wall temperature is 400°C

2.5 Fuel Channel Design Concepts

The current CANDU fuel-channel found in operating CANDU reactors consists of two tubes, the pressure tube and the calandria tube. The fuel bundles are located within the pressure tube. An annulus gas gap, which provides thermal insulation, separates the calandria tube and the pressure tube. The moderator flows outside the calandria tube. The pressure tube is made from a zirconium niobium alloy while the calandria tube is made from zirconium [**11**]. Figure 2.7 shows the present CANDU type fuel-channel.

CANDU 6 reactors have an operating pressure of 9.9 – 11.2 MPa and inlet and outlet temperatures of 260°C and 310°C respectively while SCWRs will have an operating pressure of 25 MPa and inlet and outlet temperatures of 350°C and 625°C [**11**]. The higher pressures associated with SCWRs are above the pressure tube burst pressure and thus the current design must be changed.

The current candidate for the CANDU SCWR PT type fuel-channel design uses only a pressure tube as shown in Figure 2.8. A ceramic liner is used to reduce heat losses to the moderator. A perforated metal insert is used to protect the ceramic liner from fuel bundles from scratching during refuelling and also reduce the erosion of the ceramic liner. The premise for this design is that the metal insert acts as a fuelling sleeve for transfer of the fuel while the ceramic acts as a thermal barrier. In doing so, the pressure tube will be at the moderator temperature and the thermal component of pressure tube creep will be significantly reduced. This design is also called the High Efficiency Channel (HEC) [**9**].

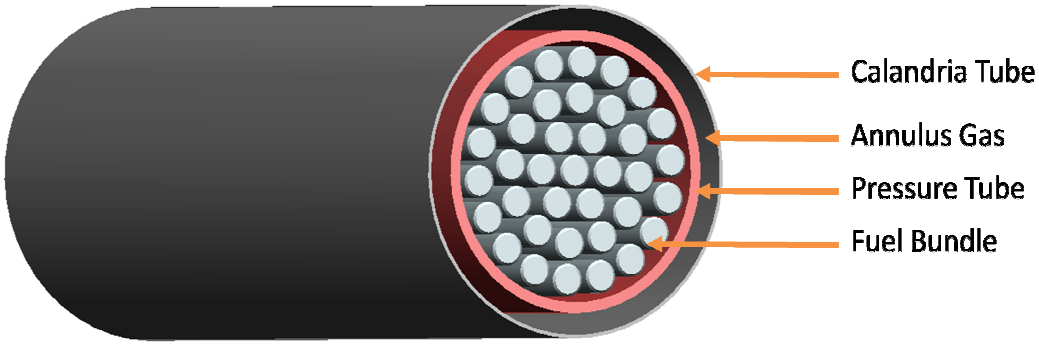

Figure 2.7: CANDU type fuel-channel

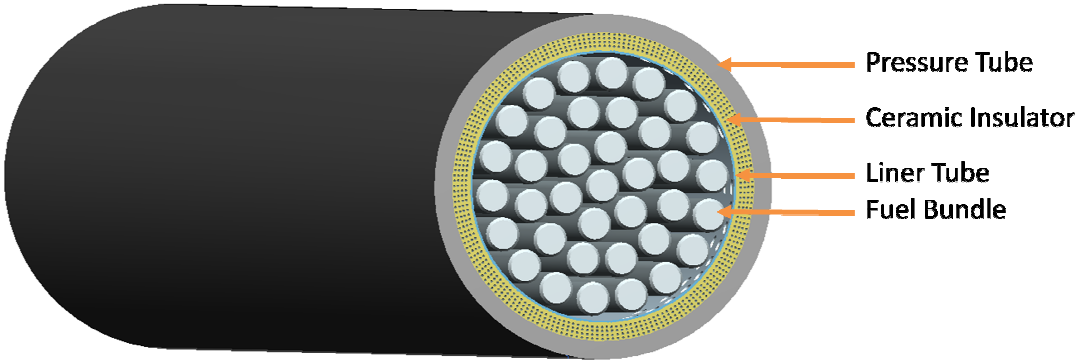

Figure 2.8: SCWR type fuel-channel concept

While such a design may work, there are concerns with the construction, assembly, and maintenance of the HEC. One potential problem with this design is that if the ceramic insulator erodes, fractures, or chips, it might be difficult to repair or replace the ceramic insulator due to the presence of the metal insert. If deterioration of the ceramic liner was to occur, then the thermal barrier is weakened and potential hotspots could occur on the pressure tube. This may result in some of the current problems such as hydriding and blistering occurring in HEC design. Hence, alternative design concepts that will not have the above mentioned problem are being considered for the SCWR channel-type reactor. One such alternative design being considered is called the Re-Entrant Fuel Channel and is explained in the following Chapter.

CHAPTER 3

PROPOSED FUEL CHANNEL DESIGN CONCEPT

The design requirements for the proposed fuel-channel concept are as follows:

1. The fuel-channel should be able to be used in a horizontal or vertical configuration.
2. The fuel-channel components should be able to withstand the high operating pressures and temperatures.
3. The fuel-channel components should be as neutron transparent as possible.
4. The fuel-channel should be insulated if required, to reduce heat losses to the moderator.

The proposed fuel-channel design concept under consideration consists of three tubes; an inner tube (flow tube), a pressure tube, and an outer tube. The fuel bundles are located within the inner tube, while a ceramic insulator or other thermal resistance barrier is placed in-between the pressure tube and the outer tube to reduce heat losses from the fuel-channel to the moderator. The outer tube protects the ceramic insulator from the heavy water moderator system. Figure 3.1 (a) shows the proposed new fuel-channel concept in a horizontal configuration in the calandria layout. The coolant inlet and outlet are in the same side of the new fuel-channel. The end fittings support the fuel-channels and allow a pressure tight connection with the fuelling machines, while a removable closure plug closes each end fitting. The end shields are filled with light water and steel balls, which thermalize and absorb neutrons. Figure 3.1 (b) shows a possible horizontal channel layout of 300 fuel-channels in the calandria vessel.

The vertical channel configuration of the proposed new fuel-channel is similar to the horizontal configuration except for the calandria vessel, which will be closer to a pressure vessel in this configuration. The vertical channel configuration is shown in Figure 3.2 (a), while a possible vertical channel layout is shown in Figure 3.2 (b).

The coolant first flows through the gap between the pressure tube and the flow tube from one end of the channel to the other before reversing direction and flowing through the inner tube. Thus, the fuel-channel effectively becomes a double-pipe heat exchanger in which the annulus acts as a preheater. The Re-Entrant channel design is shown in Figure 3.3. The fuel length of the current CANDU-type fuel-channel, 5.772 m, is chosen as the reference fuel length of the new fuel-channel. The side view of the Re-Entrant channel is shown in Figure 3.4 (a). The inner tube is referred to as the hot side and the annulus is referred to as the cold side of the Re-Entrant fuel-channel. Figures 3.4 (b) and (c) show the entrance region and the re-entrant region of the fuel-channel respectively.

The mass flow rate of the coolant in each channel is 4.37 kg/s [**24**]. The moderator temperature is estimated to be 80° C based on current operating parameters. The mean mass-flow rate of 0.95 kg/s for a mixed type flow in a CANDU-6 reactor is chosen as the reference mass flow rate of the moderator outside the Re-Entrant channel [**33**]. The reference case is a Channel Thermal Power of 8.5 MW_{th} uniformly applied in the fuelled region. Variable power profiles have also been accounted for in this work.

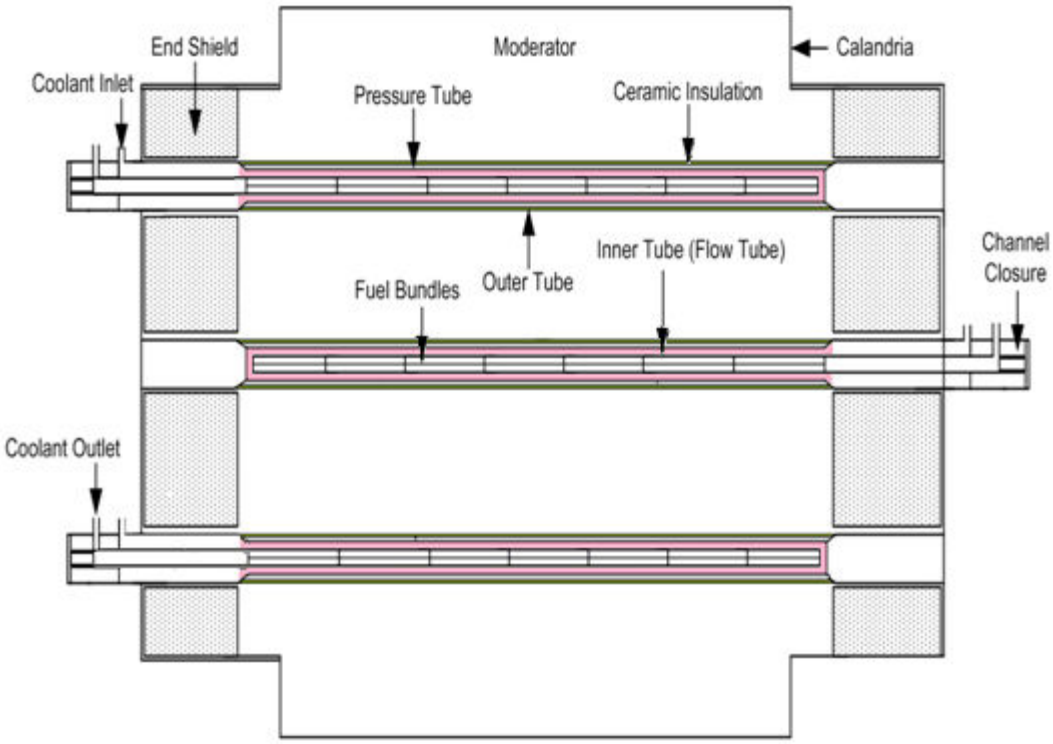

Figure 3.1 (a): Horizontal Re-Entrant channel configuration

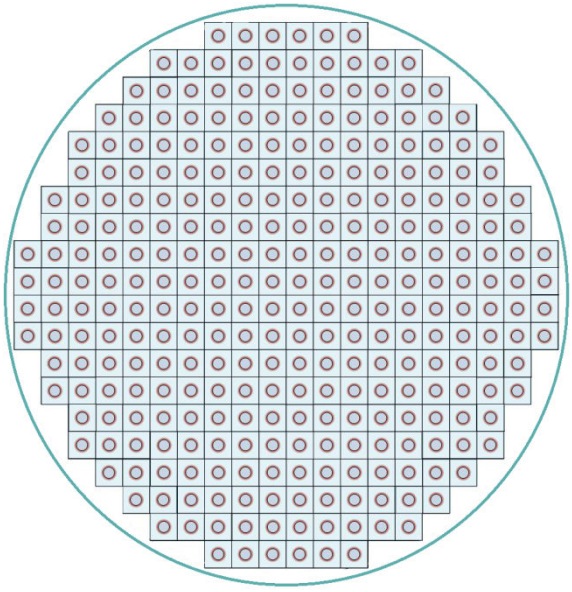

Figure 3.1 (b): Horizontal Re-Entrant channel configuration

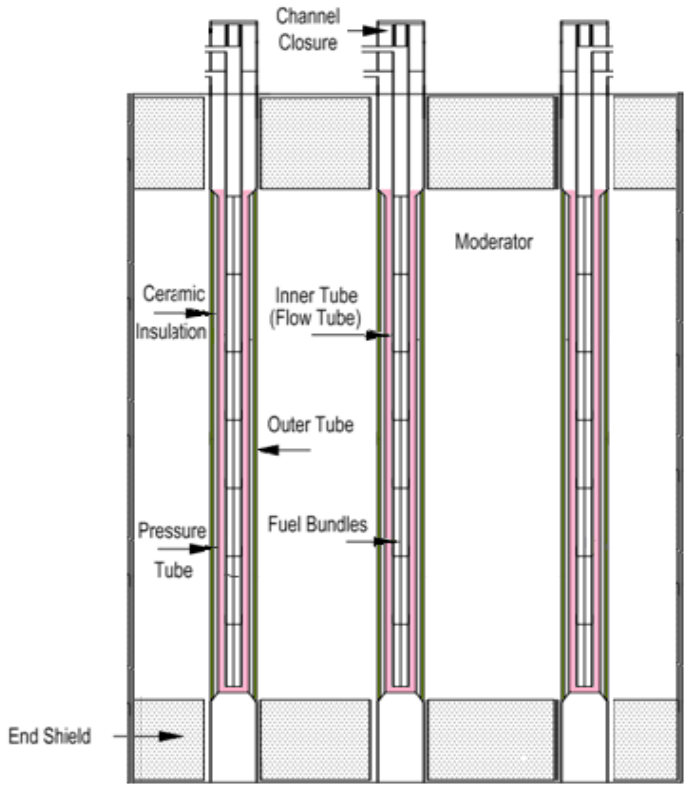

Figure 3.2 (a): Vertical Re-Entrant channel configuration

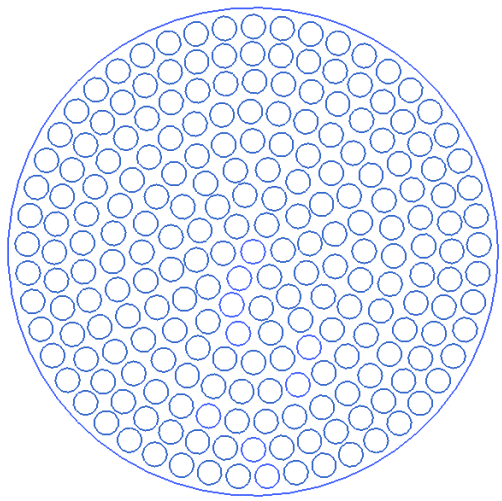

Figure 3.2 (b): Vertical Re-Entrant channel configuration

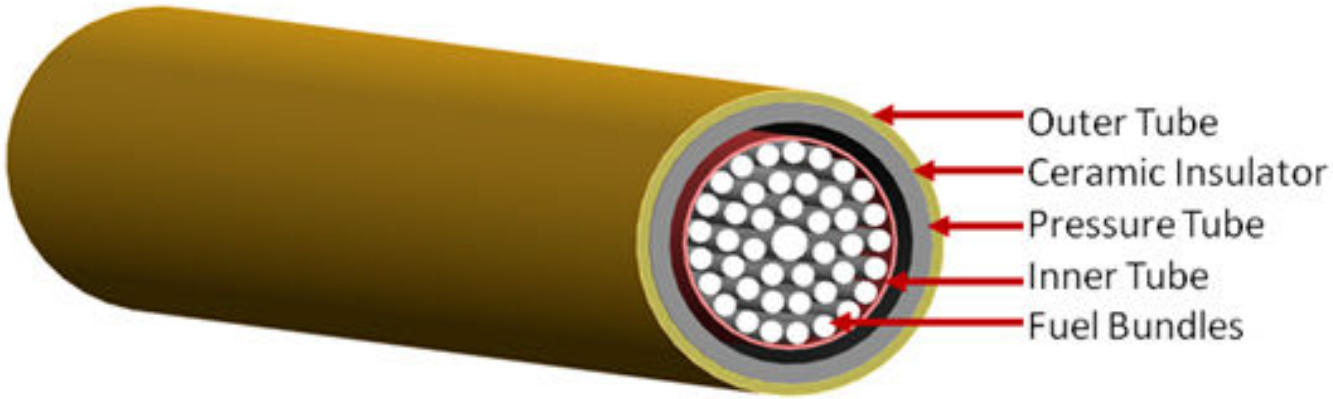

Figure 3.3: Proposed New Fuel Channel

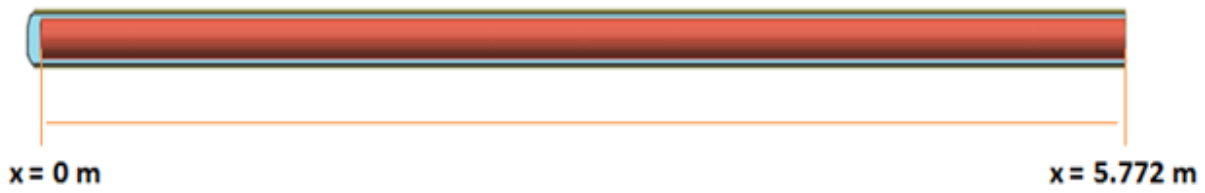

Figure 3.4 (a): Fuel length of Re-Entrant channel

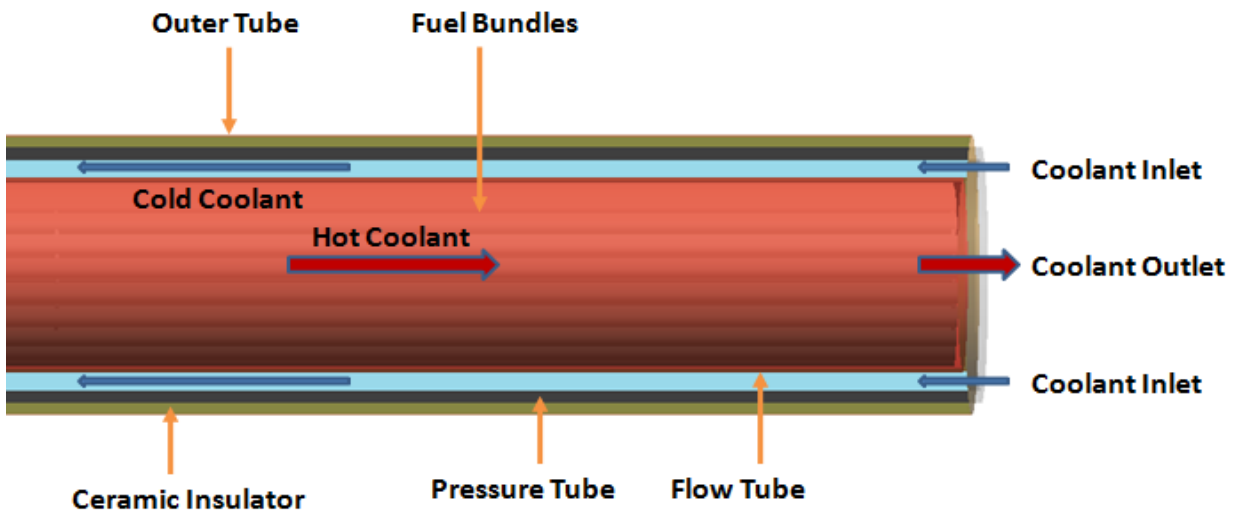

Figure 3.4 (b): Entrance Region of Re-Entrant channel

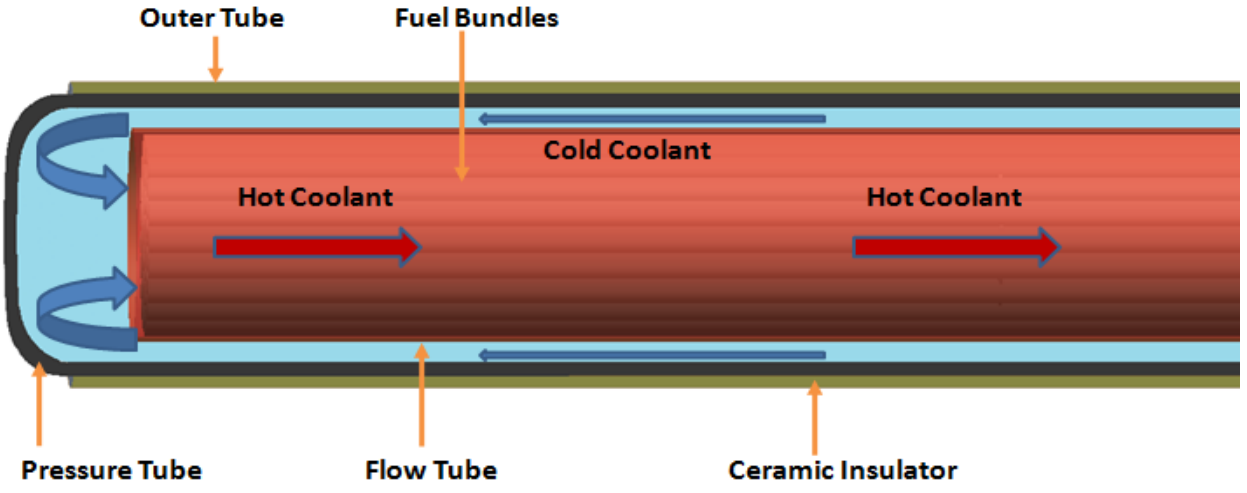

Figure 3.4 (c): Re-Entrant region of Re-Entrant channel

The inner diameter of the flow tube is kept equal to that of the current CANDU-type fuel-channel for two reasons. The first is that 103.5 mm allows current CANDU-type fuels to be used in the Re-Entrant channel. The second is that the industry has a lot of manufacturing and operating experience with this diameter range. The flow tube inner diameter is a design parameter that could be changed once more knowledge on the reactor physics and recommended fuel types is known. The four different options for the fuel bundles are shown in Table 3.1 [**34**]. They are the 37-Element bundle, the CANFLEX bundle, the Variant-18 bundle, and the Variant-20 bundle. The 37-Element and the CANFLEX bundles are currently being used, while the Variant-18 and the Variant-20 bundle concepts are variations of the CANFLEX bundle that are presently being developed. The CANFLEX, Variant-18, and the Variant-20 bundles have a total of 43 elements, while the 37-Element bundle has 37 elements. All four fuel bundles contain four rings of elements and the number of elements in each ring is different for the 37-Element bundle and the 43 element bundles, as seen in Table 3.1. Unlike the 37-Element bundle and the CANFLEX bundle, the centre element in the Variant-18 and Variant-20 bundles is unheated and filled with Dysprosium, a burnable neutron absorber which can reduce void reactivity [**35**]. The heated length of all four bundles is 481 mm, which corresponds to a total of 12 bundles in the 5.772 m long Re-Entrant fuel-channel. For the purposes of this work, the Variant-18 fuel bundle concept has been chosen for the horizontal Re-Entrant channel configuration. Note that the vertical configuration will use a fuel string and, depending on the fuelling method, a central rod might be needed to connect to the fuel string.

Table 3.1: Parameters of current fuel bundle options for the Re-Entrant channel

Parameter	Value			
	37 Element	**CANFLEX**	**Variant-18**	**Variant-20**
Total No. of Elements	37	43	43	43
No. of elements in the centre ring	1	1	1	1
No of elements in the inner ring	6	7	7	7
No. of elements in the intermediate ring	12	14	14	14
No of elements in the outer ring	18	21	21	21
Outer diameter of centre ring element (mm)	13.08	13.5	18.0	20
Outer diameter of inner ring element (mm)	13.08	13.5	11.5	11.5
Outer diameter of intermediate ring element (mm)	13.08	11.5	11.5	11.5
Outer diameter of outer ring element (mm)	13.08	11.5	11.5	11.5
Heated Bundle Length (mm)	481	481	481	481

There are few options for the material of construction of the tubes in the Re-Entrant channel. They include, Zirconium alloy with 2.5 wt% Niobium (Zr-2.5Nb) which is presently used as the material of construction of CANDU-type pressure tubes, Stainless Steel – Grade 304 (SS-304), Inconel-718, and a zirconium alloy called Excel (Zr-3.5% Sn-0.8% Nb–0.8% Mo-1130 ppm O). The Ultimate Tensile Strength (UTS) for all of the above mentioned materials is similar for the operating range of the Re-Entrant fuel-channel. Tests have shown that the creep rate in Excel is much lower than Zr-2.5Nb, however Zirconium alloys are not suitable for long term exposure to supercritical water unless they are coated to avoid corrosion [**9**]. There is little data for irradiation creep and swelling at the high temperatures associated with the Re-Entrant fuel-channel for all of the above mentioned materials [**6**]. Extensive testing needs to be conducted using all four materials before the design of the Re-Entrant channel is finalized. For the purpose of this work, SS-304 has been chosen as the material of construction of the inner tube, the pressure tube and the outer tube.

The inner tube in the Re-Entrant channel can be made as thin as possible to improve neutron economy as it is not required to bear any significant pressure difference[**9**]. A reference thickness of the inner tube is 2 mm, and a sensitivity analysis on the thickness of the inner tube is performed in Chapter 5. The inner diameter of the pressure tube is calculated to be 127.9 mm. ASME standards require that the design stress of the pressure boundary component be less than 1/3 of the UTS of the material [**9**]. The UTS of SS-304 at 400°C is 448 MPa [**36**]. Analysis in Chapter 5 indicate that the actual temperature of the pressure tube is much lower than 400°C, but the UTS of SS-304 is chosen at this temperature to account for a reasonable safety factor. Thus, the minimum thickness of the pressure tube required to satisfy the ASME standards is 10.71 mm. The reference pressure tube thickness for this work is chosen to be 11 mm.

An insulator is required so that only 1 to 2 % of the thermal energy would be lost to the moderator from the Re-Entrant channel. Two different ceramic insulators are chosen in this work. The first is the ceramic insulator which is used in the HEC channel, so that heat loss comparisons can be made between the two designs. Thus, Porous Yttria

Stabilized Zirconia (with 70% porosity) has been chosen as for the insulation. Unlike the HEC channel, the Re-Entrant channel does not have SCW flowing through the pores of the insulator as the insulator is placed outside the pressure tube. Carbon dioxide (CO_2) gas flows through the pores in the insulator. Similar to current CANDU-type reactors, the moisture content of the CO_2 gas can be analyzed to determine if there is a leak in the pressure tube. Yttria Stabilized Zirconia (YSZ) has a low neutron cross section and low thermal conductivity. Studies have shown that irradiation would not significantly embrittle YSZ at high temperature [**37**]. Porous YSZ, with open pores increases the thermal resistance and improves the thermal shock resistance. The other insulating option selected for the Re-Entrant channel is solid zirconium dioxide (ZrO_2). The solid insulator eliminates the need for the CO_2 gas system. The reference thickness of the insulator is 7 mm and a sensitivity analysis on the insulator thickness can be seen in Chapter 5, along with a detailed comparison of the performance of both insulators selected for use in the Re-Entrant channel. The rear end of the Re-Entrant channel will be insulated in the end shield of the calandria.

The main purpose of the outer tube is to prevent erosion of the ceramic insulator in the moderator. Hence, the outer tube can be as thin as possible to improve neutron economy and the reference thickness of the outer tube is 0.5 mm. Table 3.2 shows the relevant dimensions associated with the Re-Entrant channel and Figure 3.5 shows the cross-sectional view of the channel.

Table 3.2: Reference case Re-Entrant Channel Dimensions

Parameter	Value
Flow tube – Inner Diameter (mm)	103.5
Flow tube – Outer Diameter (mm)	107.5
Pressure tube – ID (mm)	127.9
Pressure tube – OD (mm)	149.9
Ceramic thickness (mm)	7
Outer tube – ID (mm)	163.9
Outer tube – OD (mm)	164.9

Notes: Flow tube, pressure tube, ceramic insulation and outer tube thicknesses may vary as a design option.

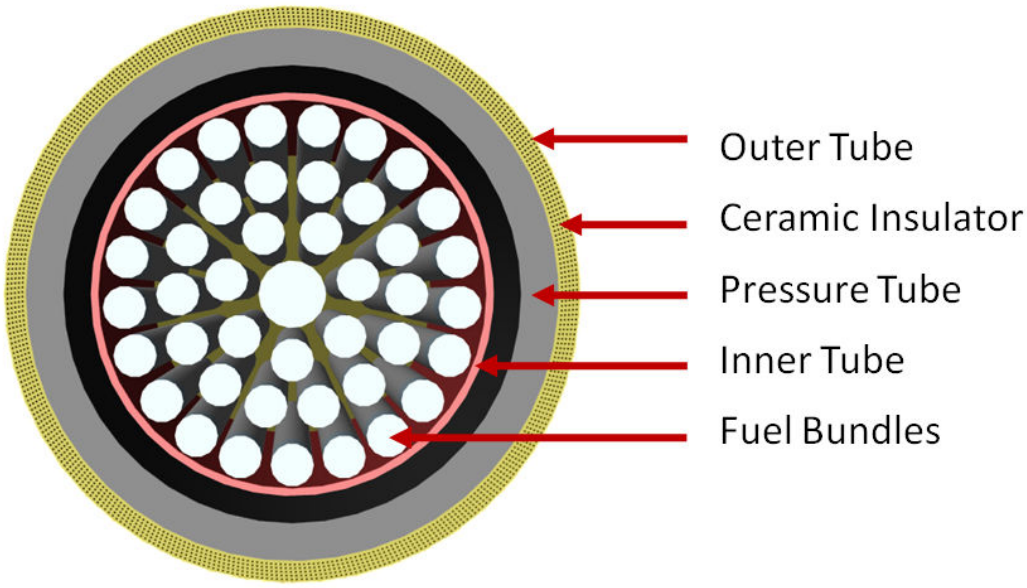

Figure 3.5: Cross sectional view of Re-Entrant channel

Unlike present CANDU reactors, the REC uses the "fuel against flow method" and can only be refuelled from one end. The single-ended refuelling concept was developed for the CANDU-3 and CANDU-80 reactor designs for fuel bundles, and experimentally demonstrated on a full-scale mockup. In single-ended refuelling, a refuelling machine pushes the bundles to the end of the channel, where a bundle stopper is present. This stopper prevents the fuel bundles from sliding during normal operation. Once the bundle has reached the end of a channel, the machine engages a latch at the front end, which keeps the bundles from sliding forward. When the bundles need to be removed from the channel, the refuelling machine disengages the latch, while the force of the coolant pushes the bundles out. For a vertical configuration, a fuel string is used. Refuelling of a vertical channel has been demonstrated for several reactor types as NRU, Gentilly-1 and RBMK.

The main advantage of the Re-Entrant channel is the elimination of the ceramic liner inside the fuel-channel where the pressures and temperatures are considerably higher than the outside of the pressure tube. This means that the ceramic insulator will never come in contact with the coolant, hence avoiding the problem of having eroded ceramic particles in the primary heat transport system. Another advantage of the Re-Entrant channel over the HEC is that if there is an issue with the ceramic in the HEC, the entire fuel-channel assembly needs to be taken apart to examine the ceramic insulator, and this will not be an easy process if the fuel-channel is irradiated. This will not be the case in the Re-Entrant channel as the ceramic liner is outside the pressure tube. The Re-Entrant channel can be used in both the horizontal and vertical channel configurations whereas the HEC is designed for use in the horizontal configuration. The location of the pseudocritical point in the REC could also be an advantage if it occurs in the cold side of the fuel-channel as it's separate from the fuelled region. This may address concerns with deteriorated heat transfer and chemistry control in the pseudocritical region. One possible disadvantage of the Re-Entrant fuel-channel is that the piping and fittings would be congested as the inlet and outlet are at the same side of the channel [**9**]. Another disadvantage of the Re-Entrant channel is that it may lead to bigger calandria vessels to accommodate the larger fuel-channels.

CHAPTER 4

NUMERICAL MODEL OF RE-ENTRANT FUEL-CHANNEL

This chapter discusses the fundamental theory and how it is applied to develop a numerical model that represents the proposed fuel-channel.

4.1 Fundamental Equations

Fourier's law states that for one-dimensional steady-state conduction in a plane wall with no heat generation and constant thermal conductivity, the temperature varies linearly with the thickness, x, as shown in Equation (4.1) below:

$$q = -kA\frac{dT}{dx} \tag{4.1}$$

where k is the thermal conductivity and A is the cross-sectional surface area [**38**].

Newton's law of cooling is used to find the heat transfer through convection and is shown in Equation (4.2) [**38**].

$$q = hA\Delta T \tag{4.2}$$

where h is called the convective heat-transfer coefficient.

The conservation of mass relation for a two-dimensional steady flow of a fluid is given by Equation (4.3) [**39**].

$$\frac{\partial u}{\partial x} + \frac{\partial v}{\partial y} = 0 \tag{4.3}$$

where the x-component of the velocity is u and the y-component is v.

The conservation of momentum in the x-direction or the x-momentum equation is given by Equation (4.4) [**39**].

$$\rho\left(u\frac{\partial u}{\partial x}+v\frac{\partial u}{\partial y}\right)=\mu\frac{\partial^2 u}{\partial y^2}-\frac{\partial P}{\partial x} \tag{4.4}$$

where ρ is the density of the fluid, μ is the dynamic viscosity and P is the pressure.

During a steady-flow process, the total energy content of a control volume remains constant, and the amount of energy entering a control volume in all forms equals the amount of energy leaving it. This implies that the net energy convected by a fluid out of a control volume is equal to the net energy transferred into the control volume by heat conduction and the energy equation for a two-dimensional steady flow of a fluid with constant properties is given by Equation (4.5) [**39**].

$$\rho C_p\left(u\frac{\partial T}{\partial x}+v\frac{\partial T}{\partial y}\right)=k\left(\frac{\partial^2 T}{\partial x^2}+\frac{\partial^2 T}{\partial y^2}\right) \tag{4.5}$$

where C_p is the specific heat. The above equations can be written in a nondimensionalized form that can be used to derive the Nusselt number (Nu), which represents the enhancement of heat transfer through a fluid layer as a result of convection relative to conduction. The Nusselt number is referred to as the dimensionless heat transfer coefficient and can be expressed in terms of the Reynolds number (Re) and Prandtl number (Pr) and hence Equation (2.7) can be used along with Equation (4.2) to find the heat transfer through a fluid.

4.2 Flow Area, Wetted Perimeter, Hydraulic Diameter

Since the diameters of the elements in the bundles are known, the cross-sectional area of the fuel bundle can be calculated using Equation (4.6).

$$\mathrm{A}_{c_B} = \frac{\pi}{4}\left[\left(\mathrm{D}_{CE}\right)^2 + 42\left(\mathrm{D}_E\right)^2\right]; [m^2] \tag{4.6}$$

The cross-sectional area of the flow tube can be found using Equation (4.7). The difference between the cross-sectional area of the flow tube and the bundles gives the flow area of the inner tube as seen in Equation (4.8).

$$\mathrm{A}_{c_{IT}} = \frac{\pi}{4}\left[\left(\mathrm{D}_{i_{IT}}\right)^2\right]; [m^2] \tag{4.7}$$

$$\mathrm{A}_f = \mathrm{A}_{c_{IT}} - \mathrm{A}_{c_B}; [m^2]$$

$$\mathrm{A}_f = \frac{\pi}{4}\left[\left(\mathrm{D}_{CE}\right)^2 + 42 \times \left(\mathrm{D}_E\right)^2 - \left(\mathrm{D}_{i_{IT}}\right)^2\right]; [m^2] \tag{4.8}$$

The hydraulic diameter of the inner tube can be calculated using the following equation:

$$\mathrm{D}_{hy_{FT}} = 4\frac{A_f}{P_{wet}}; [m] \tag{4.9}$$

where the wetted perimeter (P_{wet}) can be calculated using Equation (4.10).

$$\mathrm{P}_{wet} = \pi\left[\left(\mathrm{D}_{CE}\right) + 42 \times \left(\mathrm{D}_E\right) + \mathrm{D}_{i_{IT}}\right]; [m] \tag{4.10}$$

The flow area of the annulus is given by:

$$A_{f_A} = \frac{\pi}{4}\left(D_{i_{PT}}{}^{2} - D_{o_{OT}}{}^{2}\right) ; [m^2] \tag{4.11}$$

The hydraulic diameter of the annulus can be found using Equation (4.12).

$$D_{hy_A} = \frac{4\frac{\pi}{4}\left(D_{i_{PT}}{}^{2} - D_{o_{IT}}{}^{2}\right)}{\pi D_{i_{PT}} + \pi D_{o_{IT}}} ; [m]$$

$$D_{hy_A} = D_{i_{PT}} - D_{o_{IT}} ; [m] \tag{4.12}$$

The mass fluxes of the inner tube and the annulus can be calculated by using Equation (4.13) and Equation (4.14) respectively.

$$G_{IT} = \frac{\dot{m}}{A_f} ; \left[\frac{kg}{m^2 s}\right] \tag{4.13}$$

$$G_A = \frac{\dot{m}}{A_{f_A}} ; \left[\frac{kg}{m^2 s}\right] \tag{4.14}$$

Table 4.1: Reference case Re-Entrant Channel Parameters

Parameter	Value
Wetter perimeter of Variant-18 bundle (m)	1.5174
Cross-sectional fuelled area of bundle (m^2)	0.0046
Cross-sectional flow area of inner tube (m^2)	0.0084
Wetted perimeter of inner tube (m)	1.8989
Hydraulic diameter of inner tube (m)	0.0080
Mass flux of inner tube (kg/m^2s)	1153.6
Flow area of annulus (cold side) (m^2)	0.0038
Hydraulic diameter of annulus (cold side) (m)	0.0205
Mass flux of annulus (cold side) (kg/m^2s)	1153.6

4.3 Nodalization

To apply the heat balance model using the fundamental equations in Section 4.1, the fuel-channel needs to be divided into several nodes. The pressure is assumed to be constant in this model at 25 MPa. For the purpose of this work, the Re-Entrant channel was divided into 121 nodes; 60 for the cold side, 60 for the hot side and one for the re-entrant mixing node which is the region where the coolant from the annulus changes direction and flows in the inner tube. The coolant inlet temperature boundary condition is a temperature of 350°C and the coolant outlet temperature is initially assumed to be 625°C. The temperature of the mixing node is initially assumed to be 400°C. Figure 4.1 shows the nodes in the Re-Entrant fuel-channel along with the initial estimates of the coolant exit temperature and the mixing node.

4.4 Initial Estimate of Temperature profiles for Hot and Cold Side

With the three temperatures shown in Figure 4.1, the temperature profile for the coolant for the Re-Entrant fuel-channel can initially be assumed to be linear.

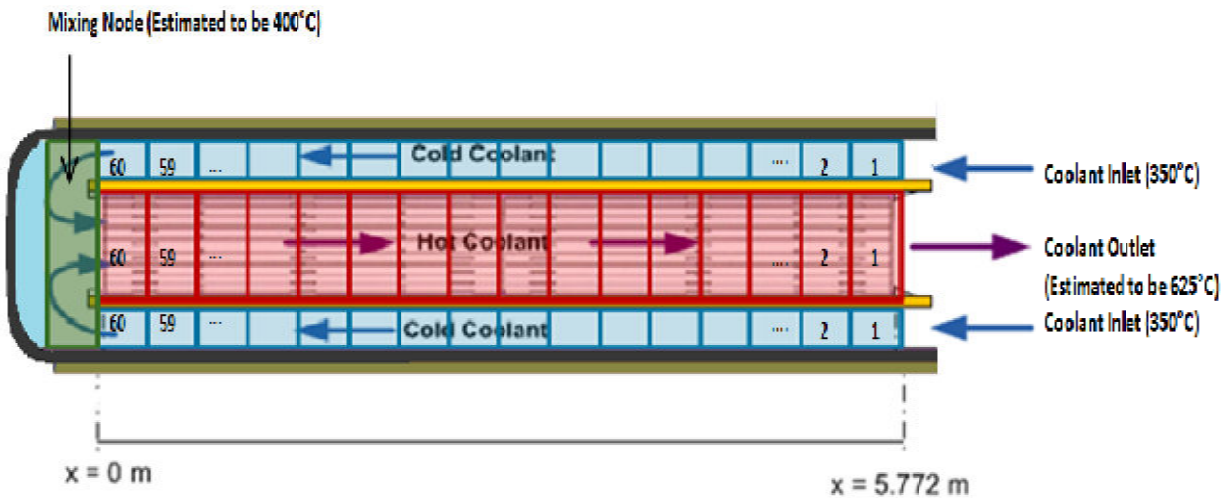

Figure 4.1: Re-Entrant flow channel showing nodes and initial temperature estimates

4.5 Initial Estimate of Temperature of Fuel Sheath

The temperature of the fuel sheath in each node is initially assumed to be 300°C higher than the temperature of the hot coolant. Since the pressure at the node is known, the bulk fluid enthalpy of the coolant, enthalpy of the coolant at the wall, i.e. fuel sheath, density of the bulk fluid, and the density of the coolant at the wall, can be obtained using NIST REFPROP, along with the thermal conductivity and viscosity of the coolant in the hot side.

As the wall temperature of the outer sheath is much higher than the coolant in the hot side, the average specific heat and average Prandtl numbers are used to calculate the flow parameters of the hot coolant as they account for the difference in temperature. The average specific heat and the average Prandtl number for each node in the hot side can be calculated using the following equations:

$$\bar{C}_p = \frac{H_w - H_b}{T_w - T_b} ; \left[\frac{J}{kg \cdot K}\right] \tag{4.15}$$

$$\overline{\mathbf{Pr}} = \frac{\mu_{hs} \cdot \bar{C}_p}{k_{hs}} \tag{4.16}$$

Equation (4.17) below is used to calculate the Reynolds number of the coolant in the hot side.

$$\mathbf{Re} = G \cdot \frac{\mathrm{D}_{hy_{FT}}}{\mu_{hs}} \tag{4.17}$$

With the above equations for the Reynolds and Prandtl numbers, the Nusselt number can be calculated using Equation (2.7). The convection heat transfer coefficient can be calculated using Equation (4.18).

$$h_{hs} = \mathbf{Nu}_D \frac{k_{hs}}{\mathrm{D}_{hy_{FT}}} \; ; \left[\frac{W}{m^2 \cdot K}\right] \tag{4.18}$$

The fuel sheath temperature is calculated using the equation below [**28**]:

$$T_{fs} = \frac{q}{h_{hs}} + T_{hs} \; ; [°C] \tag{4.19}$$

Since the fuel sheath temperature was first estimated to be 300°C higher than the hot coolant and the above equation calculates the temperature of the fuel sheath based on that estimate, the above process is repeated until the value of one iteration and the value of the previous iteration are within 0.1°C of each other to determine the actual estimate of the fuel sheath temperature.

4.6 Thermal Resistances

The thermal resistance of the hot fluid can be calculated using Equation (4.20).

$$R_{hs} = \frac{1}{h_{hs} A_{FT}} \; ; \left[\frac{°C}{W}\right] \tag{4.20}$$

Equation (4.21) can be used to calculate the thermal resistances of the flow tube, the pressure tube, and the outer tube.

$$R_{\,tube} = \frac{\ln\left(\frac{r_o}{r_i}\right)}{2\pi L k} \; ; \left[\frac{°C}{W}\right] \tag{4.21}$$

The thermal conductivity of SS-304 is calculated using Equation (4.22) [**40**].

$$k_{SS-304} = 2.0 \cdot 10^{-6} {T_s}^2 + 0.0134\, T_s + 10.689 \; ; \left[\frac{W}{m^2 \cdot K}\right] \tag{4.22}$$

The heat transfer coefficient for the cold side can be calculated using Equations (4.15) to (4.18) by using the appropriate thermophysical properties for the cold side, which can be obtained from NIST REFPROP. Once the heat transfer coefficient for the cold side is known, the thermal resistance for the cold fluid can be calculated using the following equation:

$$R_{cs} = \frac{1}{h_{cs}A_{PT}}\,;\left[\frac{°C}{W}\right] \tag{4.23}$$

A rough upper-bound estimate of the thermal conductivity of Porous YSZ (70% porosity) is given by Equation (4.24) [**9**].

$$k_{YSZ} = 0.3\ \mathrm{k}_{ZrO_2} + 0.7\ k_{CO_2};\left[\frac{W}{m^2 \cdot K}\right] \tag{4.24}$$

The average thermal conductivity of ZrO_2 is 2.7 $(W/m \cdot K)$ in the temperature range of this analysis. The thermal conductivity of carbon dioxide is a function of temperature and the thermal conductivity of the Porous YSZ insulation with CO_2 is shown in Figure 4.2.

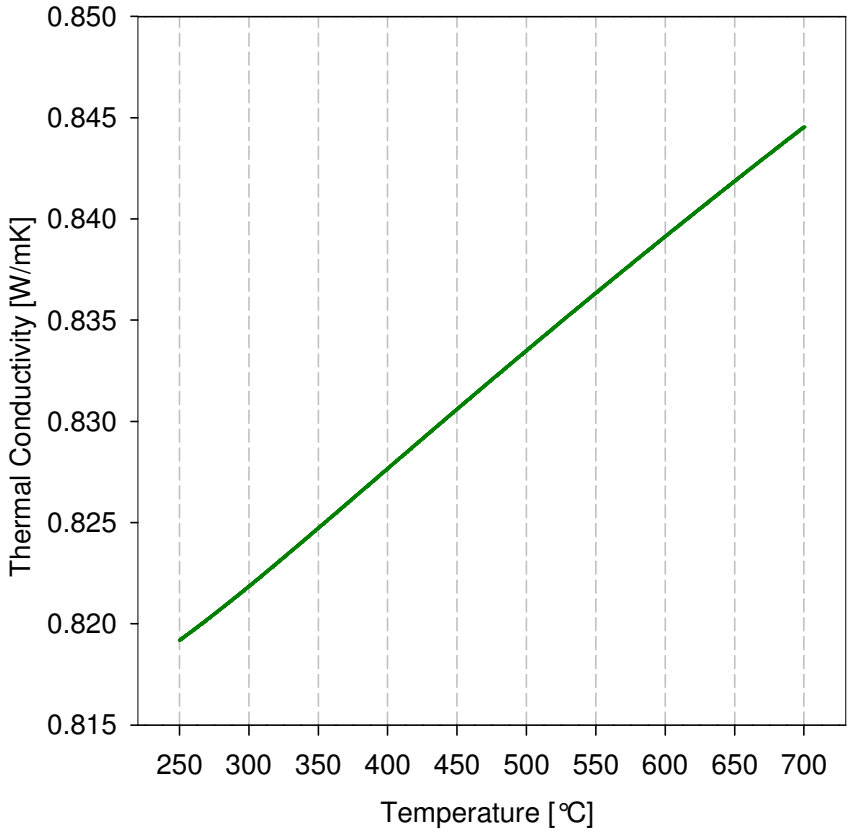

Figure 4.2: Thermal Conductivity of Porous YSZ

4.7 Heat Transferred from Hot Side to Cold Side and Heat Loss to Moderator from Cold Side

When the reactor is under normal operation, heat loss from the channel to the moderator is assumed to be via mixed forced and free convection. This is because the Rayleigh number from free convection is high enough, that the thermal buoyancy cannot be ignored. An empirical combining rule shown in Equation (4.25) is used to calculate the Nusselt number for mixed flow [**41**].

$$\mathbf{Nu}_{total} = \left[\left(\mathbf{Nu}_{forced}\right)^3 + \left(\mathbf{Nu}_{free}\right)^3\right]^{1/3} \tag{4.25}$$

where $\mathbf{Nu}_{forced}$ is the Nusselt number for forced convection, $\mathbf{Nu}_{free}$ is the Nusselt number for free convection and $\mathbf{Nu}_{total}$ is the Nusselt number for mixed flow. The Nusselt number for forced convection is a function of Reynolds number and Prandtl number and is given by the Churchill and Bernstein correlation [**42**].

$$\mathbf{Nu}_{forced} = 0.30 + \frac{0.62\mathbf{Re}^{1/2}\mathbf{Pr}^{1/3}}{\left[1+(0.4/\mathbf{Pr})^{2/3}\right]^{1/4}}\left[1 + \left(\frac{\mathbf{Re}}{282{,}000}\right)^{5/8}\right]^{4/5} \tag{4.26}$$

The above equation is valid for $10^2 < Re < 10^7$. However, it underpredicts the data in the midrange of Reynolds numbers between 20000 and 400000 and Equation (4.27) is used instead in that range [**42**].

$$\mathbf{Nu}_{forced} = 0.30 + \frac{0.62\mathbf{Re}^{1/2}\mathbf{Pr}^{1/3}}{\left[1+(0.4/\mathbf{Pr})^{2/3}\right]^{1/4}}\left[1 + \left(\frac{\mathbf{Re}}{282{,}000}\right)^{1/2}\right] \tag{4.27}$$

The Nusselt number for free convection can be calculated using the Churchill and Chu correlation [**43**]:

$$\mathbf{Nu}_{free} = \left\{ 0.60 + \frac{0.386\mathbf{Ra}_D{}^{1/6}}{\left[1+\left(\frac{0.559}{\mathbf{Pr}}\right)^{9/16}\right]^{8/27}} \right\}^2 \tag{4.28}$$

The Rayleigh number can be calculated using Equation (4.29) [**28**].

$$\mathbf{Ra}_D = \frac{g\beta(T_i - T_o)D^3}{\nu\alpha} \tag{4.29}$$

Once the temperature of the coolant at each node is known, and the total thermal resistances of the fuel-channel components are calculated, the heat loss to the moderator and the heat transferred from the hot side to the cold side can be calculated using:

$$q = \frac{\Delta T}{R_{total}} \; ; [W] \tag{4.30}$$

$$q = \frac{T_{os} - T_{mod}}{R_{hot\ side} + R_{flow\ tube} + R_{cold\ side} + R_{pressure\ tube} + R_{insulator} + R_{outer\ tube} + R_{mod}} ; [W] \tag{4.31}$$

$$q = \frac{T_{os} - T_{mod}}{\left(\frac{1}{hA}\right)_{hs} + \left(\frac{\ln\left(\frac{r_o}{r_i}\right)}{2\pi Lk}\right)_{FT} + \left(\frac{1}{hA}\right)_{cs} + \left(\frac{\ln\left(\frac{r_o}{r_i}\right)}{2\pi Lk}\right)_{PT} + \left(\frac{\ln\left(\frac{r_o}{r_i}\right)}{2\pi Lk}\right)_{ins} + \left(\frac{\ln\left(\frac{r_o}{r_i}\right)}{2\pi Lk}\right)_{OT} + \left(\frac{1}{hA}\right)_{mod}} ; [W] \tag{4.32}$$

4.8 Actual Temperature Profile of Cold Side, Hot Side & Fuel Sheath

The net heat loss is the difference between the heat transferred to the cold side from the hot side and the heat loss to the moderator. Since the pressure and temperature of the first node for the cold side is known, the enthalpy of Node 1 can be obtained from NIST REFPROP. Equation (4.33) can be used to calculate the enthalpy of the next node.

$$H_{n,i+1\,(cold)} = H_{n,i} + \frac{q_{net(i)}}{\dot{m}} \; ; \left[\frac{J}{kg}\right] \tag{4.33}$$

The above equation is slightly modified to calculate the enthalpy of the hot side to account for different power profiles.

$$H_{n,i+1\,(hot)} = H_{m,i} + \frac{Q_{node} \cdot p \cdot \Delta x}{\dot{m}} \; ; \left[\frac{J}{kg}\right] \tag{4.34}$$

Once the enthalpies for the hot and cold sides are calculated at each node, the temperature profiles for the coolant can be obtained from NIST REFPORP. With the actual temperature profile of the hot side, Equations (4.15) to (4.19) can be used to calculate the actual temperatures of the fuel sheath.

4.9 Surface Temperatures of Tubes

Equation (4.30) can also be used to calculate the inner and outer surfaces temperatures of the inner, pressure and outer tubes.

4.10 MATLAB code

A numerical model was developed using the equations shown above and a program was written in MATLAB to calculate the heat-transfer characteristics of the Re-Entrant fuel-channel. Figure 4.3 is a flow chart that highlights the main steps in the code, which is shown in Appendix A.

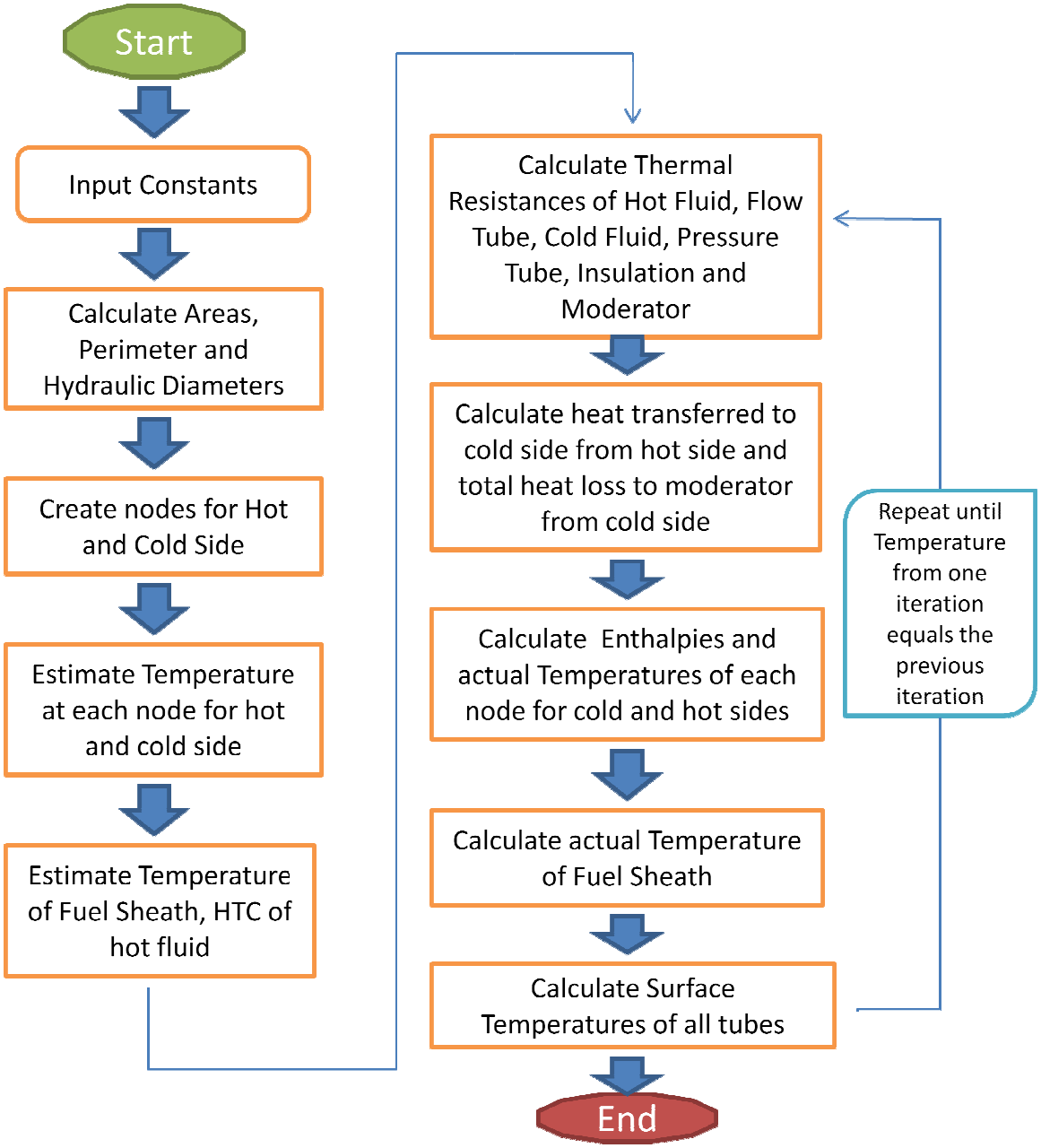

Figure 4.3: Flow chart representing Numerical Model in MATLAB

CHAPTER 5

HEAT TRANSFER ANALYSIS

Numerical analysis was done for several different parameters to study their effect on heat transfer. The objective is to determine the sensitivity of the design to the tube thickness, and material choice by using the thermal conductivity. The effect of the insulator design on heat loss and the impact of variable heat flux profiles are considered. The impact of the location of the pseudocritical point and the location of peak fuel sheath temperature is assessed in each case.

5.1 Reference Case: No Heat Loss to the Moderator

Heat-transfer analysis was performed on the Re-Entrant channel assuming no heat loss to the moderator. This case is ideal from the heat loss perspective and will result in the highest fuel temperature and highest coolant temperature. The fuel-channel power, the thickness of the flow tube, and the flow-tube thermal conductivity were varied for this analysis, while heat flux was assumed to be constant. The coolant enters the cold side of the Re-Entrant channel at x = 5.772 m, and enters the hot side at x = 0 m, as shown in Figure 4.1.

Figure 5.1 shows the axial temperature profiles of the coolant, the inner and outer surfaces of the flow tube and the outer fuel sheath along the heated length of the channel for a channel power of 8.5 MW_{th}, a coolant inlet temperature of 350°C, a mass flow rate of 4.37 kg/s, and uniform heat flux. The pressure tube is not included in the analysis and no heat transfer from the cold coolant side to the pressure tube is allowed. The temperature of the coolant on the cold side increases approximately linearly, as expected, as the heat source is the outer wall of the flow tube. The coolant temperature on the hot side increases slowly at first and then dramatically after approximately 2 m of fuelled length. The main reason for this, as will be seen in later figures, is the transition of the

coolant through the pseudocritical point. The pseudocritical temperature for light water at 25 MPa is 384.9°C. The outer-sheath temperature increases at first, decreases and then increases again. This behaviour is expected for a uniform heat flux and constant mass flux as there is a significant improvement in heat transfer as the coolant passes through the pseudocritical point [**44**]. The outer sheath temperature is below the design limit of 850°C. This case will be used as the reference case for the remainder of the analysis.

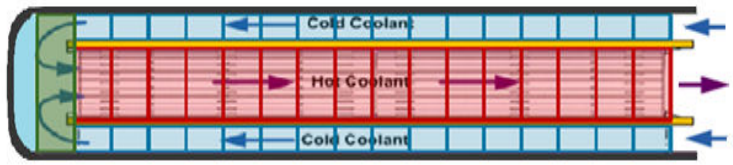

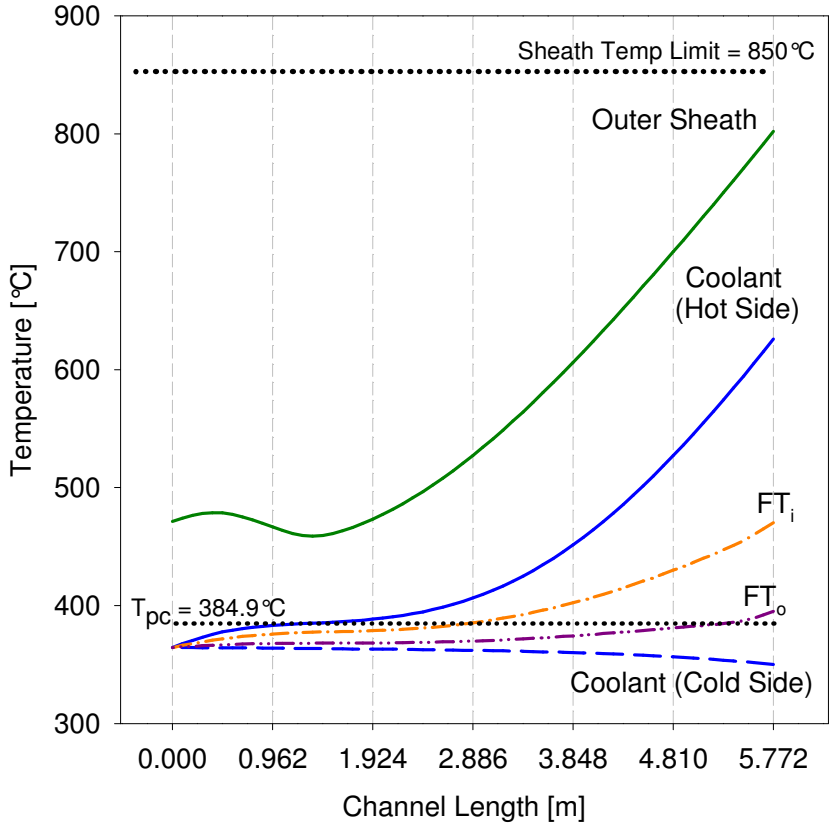

Figure 5.1: Axial temperature profile along the fuelled channel length for a channel power of 8.5 MW_{th}, inner-tube thickness of 2 mm, inlet temperature of 350°C, mass flow rate of 4.37 kg/s and uniform heat flux

The location of the pseudocritical point in the channel can be identified by the peak in the specific heat profile for the coolant as shown in Figure 5.2. Thermophysical properties such as thermal conductivity, Prandtl number, and specific heat drastically change within the pseudocritical region, as seen in Figure 5.2. These changes result in the variation in slopes of the coolant temperature and outer sheath temperature profiles at these locations in Figure 5.1. The thermophysical properties shown in Figure 5.2 are calculated using the bulk-fluid temperature along the channel. The thermal conductivity of the coolant decreases slightly along the cold side of the channel. Once the coolant enters the hot side, the thermal conductivity decreases significantly due to the higher bulk fluid temperatures of the coolant, before being almost constant just before the pseudocritical point. The thermal conductivity decreases drastically once the coolant becomes supercritical. The specific heat and Prandtl number profiles slightly increase as the coolant passes thought the cold side of the fuel-channel. As the coolant enters the fuelled region, the profiles increase drastically up to the pseudocritical point when the coolant enters the fuelled region due to higher bulk fluid temperatures, and then decrease until to the end of the hot side of the fuel-channel.

The average Prandtl number and average specific heat from Equations 4.15 and 4.16 were calculated using the bulk-fluid and wall temperatures and the resulting profiles are shown in Figure 5.3. The heat transfer coefficient profile which is calculated using Equation 4.13 is also shown in Figure 5.3 along with the heat flux for the hot side. The average specific heat is the ratio between the difference in the enthalpies of the coolant at the wall temperature and the bulk fluid temperature to the difference in the temperature of the coolant at the wall and the bulk fluid temperature. As the coolant enters the fuelled region, there is an increase in the wall temperature of the fuel sheath and the enthalpy of the coolant at the wall. This accounts for the significant increase in the specific heat profile at the entrance of the hot side. The average Prandtl number is directly proportional to the average specific heat. Thus, there is also a significant increase in the average Prandtl number profile.

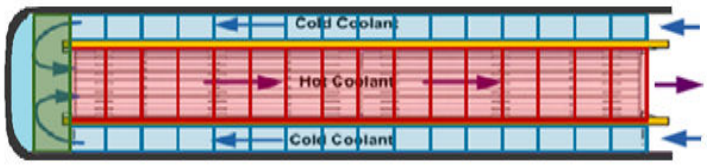

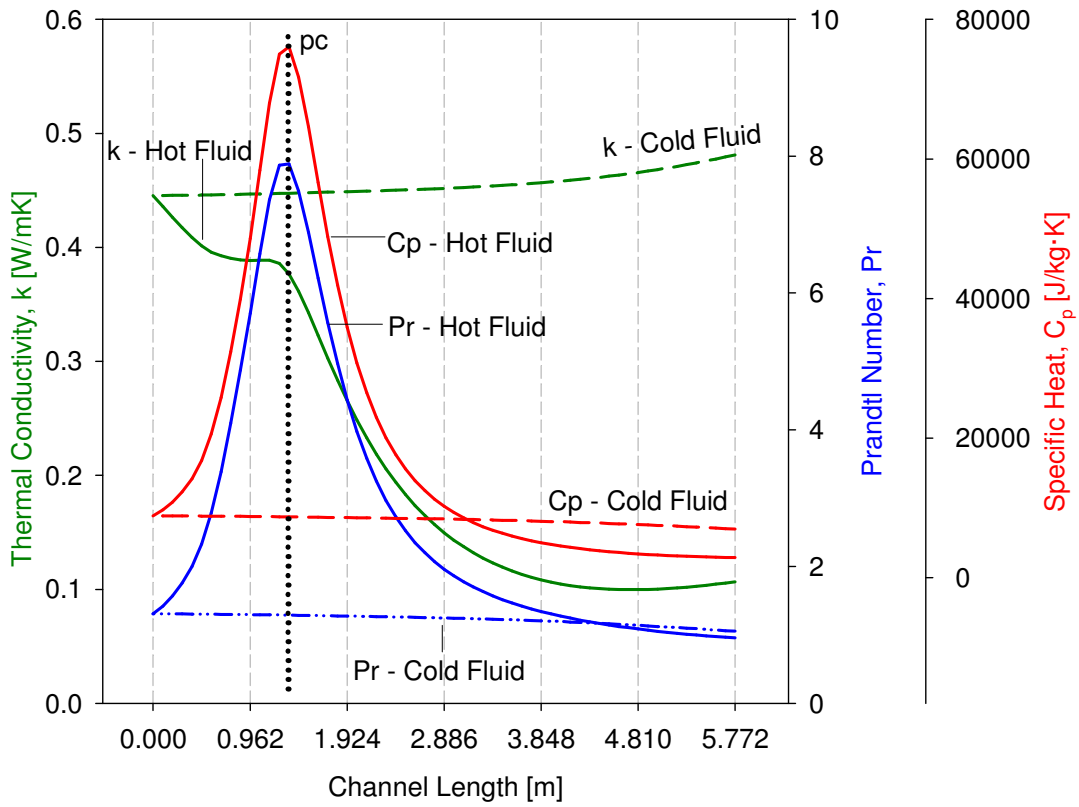

Figure 5.2: Specific heat, thermal conductivity and Prandtl number profiles along the fuel-channel for a channel power of 8.5 MW_{th}, inner-tube thickness of 2 mm, inlet temperature of 350°C, mass flow rate of 4.37 kg/s and uniform heat flux

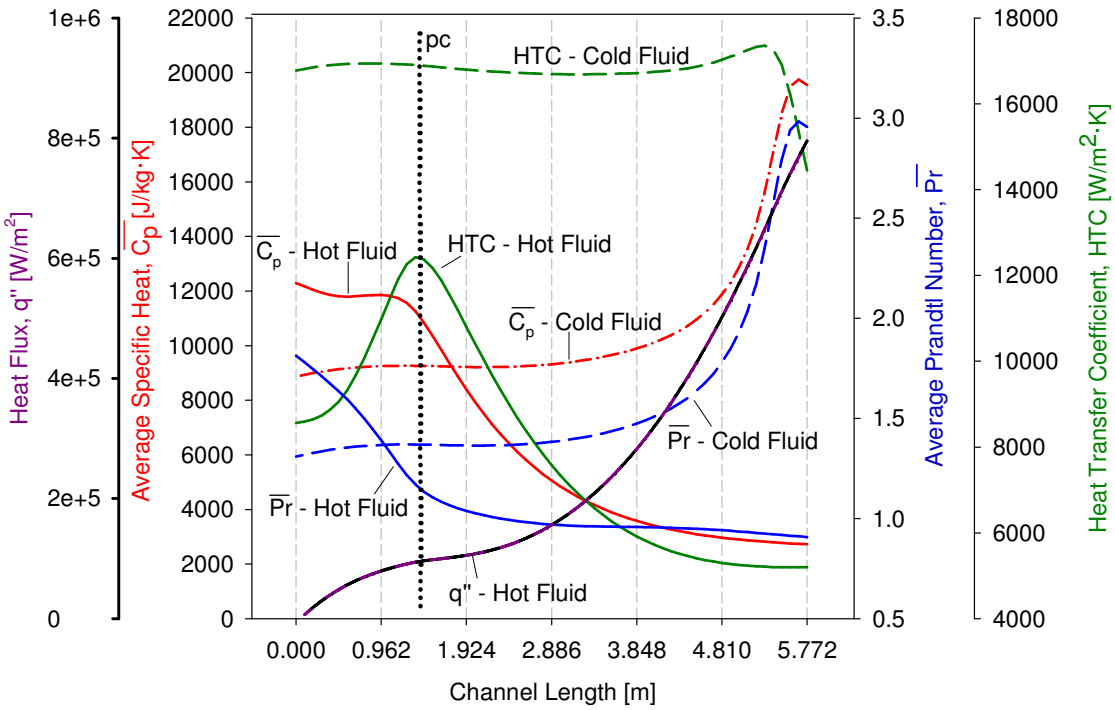

Figure 5.3: Average specific heat, average Prandtl number, Heat Flux and HTC profiles along the fuel-channel for a channel power of 8.5 MW_{th}, inner-tube thickness of 2 mm, inlet temperature of 350°C, mass flow rate of 4.37 kg/s and uniform heat flux

Not all fuel-channels have the same power in the core. Refuelling and balancing the neutron flux are two instances where fuel-channel power is varied among the fuel-channels in the core. The effect of power on the outer sheath temperature profile is shown in Figure 5.4. As expected, the maximum outer sheath temperature at the outlet of the fuelled region (hot side) increases with increasing power. This also means the coolant will reach the pseudocritical region earlier along the axial length of the channel with increasing power. Thus, the pseudocritical point shifts along the channel from the outlet towards the inlet with increasing channel power as shown in Figure 5.4.

As there is no pressure boundary requirement for the flow tube, the thickness of the flow tube is dominated by heat transfer characteristics and physical strength. The reference flow tube thickness for this analysis was chosen to be 2 mm. As this work only consisted of a heat transfer analysis, the flow tube thickness might change once a detailed analysis on the physical strength of the REC is performed. A sensitivity analysis for variable thickness of the flow tube was performed and Figure 5.5 shows the variation of the outer-sheath temperature for flow tube thicknesses of 2 mm, 3 mm and 5 mm. Thicker tubes reduce neutron economy, but they may reduce the heat transfer characteristics of the hot fluid. However, there is a very slight difference in the outer sheath temperature for all three cases as seen in Figure 5.5. This suggests that the heat transfer is not significantly affected by the thickness of the inner flow tube, and thus, the thickness of the inner flow tube can be determined by neutron economy.

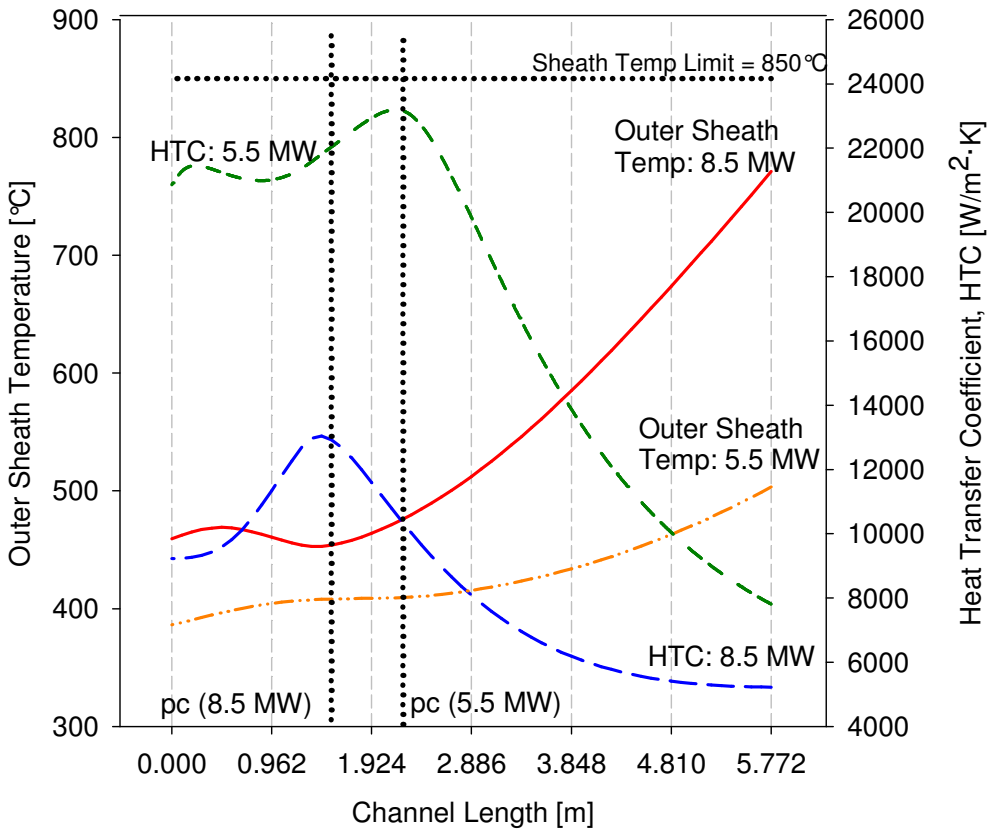

Figure 5.4: Outer-sheath-temperature profile along the channel length for powers of 8.5 MW_{th} and 5.5 MW_{th}, inner-tube thickness of 2 mm, inlet temperature of 350°C, mass flow rate of 4.37 kg/s and uniform heat flux

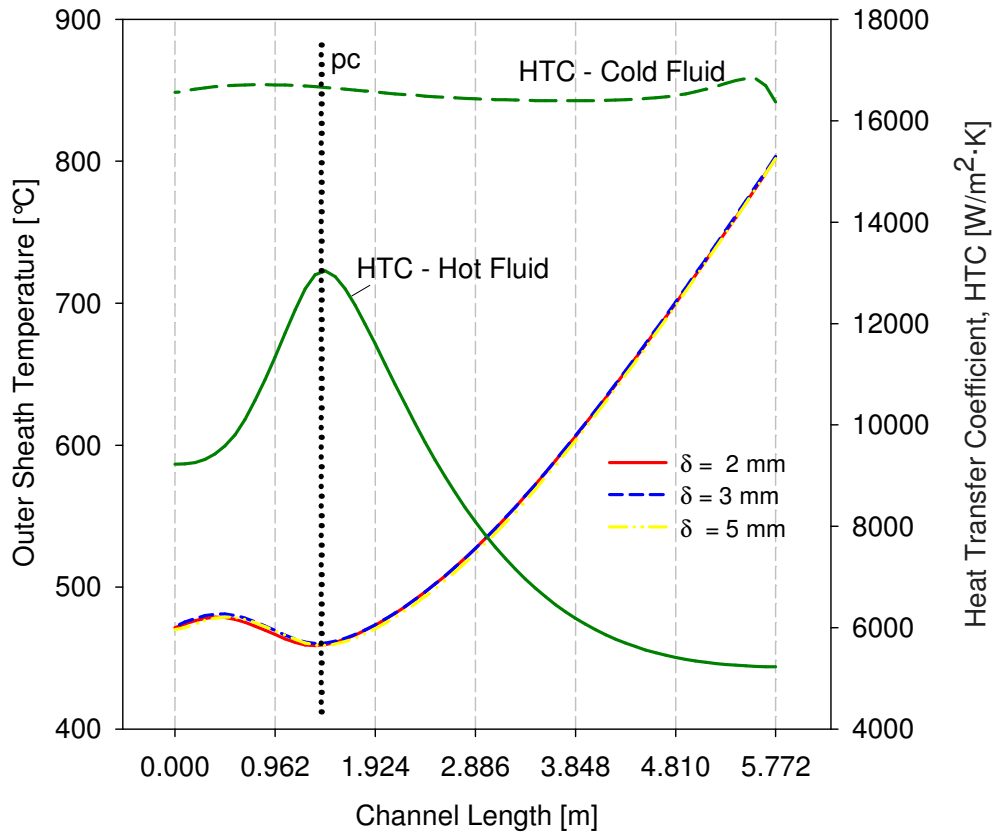

Figure 5.5: Outer-sheath temperature profiles with variable flow-tube thickness, inlet temperature of 350°C, mass flow rate of 4.37 kg/s and uniform heat flux

The thermal resistance of the inner tube is inversely proportional to the thermal conductivity of the material of construction, and directly proportional to the change in temperature across the inner tube. The higher the thermal conductivity of the inner tube, the larger the temperature difference across the inner tube. This also means that more heat will be transferred from the hot side to the cold annulus. Figure 5.6 shows the change in temperature across the inner tube with various wall thermal conductivities. The figure indicates that the wall thermal conductivity will be an important consideration for the flow as it will define the heat transfer to the cold annulus of the flow channel.

Changing the inner tube material does not have the same effect on the outer sheath temperature as it does on the temperature difference across the inner tube. The change in the outer-sheath temperature for various wall thermal conductivities is nearly constant when the reference conductivity is multiplied by a factor of 0.5 and 2 as shown in Figure 5.7. The results indicate that the heat transfer characteristics of the flow tube will not significantly affect the ability to cool of the fuel. The main reason for this is that heat loss to the cold annulus is low, and also, the cold annulus is essentially acting as a fluid preheater, and the lost heat is recovered.

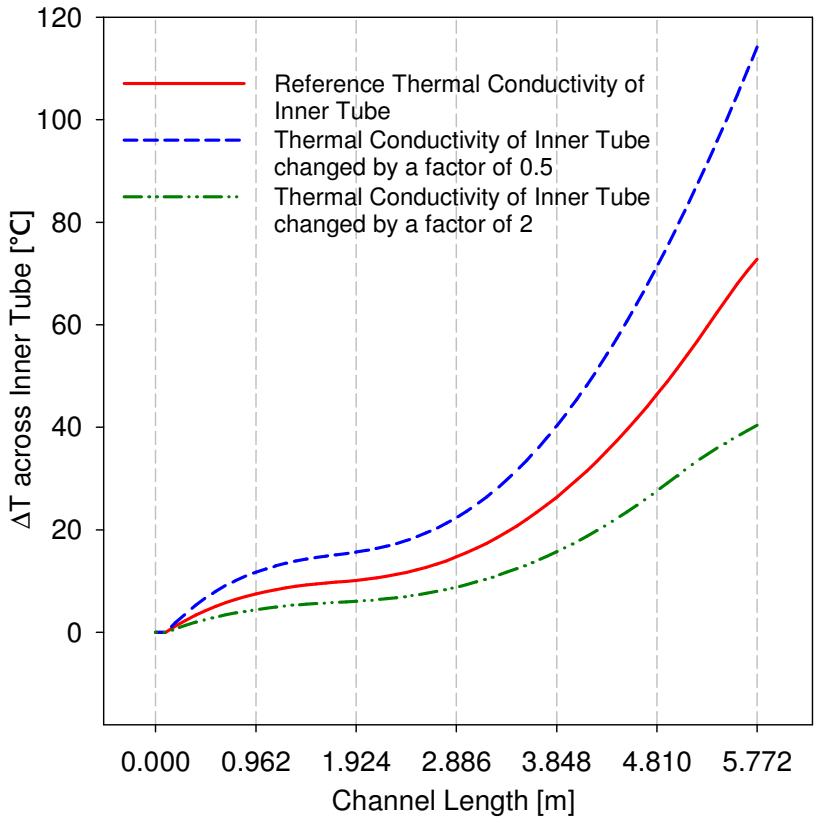

Figure 5.6: Change in temperature across the flow tube for different wall thermal conductivities, inner-tube thickness of 2 mm, inlet temperature of 350°C, mass flow rate of 4.37 kg/s and uniform heat flux

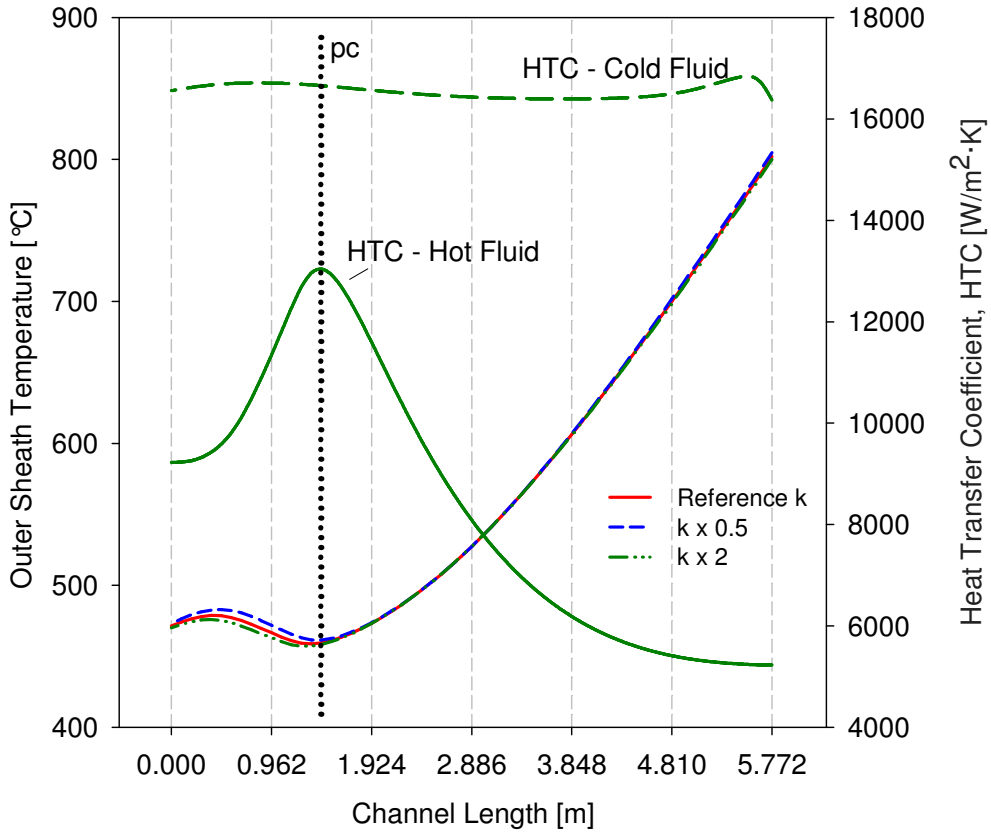

Figure 5.7: Temperature Profile of Outer Sheath Temperature for variable wall thermal conductivity, inner-tube thickness of 2 mm, inlet temperature of 350°C, mass flow rate of 4.37 kg/s and uniform heat flux

The heat-transfer analysis performed for the reference Re-Entrant channel assumes no heat loss to the moderator. The temperature profiles of the coolant, outer sheath, inner surface of the flow tube and outer surface of the flow tube were estimated at different operating conditions. The temperature profiles of the coolant in the hot side and of the outer sheath change considerably within the pseudocritical region. The pseudocritical point occurs close to the entrance of the coolant into the flow tube, approximately near fuel bundle #3 for the reference case. The location of the pseudocritical point changes with channel power as expected, but is not significantly affected by the wall thickness of the inner tube or the thermal conductivity of the inner tube. Note that with significant overpower, it may be possible for the pseudocritical point to move to a region upstream of the fuelled length as seen in Figure 5.8 when the channel power is 10 MW. For this case, the location of the pseudocritical moves from x = 1.54 m to x = 1.2506 m. This shows that at 10 MW_{th}, the pseudocritical point is still in the hot side of the fuel-channel. However, the outer sheath temperature is much higher than the sheath temperature limit indicating that the outer sheath may melt. The coolant exit temperature also is over 100°C higher than the desired exit temperature of 625°C.

In reality, there are heat losses to the moderator from the cold side of the Re-Entrant channel as the thermal conductivity of SS-304 cannot be zero. These losses are examined in detail in Section 5.2

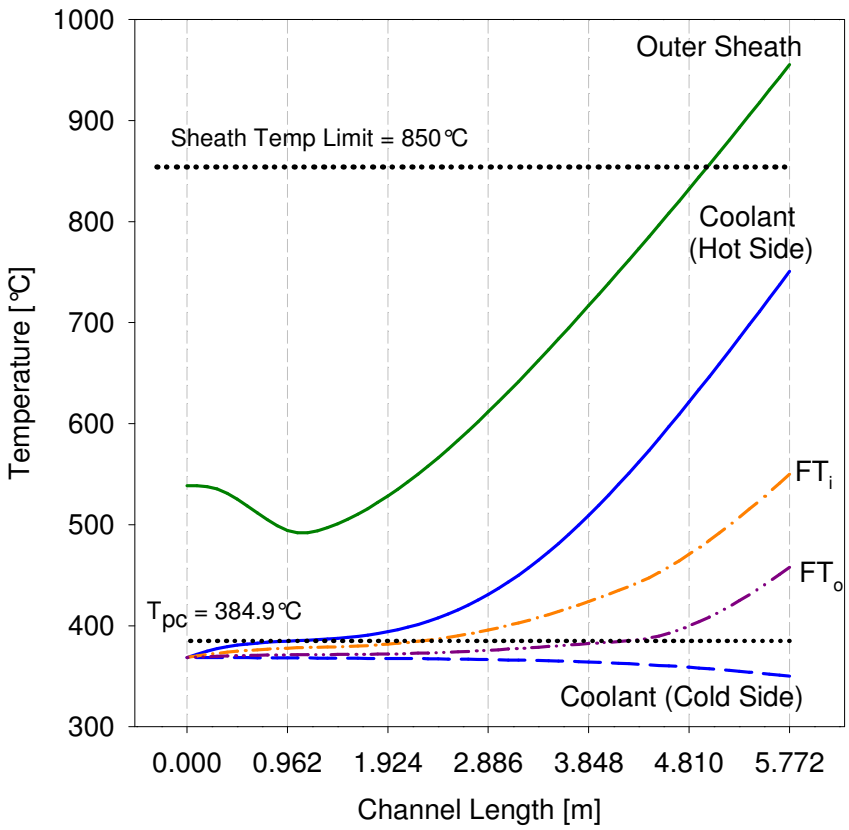

Figure 5.8: Axial temperature profile along the fuelled channel length for a channel power of 10 MW_{th}, inner-tube thickness of 2 mm, inlet temperature of 350°C, mass flow rate of 4.37 kg/s and uniform heat flux

5.2 Heat Loss to the Moderator

This section discusses heat loss to the moderator for both cases of no insulation and with insulation.

5.2.1 Non-insulated Re-Entrant channel

Heat loss to the moderator was calculated for a non-insulated Re-Entrant channel. For consistency with earlier work, Variant-18 bundles are used for the heat transfer analysis. The moderator was assumed to have a bulk fluid temperature of 80°C and a pressure of 200 kPa, based upon current moderator types. Moderator properties were calculated at 100°C to be more representative of fluid conditions at the wall. Heat transfer to the moderator was assumed to be via free convection.

Figure 5.9 shows the axial temperature profiles of the coolant, the inner and outer surfaces of the flow and pressure tube and the outer sheath along the heated length of the channel, for a channel power of 8.5 MW_{th}, inner-tube thickness of 2 mm, pressure tube thickness of 11 mm and mass flow rate of 4.27 kg/s. The outer sheath temperature is below the sheath temperature limit, but the outlet temperature of the hot side is only 550 °C. The temperature difference between the outer surface of the pressure tube and the moderator indicates that the moderator boils when no insulation is present.

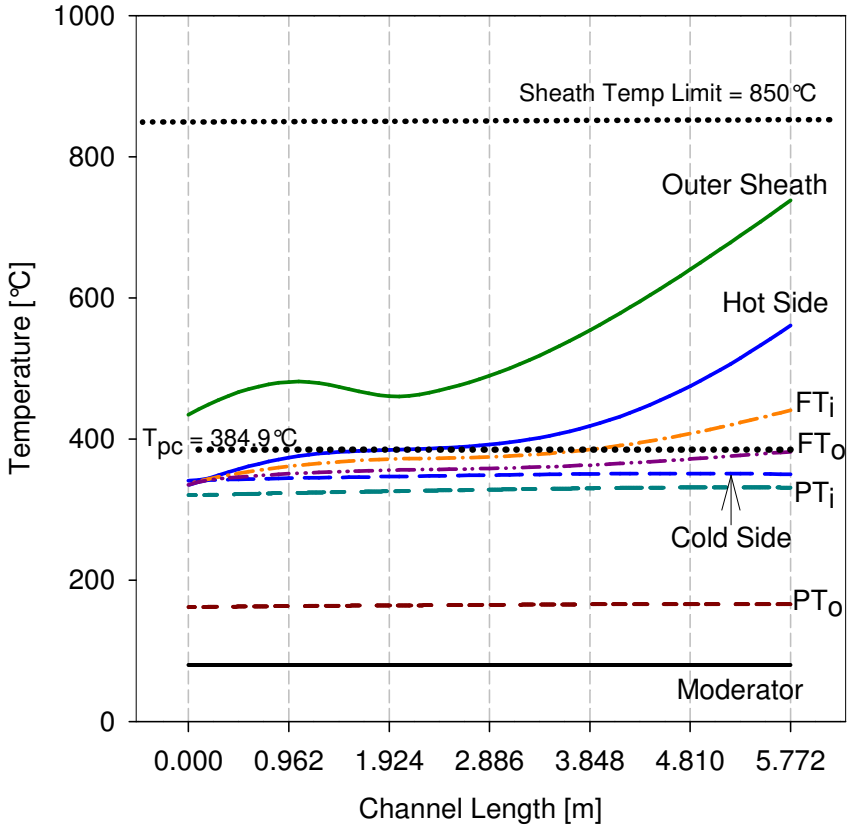

Figure 5.9: Temperature profile along the channel length for a channel power of 8.5 MW_{th}, inner-tube thickness of 2 mm, pressure tube thickness of 11 mm, inlet temperature of 350°C, mass flow rate of 4.37 kg/s and uniform heat flux

The pseudocritical point occurs in fuel bundle 5 as seen in Figure 5.10. This figure also shows the specific heat, thermal conductivity, and Prandtl number profiles along the fuel-channel for a channel power of 8.5 MW_{th}.

The average specific heat, average Prandtl number. and the heat transfer coefficient can be seen in Figure 5.11. The significant increase in these profiles at the entrance of the hot side can be accounted for by the fact that as the coolant enters the fuelled region there is a rapid increase in wall temperature of the fuel sheath.

There are three main differences between the Re-Entrant channel model with heat loss to the moderator and the reference case where there is no heat loss the moderator. The maximum outer sheath temperature in the former is much lower than the later. The pseudocritical point in the model with heat loss occurs at the start of bundle 5 whereas it is at bundle 3 in the reference case model and the outlet temperature of the hot side in the model with heat loss is much lower than the outlet temperature of the reference case. The main reason for the differences between the two models is that although the cold side acts as a preheater for both models, some of the heat transferred to the cold side from the hot side is lost to the moderator in the second model. Hence, the bulk fluid temperature of the model with heat loss to the moderator takes more time to reach the pseudocritical temperature, as seen by the shift in the location of the pseudocritical point. The outlet temperature of this model remains below 625°C because of the heat loss to the moderator and this also leads to a lower sheath temperature.

The temperature gradients across the radial section of the non insulated Re-Entrant fuel-channel at the entrance to the hot side ($x = 0$ m), the location of the pseudocritical point ($x = 1.92$ m) and the exit of the hot side ($x = 5.772$ m) are shown in Figure 5.12. The dotted line indicates the expected temperature profile in the liquid.

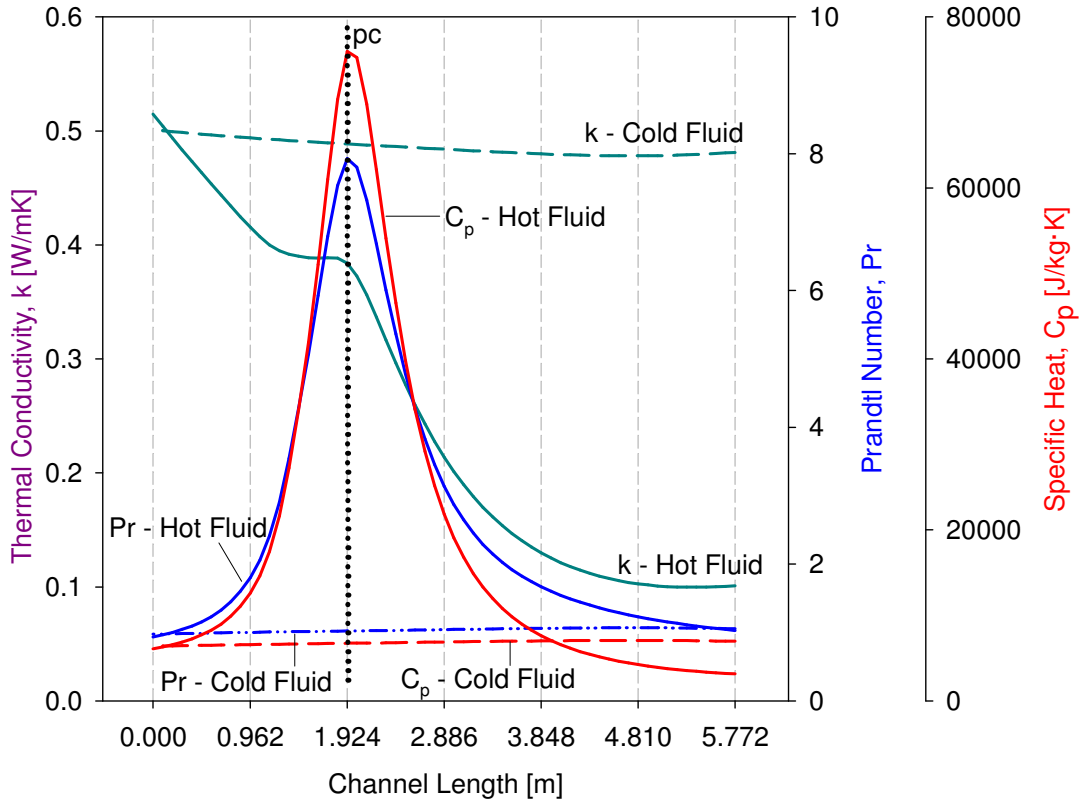

Figure 5.10: Specific heat, thermal conductivity and Prandtl number profiles along the fuel-channel for a channel power of 8.5 MW, inner-tube thickness of 2 mm, pressure tube thickness of 11 mm, inlet temperature of 350°C, mass flow rate of 4.37 kg/s and uniform heat flux

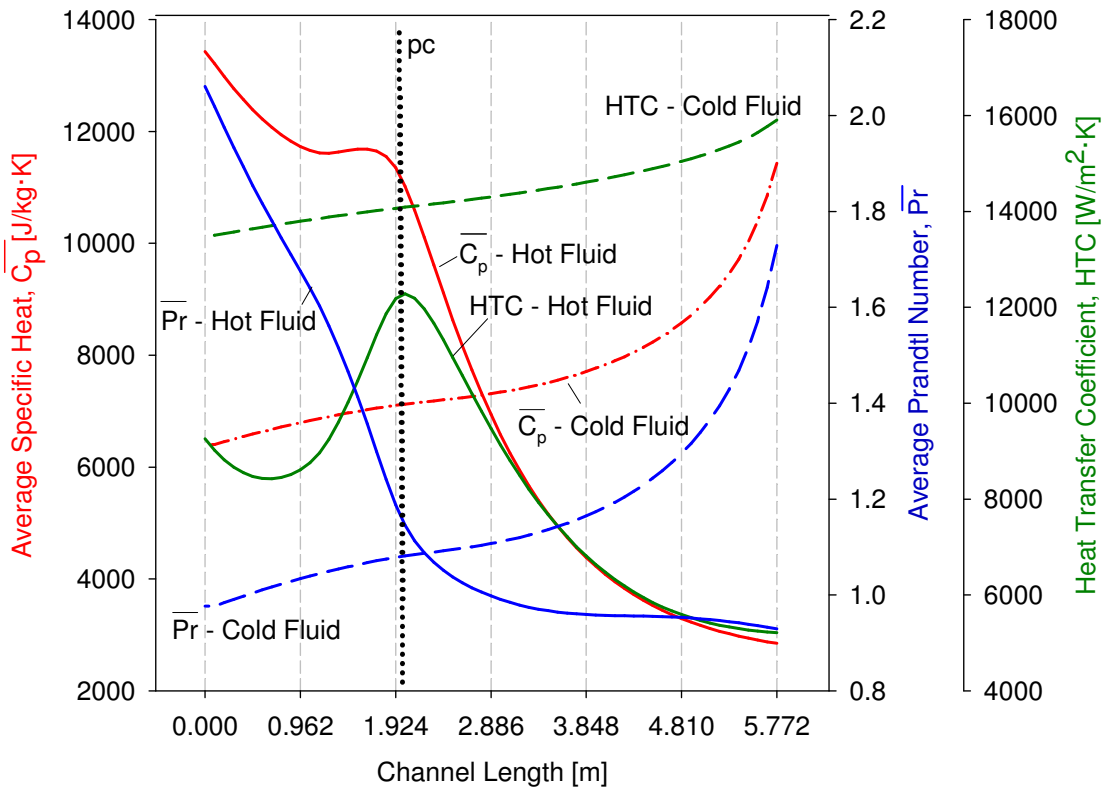

Figure 5.11: Average specific heat, average Prandtl number and HTC profiles along the fuel-channel for a channel power of 8.5 MW, inner-tube thickness of 2 mm, pressure tube thickness of 11 mm, inlet temperature of 350°C, mass flow rate of 4.37 kg/s and uniform heat flux

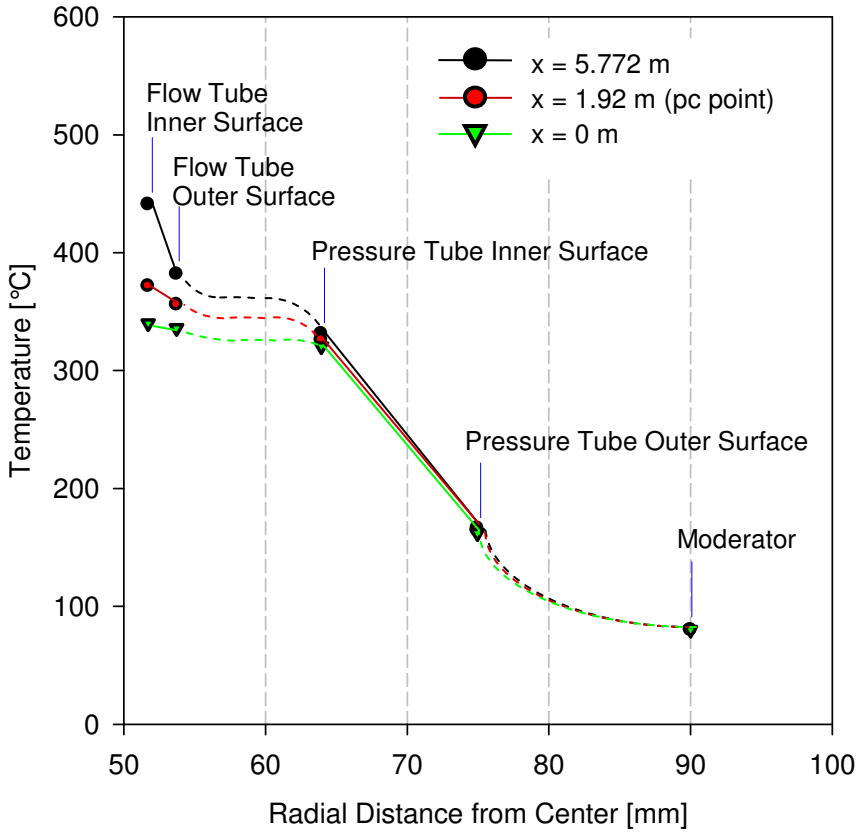

Figure 5.12: Temperature gradients along the radial distance from center for a non insulated Re-Entrant channel

The total heat loss from the cold side of the reference Re-Entrant channel to the moderator was approximately 677 kW per fuel-channel at 8.5 MW_{th} and the corresponding heat loss for 300 fuel-channels, assuming equal power, is approximately 203.1 MW. Thus, the total heat loss per channel is approximately 8% of the total channel power. This value is too high and indicates that insulation of the channel is necessary.

Table 5.1 compares the heat loss between the reference non insulated Re-Entrant channel, the reference High Efficiency Channel (HEC) and the CANDU-6 fuel-channel [**45**]. As the CANDU-6 fuel-channel is not at 8.5 MW_{th}, the values in the Table 5.1 have been scaled by a factor of 1.14 for better comparison. The heat loss in the Re-Entrant Channel is approximately 8 times the heat loss in the HEC channel when no insulation barrier is included. While a higher heat loss is expected, this does not occur, in part, as the cold annulus acts as a preheater and recovers some of the heat.

Table 5.1: Heat Loss Comparison

	Total Heat Loss Per Channel (kW)	**% of Channel Power**	**Total Heat Loss in Reactor (MW)**
Re-Entrant Channel without insulation	677	8%	203.1 MW (300 channels)
Reference HEC SCWR Fuel-Channel Concept	104	1%	31.2 MW (300 channels)
CANDU-6 Fuel Channel (scaled to 8.5 MW_{th} channel power equivalent)	13	0.1%	5 MW (380 channels)

One option to reduce heat loss in the Re-Entrant channel is to increase the thickness of the flow and pressure tubes. However, previous analysis in Section 5.1 has shown that heat transfer is not significantly affected by the thickness of the inner flow tube due to the high thermal conductivity. The total heat loss from the cold side of the Re-Entrant channel to the moderator for various pressure tube thicknesses is shown in Figure 5.13. The heat loss does not decrease significantly as the pressure tube thickness is increased, again due to high thermal conductivity. For a pressure tube thickness of 16 mm, the heat loss is approximately 5 times the heat loss of the reference HEC fuel-channel. Thicker pressure tubes are not suitable from a design perspective as it will lead to bigger calandria vessels. Neutron economy will be also lost if the pressure tube is thicker as more neutrons will be absorbed by the pressure tube, instead of passing through the tube to the moderator and back to the fuel. Thus, thicker pressure tubes are not suitable from a neutronics perspective.

A sensitivity analysis for the pressure tube material was performed. Figure 5.14 shows the difference in temperature across the pressure tube when the thermal conductivity is varied. The total heat loss to the moderator is 322 kW per channel, which is 3 times the reference HEC fuel-channel, when the thermal conductivity is changed by a factor of 0.5.

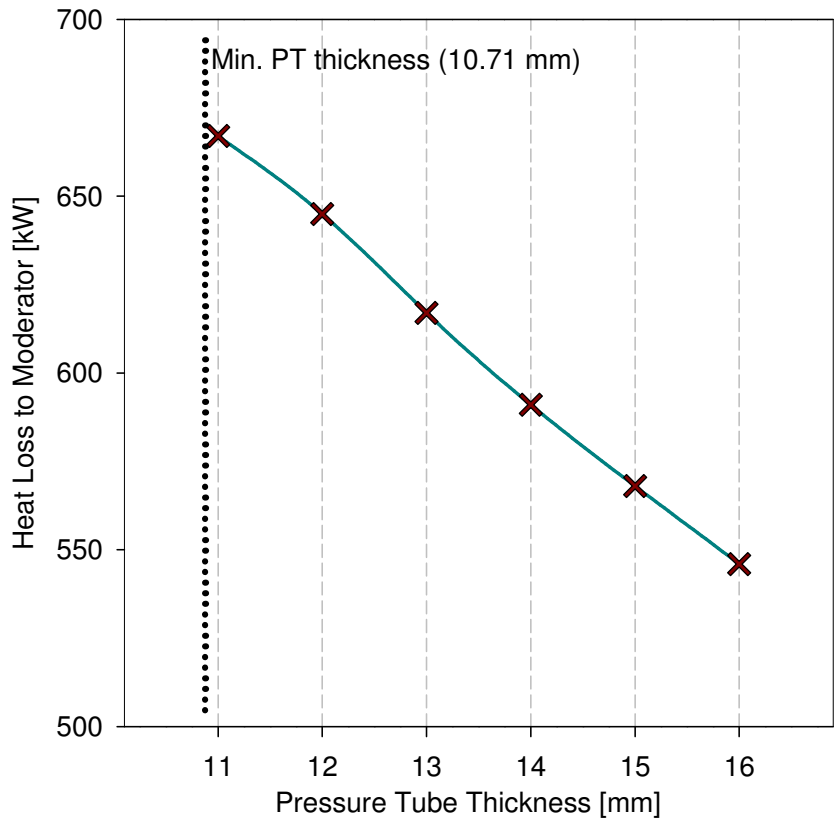

Figure 5.13: Heat loss to the moderator when pressure tube thickness is varied for a channel power of 8.5 MW_{th}, inner-tube thickness of 2 mm, inlet temperature of 350°C, mass flow rate of 4.37 kg/s and uniform heat flux

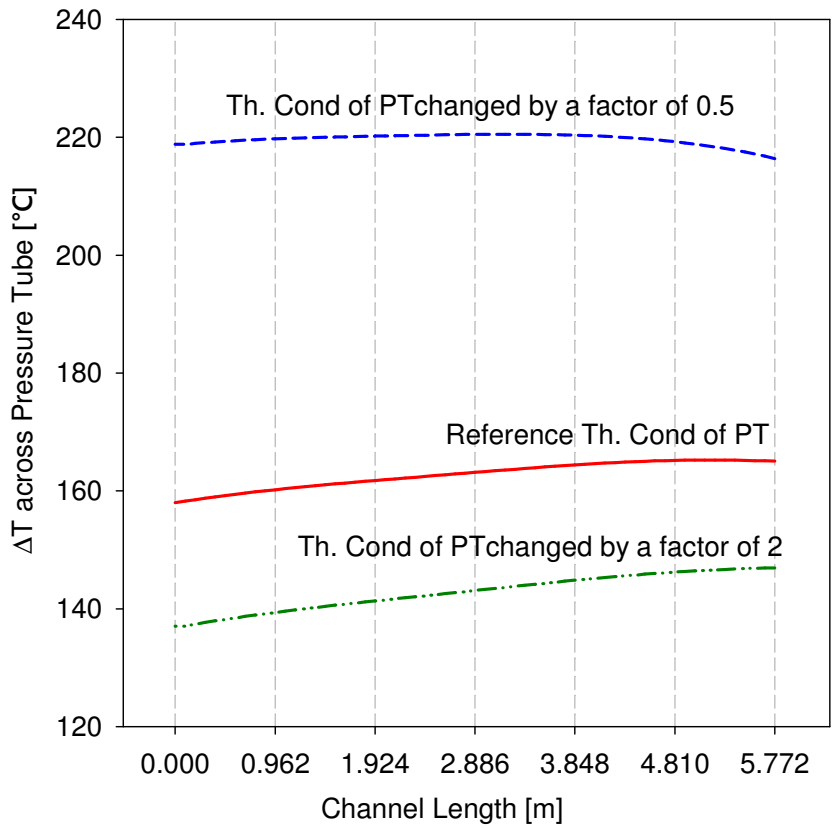

Figure 5.14: Change in temperature across the pressure tube when thermal conductivity is varied for a channel power of 8.5 MW_{th}, inner-tube thickness of 2 mm, pressure tube thickness of 11 mm, inlet temperature of 350°C, mass flow rate of 4.37 kg/s and uniform heat flux

In summary, the total heat loss to moderator when no insulation is used is much higher compared to the reference HEC and current CANDU-6 fuel-channels [**45**]. Placing a ceramic used in the HEC channel outside the pressure tube in the Re-Entrant should reduce heat loss in the Re-Entrant channel. A solid moderator could also be used to address boiling concerns. The following section examines the heat loss for an insulated Re-Entrant fuel-channel.

5.2.2 Porous Yttria Stabilized Zirconia Insulated Re-Entrant Channel

Porous Yttria Stabilized Zirconia (YSZ) with 70% porosity has been chosen as one insulating option for the Re-Entrant channel as zirconia is exceptionally resistant to irradiation damage from fast neutrons and energetic ions [**9**]. Figure 3.5 shows the insulator in the Re-Entrant fuel-channel. The pores in the insulator are in the axial direction along the fuel-channel. This allows for carbon dioxide gas to pass through them. The reference thickness of the insulator is 7 mm as an analysis on the insulator thickness indicated that the minimum thickness of the insulator required to prevent boiling of the moderator is 6 mm.

Figure 5.15 shows the temperature profiles of the coolant, the inner and outer surfaces of the flow, pressure and outer tubes, and the outer sheath along the heated length of the channel for a channel power of 8.5 MW_{th}, an inner-tube thickness of 2 mm, a pressure tube thickness of 11 mm, and a 7 mm thick porous YSZ insulator. The temperature of the outer sheath is lowest at the pseudocritical point, which can be seen in Figure 5.15. The outer tube temperature indicates that boiling does not occur in the moderator. The exit temperature of the hot side is 610°C, which is considerably higher than the Re-Entrant model with no insulation (560°C). This indicates that the insulator is reducing the thermal energy transferred to the moderator.

The temperature gradients across the radial section of the Porous YSZ insulated Re-Entrant fuel-channel at $x = 0$ m, $x = 1.44$ m and $x = 5.772$ m are shown in Figure 5.16, where $x = 1.44$ m is the location of the pseudocritical point. The dotted line indicates the expected temperature profile in the liquid. As mentioned earlier, the temperature difference between the outer tube and the moderator indicates that boiling of the moderator does not occur. The thermophysical properties for the 7 mm thick porous YSZ insulated REC are shown in Appendix C.

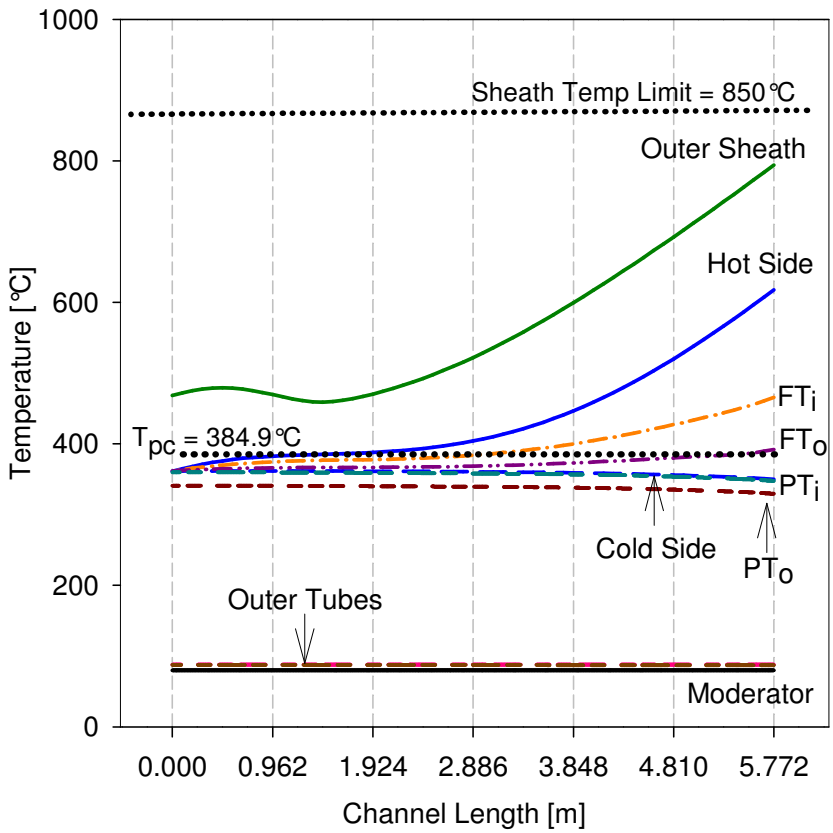

Figure 5.15: Temperature profile along the channel length for a channel power of 8.5 MW_{th}, inner-tube thickness of 2 mm, pressure tube thickness of 11 mm, inlet temperature of 350°C, mass flow rate of 4.37 kg/s and uniform heat flux

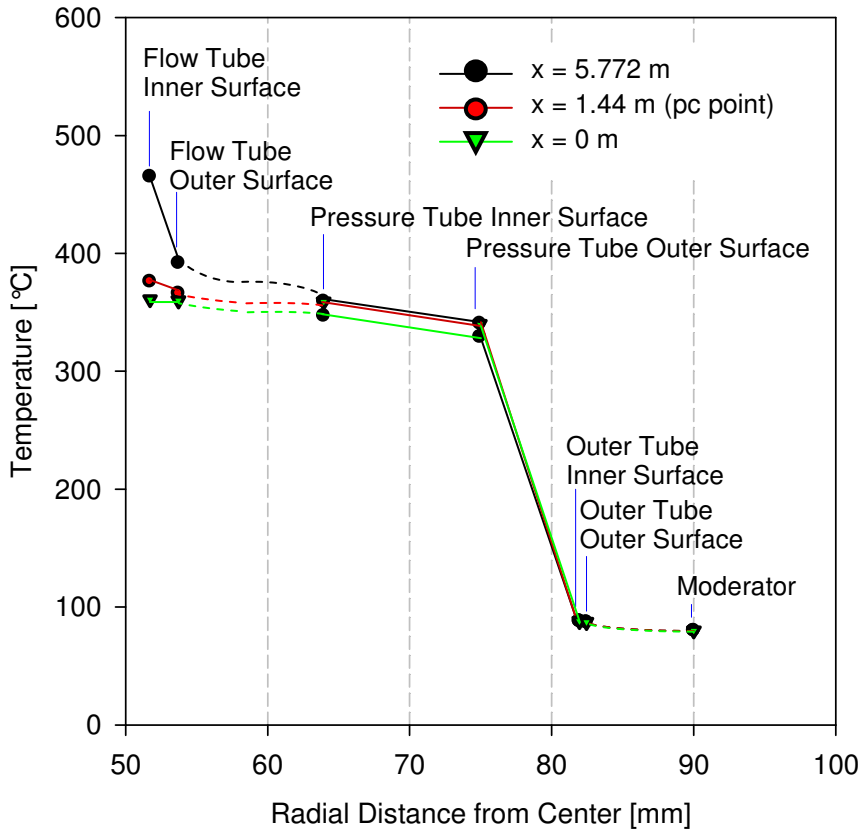

Figure 5.16: Temperature gradients along the radial distance from center for a Porous YSZ insulated Re-Entrant channel

5.2.3 Zirconium Dioxide (ZrO_2) Insulated Re-Entrant Channel

Another insulating option for the Re-Entrant channel is to use a solid Zirconium Dioxide insulation. The minimum thickness required to prevent boiling of the moderator is 5 mm. The reference thickness chosen for this analysis is 7 mm, so that the results can be compared to the Re-Entrant channel with Porous Yttria Stabilized Zirconia insulation. Heat transfer analysis was also performed for a 7 mm solid ZrO_2 insulated fuel-channel. The reference thermal conductivity of zirconium dioxide is $2.7\,W/m \cdot K$. [**9**]. The temperature profiles are shown in Figure 5.17, while thermophysical properties are shown in Appendix C. The outer temperature profile of the pressure tube in the solid zirconium dioxide channel is lower than the outer temperature profile in the YSZ insulated channel. This indicates that more heat is being lost from the cold side to the moderator in the zirconium dioxide insulated channel. The thermophysical properties profiles are similar between the two cases as the pseudocritical points are relatively close to each other.

The temperature gradients across the radial section of the reference Re-Entrant fuel-channel at $x = 0$ m, x = 1.54 m, and x = 5.772 m, are shown in Figure 5.18, where x = 1.54 m is the location of the pseudocritical point. The dotted line indicates the expected temperature profile in the liquid. The heavy water moderator does not boil boiling of the moderator does not for the ZrO_2 fuel-channel occur.

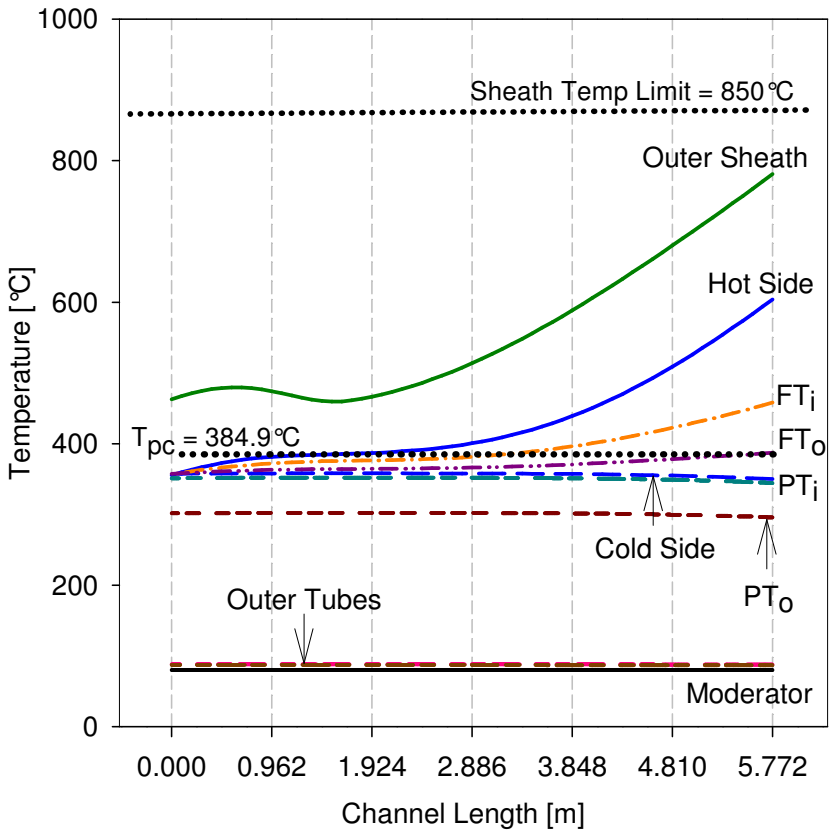

Figure 5.17: Temperature profile along the ZrO_2 insulated channel length for a channel power of 8.5 MW_{th}, inner-tube thickness of 2 mm, pressure tube thickness of 11 mm, insulation thickness of 7 mm, inlet temperature of 350°C, mass flow rate of 4.37 kg/s and uniform heat flux

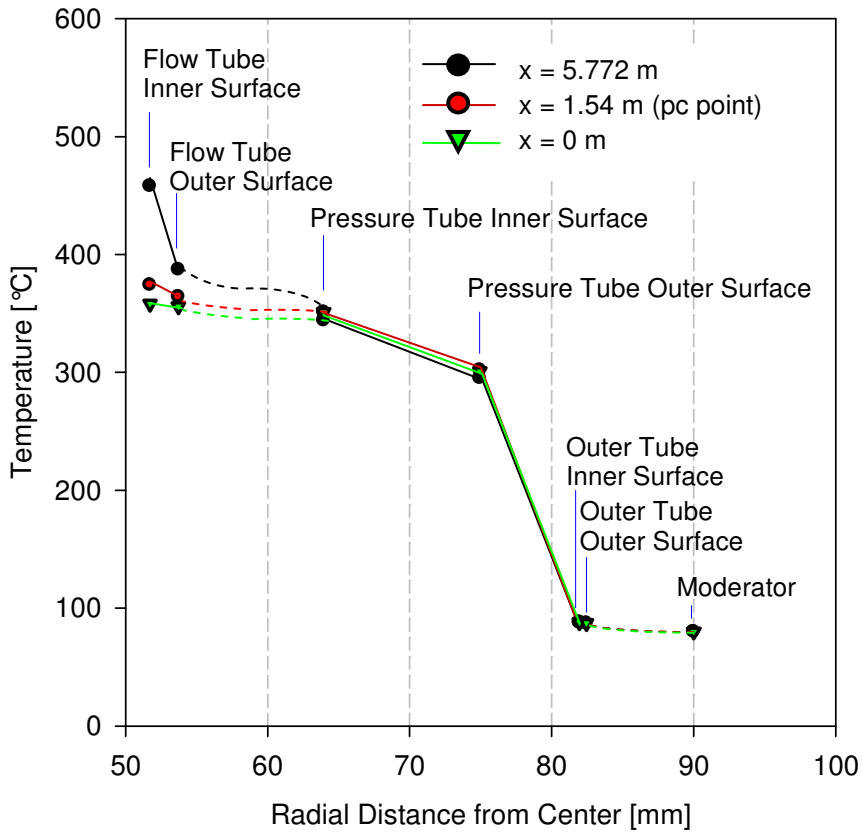

Figure 5.18: Temperature gradients along the radial distance from center for a ZrO_2 insulated Re-Entrant channel for a channel power of 8.5 MW_{th}, inner-tube thickness of 2 mm, pressure tube thickness of 11 mm, insulation thickness of 7 mm, inlet temperature of 350°C, mass flow rate of 4.37 kg/s and uniform heat flux

5.2.4 Heat Loss Comparison

When the reactor is under normal operation, heat loss from the channel to the moderator is assumed to be via mixed forced and free convection. This is because the Rayleigh number from free convection is high enough, that the thermal buoyancy cannot be ignored. Heat transfer to the moderator will occur via free convection during accident scenarios such as failure of moderator pumps. The total heat loss to the moderator from the Re-Entrant channel for both the Porous YSZ insulation and the ZrO_2 insulation when insulation thickness is varied is shown Figure 5.19 for mixed type heat loss and Figure 5.20 for free convection heat loss. The total heat loss to the moderator is much lower when the Porous YSZ insulation is used for both types of heat loss. One advantage of using solid ZrO_2 is that there is no need for an additional system for the gas that would flow through the Porous YSZ insulation. However, the CO_2 gas that flows through the insulator has other advantages such as the ability to detect leaks in the pressure tube. Thus, Porous YSZ is chosen as the insulator for the Re-Entrant fuel-channel.

A comparison between the total heat loss for a 7 mm Porous YSZ insulated channel, 7 mm ZrO_2 insulated channel, reference HEC SCWR fuel-channel, and the CANDU-6 fuel-channel is shown in Table 5.2. The heat loss from the CANDU-6 channel has been scaled to match the channel power of the Re-Entrant channel. The total heat loss in the 7 mm Porous YSZ insulation is about 1.02% of the channel's total power.

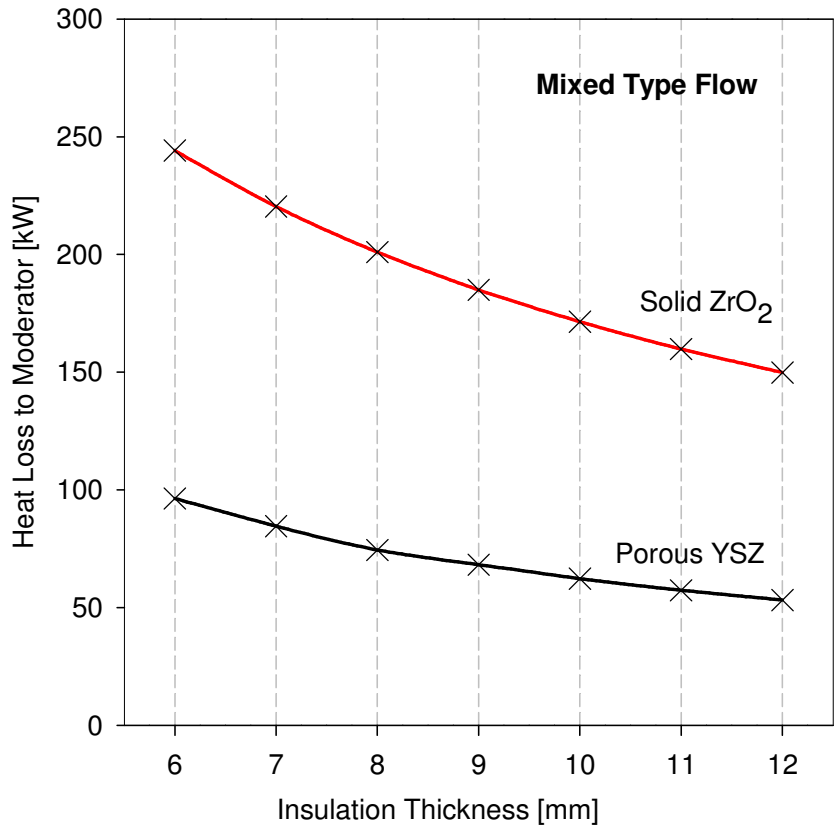

Figure 5.19: Heat loss to Moderator for cold side of Re-Entrant channel for variable Porous YSZ insulation thickness and variable solid ZrO_2 insulation thickness assuming mixed type heat loss to the moderator

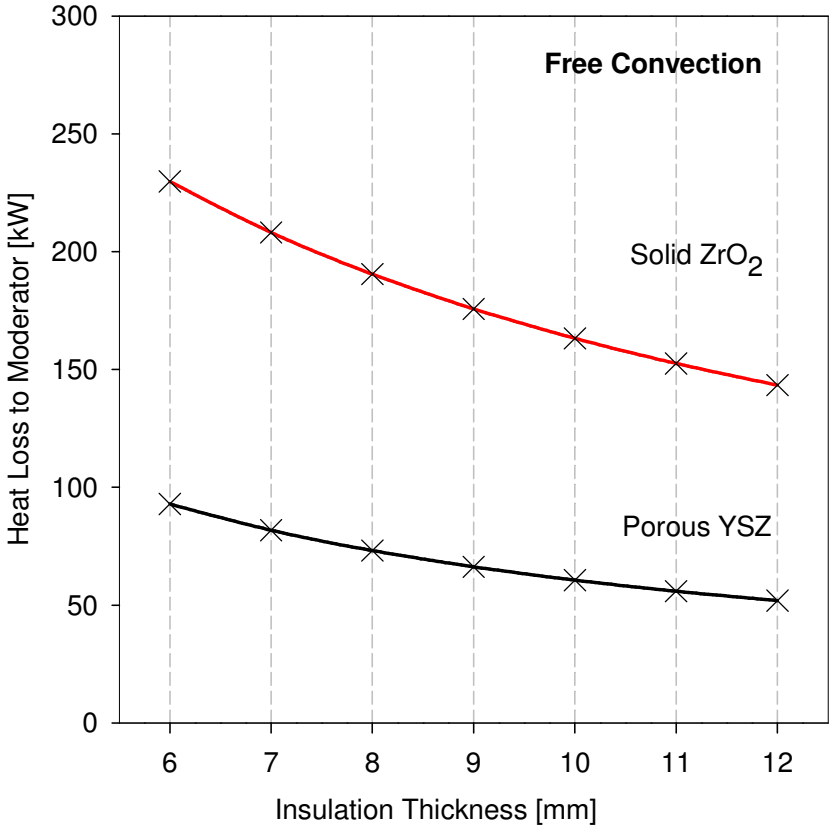

Figure 5.20: Heat loss to Moderator for cold side of Re-Entrant channel for variable Porous YSZ insulation thickness and variable solid ZrO_2 insulation thickness assuming free convection heat loss to the moderator

Table 5.2: Heat Loss Comparison for insulated Re-Entrant channel

	Total Heat Loss Per Channel (kW)	**Total Heat Loss in Reactor (MW)**
Re-Entrant Channel with 7 mm Porous YSZ insulation (Mixed Flow)	85	25.5 MW (300 channels)
Re-Entrant Channel with 7 mm ZrO_2 insulation (Mixed Flow)	225	67.5 MW (300 channels)
Re-Entrant Channel with 7 mm Porous YSZ insulation (Free Convection Heat Loss)	80	24 MW (300 channels)
Re-Entrant Channel with 7 mm ZrO_2 insulation (Free Convection Heat Loss)	212	63.3 MW (300 channels)
Reference HEC SCWR Fuel-Channel Concept	104	31.2 MW (300 channels)
CANDU-6 Fuel Channel (scaled to 8.5 MW_{th} channel power equivalent)	13	5 MW (380 channels)

In summary, the heat loss from the Re-Entrant channel is greatly reduced when an insulator is used. Two different insulators, Porous YSZ and solid ZrO_2 were used and the total heat loss was less for the Porous YSZ insulation for both free convection heat loss to moderator the mixed type flow heat loss to the moderator.

5.3 Impact of Non-Uniform Flux Shapes

For the previous analyses, the heat flux in the fuel-channel was assumed to be uniform. In this section, the heat loss to the moderator is examined for six different axial power profiles:

- Case 1: Uniform axial power profile (reference)
- Case 2: Typical nominal axial power profile
- Case 3: Peaked shaped axial power profile
- Case 4: Upstream-skewed axial power profile
- Case 5: Downstream-skewed axial power profile
- Case 6: Variable axial power profile

Case 1 is used since the majority of experimental data available for determining heat transfer models use a uniform heat flux. Hence the profile can be used for verification against experimental data.

Case 2 represents a standard case for normal operating conditions in a nuclear reactor. The flux shape is a slightly flattened cosine which occurs due to neutron leakage at the boundary of the reactor. The slight flattening of the cosine shape is caused by internal reactivity mechanisms such as adjuster rods or zone controls.

Case 3 is similar to Case 2, but represents a more severe gradient in the flux shape as there is no flattening effect by the reactivity mechanisms.

Case 4 is the inverse of Case 5. Case 5 is a designed flux shape that envelopes several refuelling scenarios in such a way as to be the most severe flux shape in critical heat flux studies. Hence, recent experimental data was obtained using these flux shapes.

The first 5 cases are typically used in research related analysis as they are usually sufficient to capture the phenomena for existing plants. In actual safety analysis of a

CANDU-6, over 900 flux shapes representing different normal and abnormal operating scenarios are used. As the reactor physics flux shapes for SCWRs are not known, one additional case is added for interest.

Case 6 is a disturbed flux shape usually caused by a reactivity device that is an outof-normal configuration. The result is a two-peak flux shape. This slope was chosen as it implies the possibilities of having the pseudocritical point in two locations or extended over a region and hence could represent a scenario of significant safety concern.

Once the reactor physics flux shapes for SCWRs are known, the choice of flux shapes can be revisited.

A 7 mm thick Porous YSZ insulated channel was used to analyze the impact of non-uniform flux shapes. The total channel power was assumed to be 8.5 MW_{th} for all cases, while the inlet temperature was 350°C and mass flow rate was 4.37 kg/s. Heat loss to the moderator was assumed to be via mixed flow.

The various axial power profiles are shown in Figures 5.21. The corresponding temperature profiles are shown in Figures 5.22 to 5.27. The thermophysical properties are shown in Appendix C for Case 1 and in Appendix D for Case 2 to 6.

The temperature profiles for all the five different axial power profiles indicate that the coolant outlet temperature is approximately 600°C which is close to the desired value of 625°C. The outer sheath temperature is below the sheath temperature limit of 850°C for all five different flux shapes, although it is close to the sheath limit for the down-skew power profile.

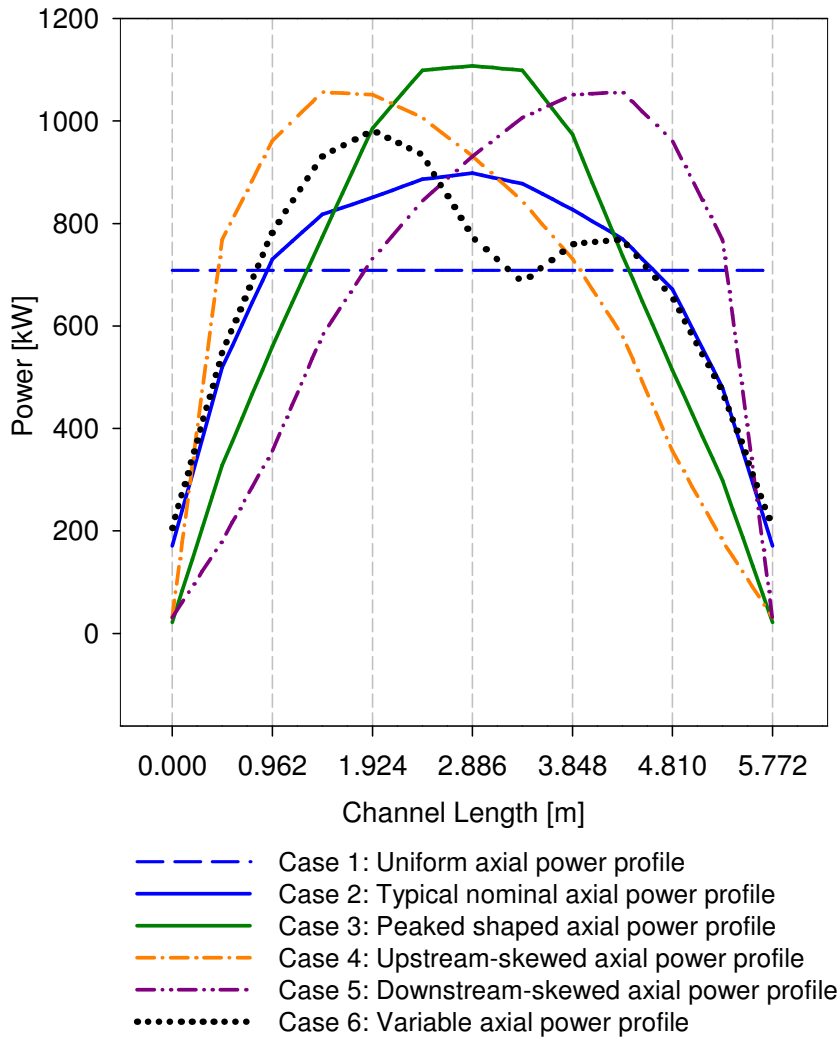

Figure 5.21: Axial Power Profiles

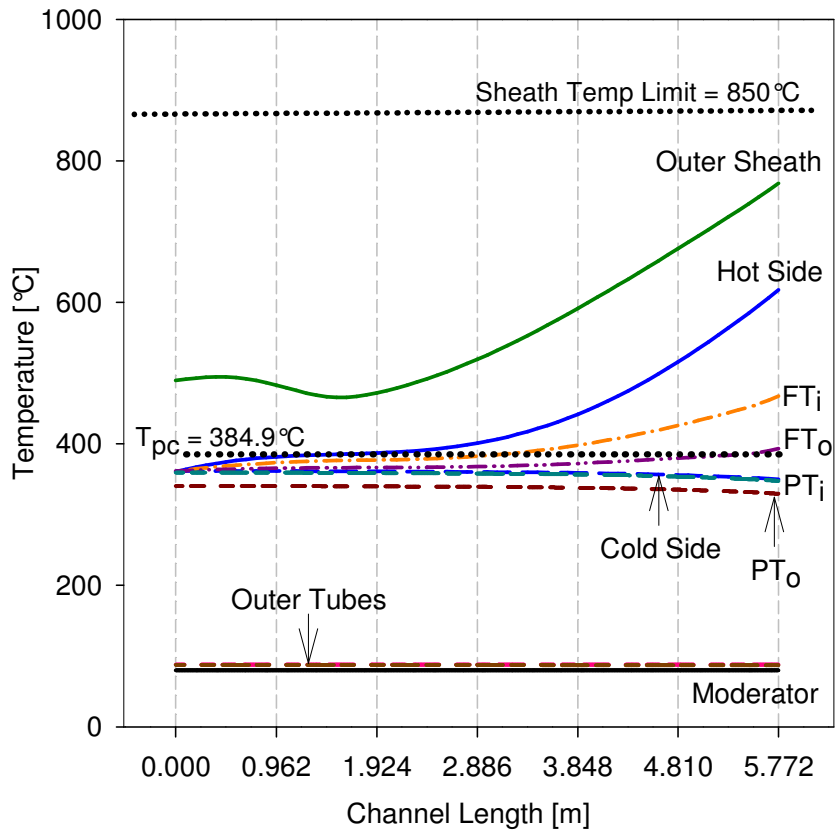

Figure 5.22: Case 1 (Uniform Power Profile): Temperature profiles along the 7 mm thick Porous YSZ insulated fuel-channel for a total channel power of 8.5 MW_{th}, inner-tube thickness of 2 mm, pressure tube thickness of 11 mm, inlet temperature of 350°C and mass flow rate of 4.37 kg/s

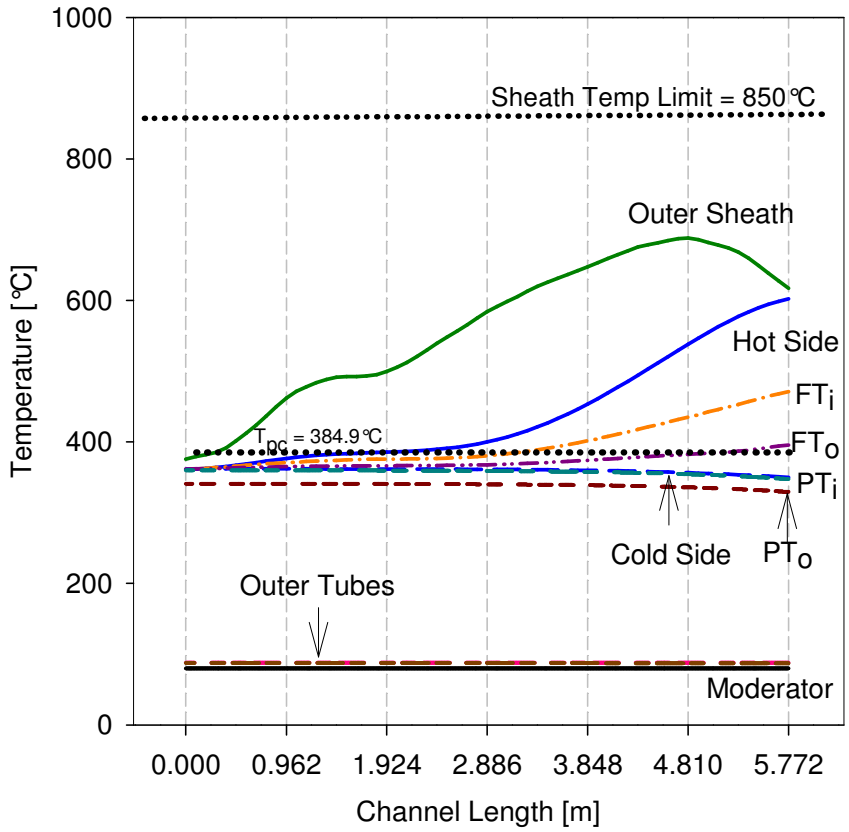

Figure 5.23: Case 2 (Typical Nominal Power Profile): Temperature profiles along the 7 mm thick Porous YSZ insulated fuel-channel for a total channel power of 8.5 MW_{th}, inner-tube thickness of 2 mm, pressure tube thickness of 11 mm, inlet temperature of 350°C and mass flow rate of 4.37 kg/s

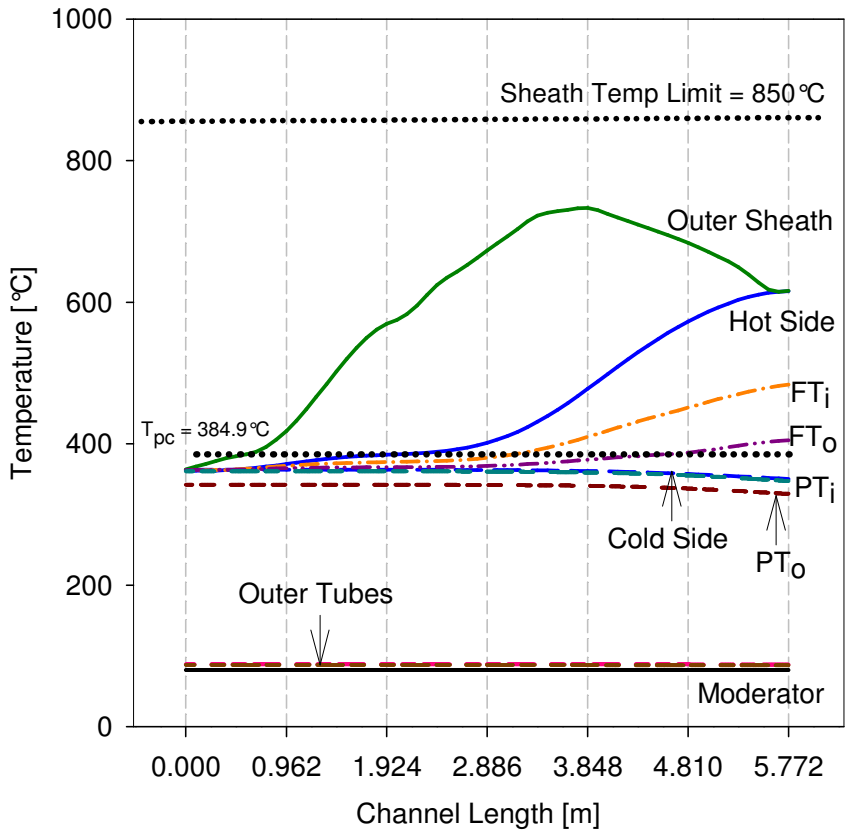

Figure 5.24: Case 3 (Peaked Shape Power Profile): Temperature profiles along the 7 mm thick Porous YSZ insulated fuel-channel for a total channel power of 8.5 MW_{th}, inner-tube thickness of 2 mm, pressure tube thickness of 11 mm, inlet temperature of 350°C and mass flow rate of 4.37 kg/s

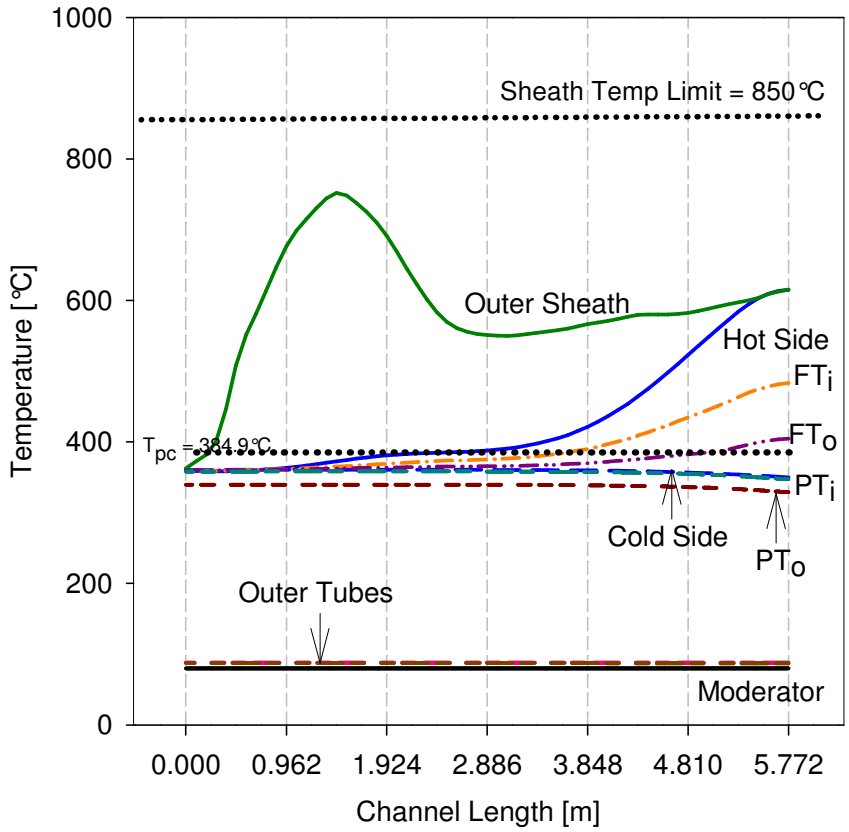

Figure 5.25: Case 4 (Upstream-skewed Power Profile): Temperature profiles along the 7 mm thick Porous YSZ insulated fuel-channel for a total channel power of 8.5 MW_{th}, inner-tube thickness of 2 mm, pressure tube thickness of 11 mm, inlet temperature of 350°C and mass flow rate of 4.37 kg/s

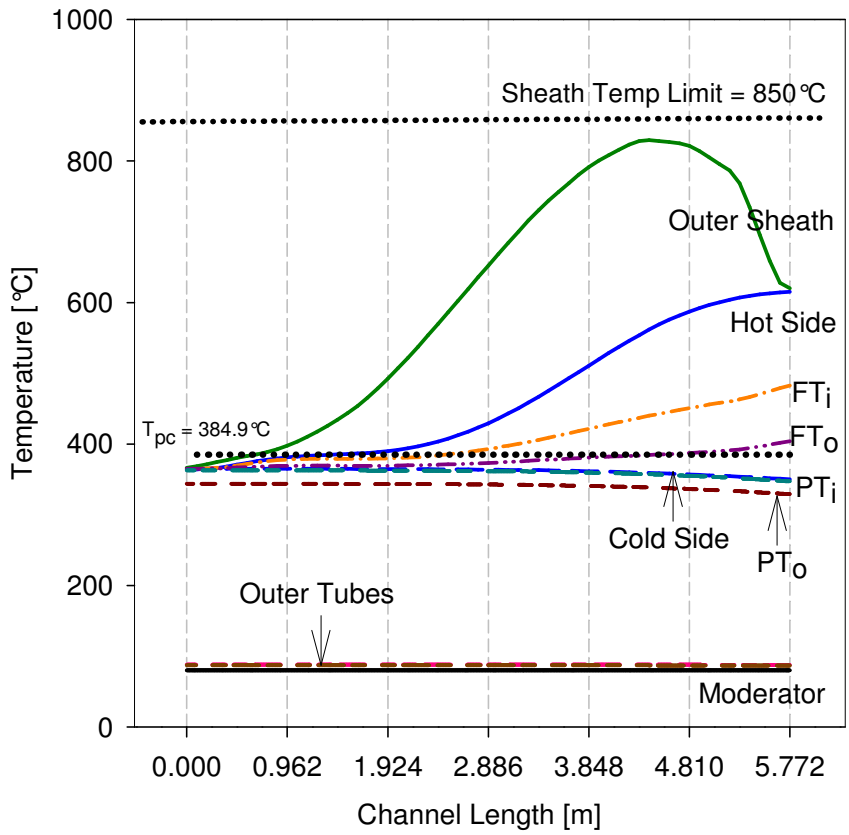

Figure 5.26: Case 5 (Downstream-skewed Power Profile): Temperature profiles along the 7 mm thick Porous YSZ insulated fuel-channel for a total channel power of 8.5 MW_{th}, inner-tube thickness of 2 mm, pressure tube thickness of 11 mm, inlet temperature of 350°C and mass flow rate of 4.37 kg/s

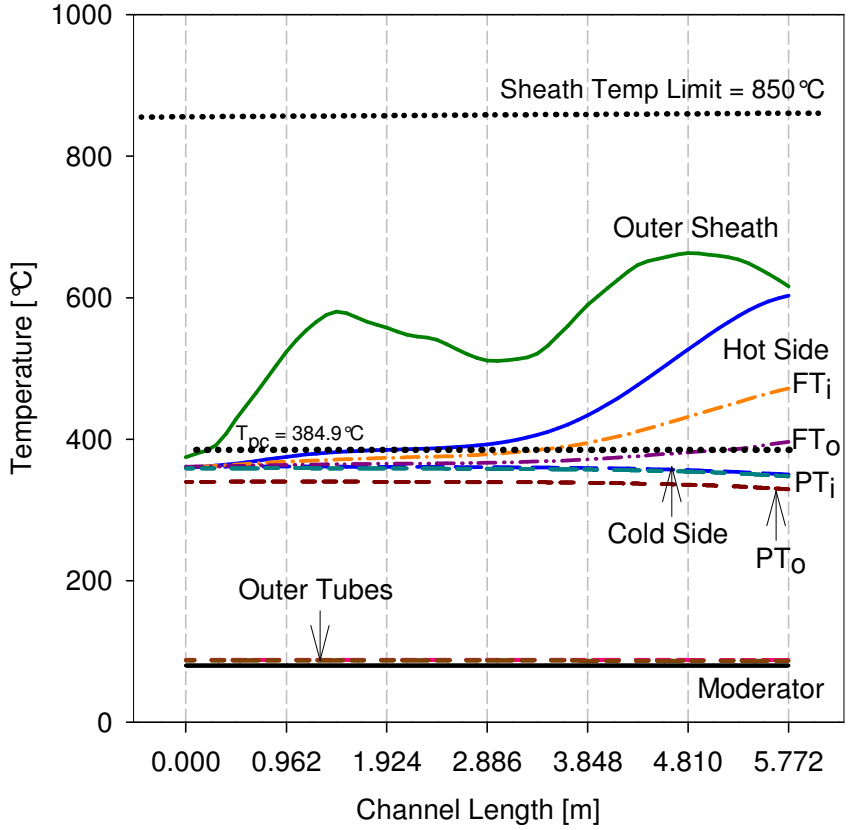

Figure 5.27: Case 6 (Variable Power Profile): Temperature profiles along the 7 mm thick Porous YSZ insulated fuel-channel for a total channel power of 8.5 MW_{th}, inner-tube thickness of 2 mm, pressure tube thickness of 11 mm, inlet temperature of 350°C and mass flow rate of 4.37 kg/s

The total heat loss from the reference 7 mm thick Porous YSZ insulated Re-Entrant channel for the five different axial heat flux profiles is shown in Table 5.3. As expected, the total heat loss is similar in all five cases as the total channel power is 8.5 MW_{th}. Table 5.4 shows the peak sheath temperature and its axial location in the Re-Entrant fuel-channel for the six different cases. The peak sheath temperature of the downstream-skewed profile is close to the sheath temperature limit which is 850°C. This maybe an issue when the reactor is in operation as there are several hundred possible power profiles, and power profiles similar to the downstream-skewed profile used in this analysis may cause the sheath temperature to exceed the limit.

The location of the pseudocritical point for all six cases is shown in Table 5.5. The pseudocritical point is located in bundle #3 for the uniform power profile, the typical nominal power profile and the two peak power profile and in bundle #4 for the peaked shape power profile. As expected, the pseudocritical point for the upstream-skewed power profile occurs before the other cases, in bundle #2, while the pseudocritical point for the downstream-skewed power profile occurs in bundle #5. The location of the pseudocritical point for different power profiles in the Re-Entrant channel is important because it affects the thermophysical properties, which in turn affects the heat transfer characteristics of the fuel-channel.

Table 5.3: Heat Loss Comparison for insulated Re-Entrant channel with different axial power profiles

Power Profile	Total Heat Loss Per Channel (kW)
Case 1: Uniform power profile	84.52
Case 2: Typical nominal power profile	84.73
Case 3: Peaked shaped power profile	85.11
Case 4: Upstream-skewed power profile	85.41
Case 5: Downstream-skewed power profile	84.53
Case 6: Two peak power profile	84.73

Table 5.4: Peak sheath temperature and location of peak sheath temperature for insulated Re-Entrant channel with different axial power profiles

Power Profile	Peak Sheath Temperature (°C)	Location of Peak Sheath Temp (m)
Case 1: Uniform power profile	768.3	5.772
Case 2: Typical nominal power profile	688.1	4.81
Case 3: Peaked shaped power profile	733.2	3.85
Case 4: Upstream-skewed power profile	752.1	1.44
Case 5: Downstream-skewed power profile	829.4	4.43
Case 6: Two peak power profile	663.1	4.81

Table 5.5: Location of pseudocritical point in the Re-Entrant channel with different axial power profiles

Power Profile	Location of pc point (m)
Case 1: Uniform power profile	1.54
Case 2: Typical nominal power profile	1.83
Case 3: Peaked shaped power profile	2.02
Case 4: Upstream-skewed power profile	1.35
Case 5: Downstream-skewed power profile	2.50
Case 6: Two peak power profile	1.64

CHAPTER 6

CONCLUDING REMARKS

An alternate fuel-channel concept called the Re-Entrant Channel for SuperCritical Water-cooled Reactors was conceptually designed and a preliminary heat transfer analysis was performed to assess the thermal hydraulic behaviour under normal operating conditions.

- The temperature profiles of the coolant, outer sheath, inner and outer surfaces of the flow tube, pressure tube and the outer tube were estimated at different operating conditions. The temperature profiles of the coolant in the hot side and of the outer sheath change considerably within the pseudocritical region. The outer sheath temperature was below the sheath temperature limit for normal operating conditions.

- The pseudocritical point was located in the hot side of the Re-Entrant fuel-channel for various power profiles. The location of the pseudocritical point changes for different axial power profiles and is important as it affects the heat transfer characteristics and may affect the materials and chemistry characteristics of the Re-Entrant channel.

- The cold side (annulus) acts as a preheater and recovers some of the heat lost. The preheating concept also allowed for the pseudocritical point to be upstream of the fuelled length.

- The Re-Entrant channel can be used in both horizontal and vertical configurations and the design allowed for the insulator to be placed outside of the fuel-channel.

- Various axial power profiles did not have a significant impact on the total heat loss to the moderator.

- Porous Yttria Stabilized Zirconia is found to be a more effective insulator than Zirconium dioxide in terms of heat loss for the Re-Entrant channel.

- The total heat loss to the moderator for the porous Yttria Stabilized Zirconia insulated Re-Entrant channel is 85 kW per channel for a channel power of 8.5 MW_{th}, which is approximately 1% of the channel's total power, and is 18% less than the heat loss in the existing SCWR channel-type design concept. Thus, the Re-Entrant channel is more efficient than the High Efficiency Channel in terms of total heat loss to the moderator.

CHAPTER 7

FUTURE WORK

Future work should include optimizing the design of the Re-Entrant fuel-channel to further reduce the heat loss from the cold side to the moderator and to see if it's possible to move the location of the pseudocritical point from the hot side to the cold side of the fuel-channel.

A 2-D model of the re-entrant zone should be developed to investigate heat transfer characteristics of the mixing node.

The use of a gaseous insulation similar to that used in the present CANDUs should also be investigated as this may reduce heat loss. The effect of increasing the temperature and pressure of the heavy water moderator on the minimum thickness of the insulator required to prevent boiling should be studied as this will lead to a thinner insulator for the fuel-channel design.

Using different solid and liquid moderators should also be considered as this may eliminate the need for an insulator.

A detailed sensitivity analysis on the materials used for the flow and pressure tubes should be conducted as data on how the metals perform at supercritical pressures and temperatures becomes available.

The support structure for the flow and pressure tubes should be designed and the pressure drop along the fuel-channel should be added to the heat transfer model as it may impact the thermophysical properties of the coolant.

Changing operating conditions, such as mass flow and inlet temperatures, to account for accident scenarios would also be useful.

REFERENCES

[1] I Hore-Lacy, *Nuclear Energy in the 21st Century*. London: World Nuclear University Press, 2006.

[2] Organisation for Economic Co-Operation and Development / International Energy Agency, "World Enery Outlook," Paris, 2004.

[3] Ontario Power Generation. (2007, May) Energy Today Magazine. [Online]. http://www.energytodaymagazine.com/index.php?option=com_content&task=view&id=5750

[4] The International Association for the Properties of Water and Steam, "IAPWS Release on the Values of Temperature, Pressure and Density of Ordinary Water Substances at their Respective Critical Points," St. Petersburg, Russia, 1983.

[5] I. L. Pioro and R.B. Duffey, *Heat Transfer and Hydraulic Resistance at Supercritical Pressures in Power Engineering Applications*. New York: ASME Press, 2007.

[6] C. K. Chow, S. J. Bushby, and H. F. Khartabil, "A Fuel Channel Design for CANDU-SCWR," in *14th International Conference on Nuclear Engineering (ICONE14)*, Miami, 2006, pp. 677-685.

[7] I. L. Pioro, H. F. Khartabil, and R. B. Duffey, "Heat Transfer of Supercritical Fluids Flowing in Channels - Emperical Correlations (Survey)," *Nuclear Engineering and Design*, vol. 230 (1-3), pp. 69-91, 2004.

[8] S. Mokry, "Development of a Heat-Transfer Correlation for Supercritical Water in Supercritical Water-Cooled Reactor Applications," UOIT, Oshawa, Canada, 2009.

[9] C. K. Chow and H. F. Khartabil, "Conceptual Fuel Channel Designs for CANDU-SCWR," *Nuclear Engineering and Technology*, vol. 40 (1), 2008.

[10] G.L Brooks, "A Short History of the CANDU Nuclear Power System," 2002.

[11] AECL, "C-6 Technical Summary," Mississauga, Canada, 2005.

[12] AECL, "Enhanced CANDU 6 Technical Summary," Mississauga, Canada, 2009.

[13] AECL, "ACR-1000 Technical Summary," Mississauga, Canada, 2007.

[14] AECL, "CANDU: The Evolution," *Nuclear Engineering International (NEI)*, 2007.

[15] GEN IV International Forum, "GIF R&D Outlook for Generation IV Nuclear Energy Systems," 2007.

[16] U.S. DOE Nuclear Energy Research Advisory Committee and Generation IV International Forum, "A Technology Roadmap for Generation IV Nuclear Energy Systems," 2002.

[17] D. Hahn et al., "Conceptual Design of the Sodium-Cooled Fast Reactor Kalimer-600," Korea Atomic Energy Research Institution, Daejeon, 2007.

[18] JC Garnier, F, Morin, J. Y. Malo, and Y. Lejeail, "GFR System: Progress of CEA pre-conceptual design studies," in *International Congress on Advances in Nuclear Power Plants (ICAPP 05)*, Seoul, 2005, p. 5305.

[19] L. Mathieu et al., "The thorium molten salt reactor: Moving on from the MSBR," *Progress in Nuclear Energy*, vol. 48, no. 7, pp. 664-679, September 2006.

[20] L. Cinnoti et al., "The Potential of LFR and ELSY Project," in *International Congress on Advances in Nuclear Power Plants (ICAPP)*, Nice, 2007, p. 7585.

[21] Y. Oka and S. Koshizuka, "Coceptual design study of advanced power reactors," *Progress in Nuclear Energy*, vol. 32, no. 1-2, pp. 167-177, 1998.

[22] H. Thind, I. Pioro, and G. Harvel, "SuperCritical Water-Cooled Nuclear Reactor with Intermediate Heat Exchanges ," in *18th International Conference on Nuclear Engineering*, Xi'an, 2010, p. 30104.

[23] R. Monichan, "Steam Re-Heat Options for Supercritical Water Reactors," UOIT, Oshawa, Canada, 2009.

[24] M Naidin, I Pioro, U Zirn, S Mokry, and G Naterer, "Supercritical Water-Cooled NPPs with Co-Generation of Hydrogen: General Layout and Thermodynamic-Cycles Options," in *The 4th International Symposium on Supercritical Water-Cooled Reactors*, Heidelberg, Germany, 2009.

[25] B. V. Dyadyakin and A. S. Popov, "Heat Transfer and thermal resistance of tight seven-rod bundle, cooled with water flow at supercritical pressures," *Transactions of VTI*, vol. 11, pp. 244 - 253, 1977.

[26] W.H. McAdams, *Heat Transmission*, 2nd ed. New York, USA: McGraw-Hill, 1942.

[27] N. M. Schnurr, V. S. Sastry, and A. B. Shapiro, "A numerical analysis of heat transfer to fluids near the thermodynamic critical point including the thermal entrance region," *Journal of Heat Transfer*, vol. 98 (4), pp. 609 - 615, 1976.

[28] F. Incropera, D. DeWitt, T. Bergman, and A. Lavine, *Fundamentals of Heat and Mass Transfer*.: Wiley, 2006.

[29] A.A. Bishop, R.O. Sandberg, and L.S. Tong, "Forced convection heat transfer to water at near-critical temperatures and super-critcial pressures," Atomic Power Division, Westinghouse Electric Corporation, Pittsburgh, USA, 1964.

[30] H.S. Swenson, J.R. Carver, and C.R. Kakarala, "Heat transfer to supercritical water in smooth-bore tubes," *Journal of Heat Transfer*, vol. 87 (4), 1965.

[31] P. Kirillov et al., "Experimental Study on Heat Transfer to Supercritical Water Flowing in Vertical Tubes," in *GLOBAL 2005 International Conference, Nuclear Energy Systems for Future Generation and Global Sustainability (GLOBAL '05)*, Tsukuba, 2005.

[32] H. Zahlan, D.C. Groeneveld, and S. Tavoularis, "Look-up Table for Trans-Critical Heat Transfer," in *The 2nd Canada-China Joint Workshop on Supercritical Water Cooled Reactors (CCSC 2010)*, Toronto, 2010.

[33] Y. M. Kim and H. J. Kim, "Analysis of fluid flow and heat transfer inside Calandria vessel of CANDU-6 reactor using CFD," *Nuclear Engineering and Technology* , vol. 37 (6), pp. 575 - 586, 2005.

[34] L. Leung, "Effect of CANDU Bundle-Geometry Variation on Dryout Power," in *16th International Conference on Nuclear Engineering*, Florida, 2008, p. 48827.

[35] S. Hebert, "Identification and leaching of defective low void reactivity fuel," Royal Military College of Canada, Kingston, MR52302, 2009.

[36] AK Steel, Product Data Bulletin - 304/304L Stainless Steel, 2007.

[37] B. Savioni, D. Caceres, I Vergara, R. Gonzalez, and J. Santiuste, "Radiation damage in Neutron Irradiated Yttria-Stabilized-Zirconia Single Crystals," *Journal of Nuclear Materials*, vol. 227, pp. 199-203, 2000.

[38] J. Holman, *Heat Transfer*, 9th ed. New York: McGrawHill, 2002.

[39] Y. Cengel and A. Ghajar, *Heat and Mass Transfer*, 4th ed. New York: McGraw Hill, 2010.

[40] J. Sweet, E. Roth, and M Moss, "Thermal Conductivity of Inconel 718 and Stainless Steel," *International Journal of Thermophysics*, 1987.

[41] E. Ruckestein and R. Rajagopalan, "A Simple Algebraic Method for Obtaining the Heat or Mass Transfer Coefficients Under Mixed Convection," *Chemical Engineering Communications*, 1980.

[42] S.W. Churchill and M. Bernstein, "A Correlating Equation for Forced Convection from Gases and Liquids to a Circular Cylinder in Crossflow," *Journal of Heat Transfer*, vol. 19, pp. 300 - 306, 1977.

[43] S.W. Churchill and H.H.S Chu, "Correlating Equations for Laminar and Turbulent Free Convection from a Horizontal Cylinder," *International Journal of Heat & Mass Transfer*, vol. 18, p. 1049.

[44] M. Kao, M. Lee, Y. Ferng, and C Chieng, "Heat transfer deterioration in a supercritical water channel," *Nuclear Engineering and Design*, vol. 240, pp. 3321 - 3328, 2010.

[45] W. Peiman, E. Saltanov, K. Gabriel, and Pioro. I, "Heat Loss Calculations in a SCWR Fuel-Channel," in *18th International Conference in Nuclear Engineering*, Xi'an, China, 2010.

[46] L. Grande, "Thermal Aspects of Using Alternative Nuclear Fuels in Supercritical Water-Cooled Reactors," UOIT, Oshawa, Canada, 2010.

APPENDIX A: NUMERICAL MODEL IN MATLAB

```
clear all;
clc

P=25000; % Pressure
mdot = 4.37;  % Mass flow rate
d_bundle_centre = 18*10^-3;    % Diameter of unheated fuel rod
d_bundle_elements = 11.5*10^-3; % Diameter of heated fuel rods
p_bundle = pi* 42*d_bundle_elements; % Perimeter of the bundle
A_bundle = (pi/4)*(1*d_bundle_centre^2+ 42*d_bundle_elements^2); % Cross Sectional Area of
bundle
di  = 0.10345;  % Inner diameter of inner(flow) tube
ri = di/2; % Inner radius of inner(flow) tube
do = di + 4*10^-3; % Outer diameter of inner(flow) tube
ro = do/2; % Outer radius of inner(flow) tube
Ac_flow_tube = (pi/4)*di^2; % Cross sectional area of flow tube
A_fl = Ac_flow_tube - A_bundle; % Flow Area of inner(flow) tube
p_wetted = pi*(42*d_bundle_elements + 1*d_bundle_centre + di);  %  Wetted perimeter of
inner(flow) tube
D_hy = 4*A_fl/p_wetted; % Hydraulic diameter of inner(flow) tube
G = mdot/A_fl;  % Mass flux of inner(flow tube)
Di = sqrt((A_fl*4/pi)+do^2);    % Inner d iameter of outer(pressure) tube
Ri = Di/2; % Inner radius of outer(pressure) tube
Do = Di + 14*10^-3; % Outer diameter of outer(pressure) tube
Ro = Do/2; % Outer radius of outer(pressure) tube
A_flow_annulus = (pi/4)*(Di^2 - do^2); % Flow area of annulus
D_hy_annulus = Di - do; % Flow area of annulus
G_annulus = mdot / A_flow_annulus;  % Mass flow of annulus


% INSULATOR
d_ins_in = Do;
r_ins_in = d_ins_in/2;

thickness_ins = 7 ;
d_ins_out = d_ins_in + thickness_ins*2*10^-3;
r_ins_out = d_ins_out/2;


%OUTER TUBE
d_out_in = d_ins_out;
r_out_in = d_out_in/2;

thickness_out = 0.5;
d_out_out = d_out_in + thickness_out*2*10^-3;
r_out_out = d_out_out/2;


 Q = 8.5*10^6; % Channel power
q =  Q / (p_bundle*5.772); % Average heat flux of channel

nodes = 61; % Total nodes
```

```
n = nodes;

x= linspace(0,5.772,nodes);
for i = 1:(n-1);
   X(i) = (x(i)+x(i+1))/2;
   L(i) = x(i+1)-x(i);
end

L1 = [L,L(1)];

for i = 1:(n-1);
   L2(i) = L1(i);
end

As_FT_i = pi * di * L; % Nodal inner surface area of inner(flow) tube
As_FT_o = pi * do * L; % Nodal outer surface area of inner(flow) tube
As_PT_i = pi * Di * L; % Nodal inner surface area of outer(pressure) tube
As_PT_o = pi * Do * L; % Nodal outer surface area of outer(pressure) tube


As_INS_i = pi* d_ins_in * L;
As_INS_o = pi* d_ins_out * L;
As_OUT_i = pi* d_out_in * L;
As_OUT_o = pi* d_out_out * L;


%***** Moderator
T_moderator = 80 + 273.15;
T_m = linspace(T_moderator,T_moderator,nodes-1);
pressure_m = 200; %101.3; % moderator pressure, kPa
g = 9.81;

T_inlet = 623.15; % Inlet temperature 350 C
Cp_cold_fluid_fluid(1) = refpropm('C','T',T_inlet,'P',P,'water'); % Cp from NIST
H_cold_fluid(1)= refpropm('H','T',T_inlet,'P',P,'water');   % Enthalpy from NIST
k_cold_fluid_fluid(1) = refpropm('L','T',T_inlet,'P',P,'water');  % Thermal Conductivity from NIST
mu_cold_fluid_fluid(1) = refpropm('V','T',T_inlet,'P',P,'water'); % Viscosity from NIST
T_cold_fluid = linspace(T_inlet,T_inlet+50,nodes+1);  % Temperature profile for cold fluid
(estimate)

T_cold_initial_guess = T_cold_fluid - 273.15;

T_hot_fluid = linspace(898.15,T_cold_fluid(n+1),nodes+1);  % Temperature profile for hot fluid
(estimate)

T_hot_initial_guess = T_hot_fluid - 273.15;

T_cold_fluid_actual(1) = T_inlet;

for i=1:n-1;
   T_hot_fluid_bulk(i) = (T_hot_fluid(i) + T_hot_fluid(i+1))/2;
   T_cold_fluid_bulk(i) = (T_cold_fluid(i) + T_cold_fluid(i+1))/2;
end;
```

```
for i=1:n-1;
   T_FT_avg(i) = (T_hot_fluid_bulk(i)+T_cold_fluid_bulk(i))/2;
   Ts_FT_i(i) = (T_hot_fluid_bulk(i) + T_FT_avg(i))/2; % Estimate for inner surface temp of flow tube
   Ts_FT_o(i) = (T_cold_fluid_bulk(i) + T_FT_avg(i))/2;

   T_INS_avg(i) = (T_cold_fluid_bulk(i)+ T_m(i))/2;

   T_PT_avg(i) = (T_INS_avg(i)+ T_cold_fluid_bulk(i))/2;
   Ts_PT_i(i) = (T_cold_fluid_bulk(i) + T_PT_avg(i))/2;
   Ts_PT_o(i) = (T_PT_avg(i)+ T_INS_avg(i))/2;

   T_OUT_avg(i) = (T_INS_avg(i)+ T_m(i))/2;
   Ts_OUT_i(i) = (T_OUT_avg(i) + T_INS_avg(i))/2;
   Ts_OUT_o(i) = (T_OUT_avg(i) + T_m(i))/2;

   Ts_INS_i(i) = Ts_PT_o(i);
   Ts_INS_o(i) = Ts_OUT_i(i);

end;

T_sheath = T_hot_fluid_bulk +300; % Initial guess for claddding temp
for i = 1:n-1; % Cladding temp calculations
   delta_T = 4;
   while (delta_T > 0.1)
      H_w =refpropm('H','T',T_sheath(i),'P',P,'water');
      H_b =refpropm('H','T',T_hot_fluid_bulk(i),'P',P,'water');
      Cp = (H_w -H_b)/(T_sheath(i)-T_hot_fluid_bulk(i));
      k =refpropm('L','T',T_hot_fluid_bulk(i),'P',P,'water');
      mu =  refpropm('V','T',T_hot_fluid_bulk(i),'P',P,'water');
      Pr = (mu *Cp )/k;
      rho_b = refpropm('D','T',T_hot_fluid_bulk(i),'P',P,'water');
      rho_w = refpropm('D','T',T_sheath(i),'P',P,'water');
      Re = G * D_hy / mu;
      Nu = 0.0061 * Re^0.904 * Pr^0.684 * (rho_w/rho_b)^0.564;
      h = Nu * k /D_hy;
      T_sheath_new = (q/h)+T_hot_fluid_bulk(i);
      delta_T = abs(T_sheath_new - T_sheath(i));
      T_min = min(T_sheath(i),T_sheath_new);
      T_sheath(i) = T_min +delta_T/2;
   end
      T_outer_sheath(i)= T_sheath(i);
      rho_hot_fluid_b(i)= rho_b;
      rho_hot_fluid_w(i)= rho_w;
      Re_hot_fluid(i)= Re;
      Nu_hot_fluid(i)= Nu;
      Pr_hot_fluid(i)= Pr;
      k_hot_fluid(i) = k;
      h_hot_fluid(i)= h;
      H_hot_fluid(i)= H_b;
end


T_hot_fluid_bulk_actual(1) = T_hot_fluid_bulk(1);
T_cold_fluid_bulk_actual(1) = T_cold_fluid_bulk(1);
```

```
trials = 1;

while(trials)<50

  R_conv_1 = 1./ (h_hot_fluid .*As_FT_i); % Resistance of Hot fluid

  for i=1:n-1;
    T_FT_avg_r(i) = (Ts_FT_i(i) + Ts_FT_o(i))/2;
    k_FT(i) =(2*10^(-6))*(T_FT_avg_r(i)^2) + 0.0134 * T_FT_avg_r(i) + 10.689; % Conductivity of
flow tube
    R_cond_1(i) = (log(ro/ri))/(2*pi*L2(i)* k_FT(i)); % Resistance of flow tube
  end

  for i =1:n-1; % Cold fluid thermophysical properties
    H_cold_fluid_w(i) = refpropm('H','T',Ts_FT_o(i),'P',P,'water');
    H_cold_fluid_b(i) = refpropm('H','T',T_cold_fluid_bulk(i),'P',P,'water');
    Cp_cold_fluid(i) = (H_cold_fluid_w(i) - H_cold_fluid_b(i))/(Ts_FT_o(i)-T_cold_fluid_bulk(i));
    k_cold_fluid(i) = refpropm('L','T',T_cold_fluid_bulk(i),'P',P,'water');
    mu_cold_fluid(i) =  refpropm('V','T',T_cold_fluid_bulk(i),'P',P,'water');
    Pr_cold_fluid(i) = (mu_cold_fluid(i) *Cp_cold_fluid(i))/k_cold_fluid(i);
    rho_cold_fluid_b(i) = refpropm('D','T',T_cold_fluid_bulk(i),'P',P,'water');
    rho_cold_fluid_w(i) = refpropm('D','T',Ts_FT_o(i),'P',P,'water');
    Re_cold_fluid(i) = G_annulus * D_hy_annulus / mu_cold_fluid(i);
    Nu_cold_fluid(i) = 0.0061 * Re_cold_fluid(i)^0.904 * Pr_cold_fluid(i)^0.684 *
(rho_cold_fluid_w(i)/rho_cold_fluid_b(i))^0.564;
    h_cold_fluid(i) = Nu_cold_fluid(i) * k_cold_fluid(i) /D_hy_annulus;
  end

  R_conv_2 = 1./(h_cold_fluid .* As_PT_i); % Resistance of cold fluid


  %******* PRESSURE TUBE
  for i = 1:n-1;
     T_PT_avg_r(i) = (Ts_PT_i(i) + Ts_PT_o(i))/2;
     k_PT(i) =((2*10^(-6))*T_PT_avg_r(i)^2 + 0.0134* T_PT_avg_r(i) + 10.689);
     R_cond_2(i) = (log(Ro/Ri))/(2 * pi * L2(i) * k_PT(i));

  end


  %********INSULATION

  for i = 1:n-1;
    T_INS_avg(i) = (Ts_INS_i(i) + Ts_INS_o(i))/ 2;
    th_cond_air(i) = 8*10^(-5)*T_INS_avg(i) - 0.0072;  %% CO2
    k_INS(i) = 2.7 *0.3 + 0.7*th_cond_air(i) ; % Conductivity of insulation
    R_cond_INS(i) = (log(r_ins_out/r_ins_in))/(2*pi*L2(i)*k_INS(i)); % Resistance of insulation
  end

  %********OUTER TUBE

  for i=1:n-1;
    T_OUT_avg_r(i) = (Ts_OUT_i(i) + Ts_OUT_o(i))/2;
    k_OUT(i) =((2*10^(-6))*(T_OUT_avg_r(i))^2 + 0.0134 * T_OUT_avg_r(i) + 10.689);
    R_cond_OUT(i) = (log(r_out_out/r_out_in))/(2 * pi * L2(i)* k_OUT(i));
```

```
end


%********MODERATOR

for i = 1:n-1;
  T_m_PT_avg(i) = (T_m(i) + Ts_OUT_o(i))/2;

  if (T_m_PT_avg(i)>394.55)
     T_m_PT_avg(i) = 394.55;
  end
  beta_m(i) = 1 /T_m_PT_avg(i);
end


for i = 1:n-1;
   density_m(i) = refpropm('D','T',T_m_PT_avg(i),'P',pressure_m,'D2O');
   viscosity_m(i) = refpropm('V','T',T_m_PT_avg(i),'P',pressure_m,'D2O');
   k_m(i) = refpropm('L','T',T_m_PT_avg(i),'P',pressure_m,'D2O');
   Cp_m(i) = refpropm('C','T',T_m_PT_avg(i),'P',pressure_m,'D2O');
end
Pr_m = viscosity_m .* Cp_m ./k_m;
k_viscosity_m = viscosity_m ./ density_m;

% FREE CONVECTION

for i = 1:n-1;

   if(Ts_OUT_o(i))<T_m(i)
      Ts_OUT_o(i) = T_m(i);
   end

   Ra_m_D4(i) = (g * beta_m(i)*(Ts_OUT_o(i) - T_m(i))*d_out_out^3*
Pr_m(i))/((k_viscosity_m(i))^2);
   Nu_m_D4_free(i) = (0.6 + (0.387 * Ra_m_D4(i)^(1/6))/(1 +
(0.559/Pr_m(i))^(9/16))^(8/27))^2;
end

% FORCED CONVECTION

for i = 1:n-1;

Re_m_D4(i) = (0.95*d_out_out)/k_viscosity_m(i); % v=0.018
Nu_m_D4_forced(i) = 0.3 +
((0.62*(Re_m_D4(i)^(1/2))*(Pr_m(i)^(1/3)))/((1+(0.4/(Pr_m(i)))^(2/3))^(1/4)))*(1+((Re_m_D
4(i)/282000)^(5/8)))^(4/5);

if (Re_m_D4(i)>20000 && Re_m_D4(i)<400000)
   Nu_m_D4_forced(i) = 0.3 +
((0.62*(Re_m_D4(i)^(1/2))*(Pr_m(i)^(1/3)))/((1+(0.4/(Pr_m(i)))^(2/3))^(1/4)))*(1+((Re_m_D
4(i)/282000)^(1/2)));
end
end
```

```
 Nu_m_D4 = (Nu_m_D4_free.^3 + Nu_m_D4_forced.^3).^(1/3);

 h_m_D4 = k_m .* Nu_m_D4 ./ d_out_out;

 R_m = 1 ./(h_m_D4 .* As_OUT_o);
 R_mm = 1 ./(h_m_D4 .* pi * d_out_out);

 MOD_HEAT_LOSS = h_m_D4.*(3.142.*d_out_out.*0.0962).*(Ts_OUT_o - T_m);

 MOD_HEAT_LOSS_TOTAL = sum(MOD_HEAT_LOSS);

R_total = R_conv_1 + R_cond_1 + R_conv_2; % Total Resistance
UA = 1./ R_total;   % UA

DeltaT = T_hot_fluid_bulk - T_cold_fluid_bulk;

Qdot = UA .* DeltaT;

Qdot_total = sum(Qdot);

%*******Heat Loss to Moderator
R_m_total = R_conv_2 + R_cond_2 + R_cond_INS + R_cond_OUT + R_m;

UA_m = (1./ R_m_total);
DeltaT_m = T_cold_fluid_bulk - T_m;
heat_loss_m = UA_m .* DeltaT_m;

heat_loss_m_total = sum(heat_loss_m);

qdot = Qdot ./ As_FT_i;

Qdot_net = Qdot - heat_loss_m;

for i=1:n-1; % Cold fluid end temp using Qdot
   H_cold_fluid(i+1) = (H_cold_fluid(i)+ (Qdot_net(i)/mdot));
   T_cold_fluid_actual(i+1) =  refpropm('T','H',H_cold_fluid(i+1),'P',P,'water');
end

for i=1:n-1;
   T_cold_fluid_bulk_actual(i) = (T_cold_fluid_actual(i) + T_cold_fluid_actual(i+1))/2;
end


Q_net = Q - Qdot_total; %Net Heat (Power - Total Heat loss)

q =  Q_net/ (p_bundle*5.772);   % Avg heat flux for hot side

%Variable Power Profile

bp = [182.13 420.71 561.36 600.54 664.07 713.65 713.56 663.83 583.41 518.38 377.96 165.55];
bp =  [.21188E+03  .48466E+03  .63500E+03  .65889E+03  .70094E+03  .72986E+03
.72492E+03  .68886E+03  .62404E+03  .57426E+03  .42741E+03  .18914E+03 ];
bp =   [.20216E+03  .48237E+03  .67457E+03  .77740E+03  .77341E+03 68315E+03  .45170E+03
.50743E+03  .60024E+03  .52531E+03  .37295E+03  .15740E+03];
```

```
bp =  [.18057E+03  .43223E+03  .64382E+03  .85966E+03  .10684E+04  .10857E+04
.10855E+04  .10681E+04  .83568E+03  .59492E+03  .38855E+03  .16415E+03];
bp = [625 850 1010 1040 1000 950 850 775 625 475 175 125];
bp = [125 175  475 625 775 850 950 1000 1040 1010 850 625];
bp = [708.33 708.33 708.33 708.33 708.33 708.33 708.33 708.33 708.33 708.33 708.33 708.33];

bp(end:-1:1);

test_bp_total = sum(bp);

for k=1:11
   avg(k) = (bp(k)+bp(k+1))/2;
   bundlepower_old(k+1) = avg(k);
end
bundlepower_old(1) = 0;
bundlepower_old(13)= 0;


sum_bundlepower_old = sum(bundlepower_old);
diff_bundlepower_old = 8500 - sum_bundlepower_old;
add_bundlepower = diff_bundlepower_old/12;
bundlepower = bundlepower_old + add_bundlepower;
sum_bundlepower_new = sum(bundlepower);
y = bundlepower.*2.079;

% Node 1

a = 1;
b = 2;
i = 1;
j = 1;

while(a<13)

y1 = y(a);
y2 = y(b);

for mu = 0: 0.2: 1
   val(i) = (y1*(1-mu)+y2*mu);
   i = i+1;
end


for j=j:i-2;
   nodalpower(j) = ((val(j)+val(j+1))/2)*0.0962;
end;

i = i - 1;
j = j + 1;

a = a + 1;
b = b + 1;

end
```

```
totalnodalpower = sum(nodalpower);

x = linspace(0,5.772,61);
val=val./2.079;

plot(x,val)


   q_diff = (nodalpower.*1000)- Qdot;
   q_prime = (q_diff)./(p_bundle*0.0962);



   T_mixing =  T_cold_fluid_actual(n-1)+ ((6.1 - (5.772-L1(1)))/((5.772-L1(1)/2) - (5.772-
L1(1))))*(T_cold_fluid_actual(n)-T_cold_fluid_actual(n-1));


   T_hot_fluid_actual(n)= 2*T_mixing - T_cold_fluid_actual(n);
   H_hot_fluid_actual(n) = refpropm('H','T',T_hot_fluid_actual(n),'P',P,'water'); % Enthalpy for first
node



temp1 = n;
for i = 1:n-1; % Actual enthalpies & temp for hot fluid
   H_hot_fluid_actual(temp1-1) = (H_hot_fluid_actual(temp1)+ (p_bundle * q_prime(i)* L(i))/(mdot
));
   T_hot_fluid_actual(temp1-1) =  refpropm('T','H',H_hot_fluid_actual(temp1-1),'P',P,'water');
   temp1 = temp1 - 1;
end

for i=1:n-1;
   T_hot_fluid_bulk_actual(i) = (T_hot_fluid_actual(i) + T_hot_fluid_actual(i+1))/2;
end


T_sheath_actual = T_hot_fluid_bulk_actual +300;

   for i = 1:n-1;
      delta_T = 4;
      while (delta_T > 0.1)
      H_w =refpropm('H','T',T_sheath_actual(i),'P',P,'water');
      H_b =refpropm('H','T',T_hot_fluid_bulk_actual(i),'P',P,'water');
      Cp = (H_w -H_b)/(T_sheath_actual(i)-T_hot_fluid_bulk_actual(i));
      k =refpropm('L','T',T_hot_fluid_bulk_actual(i),'P',P,'water');
      mu =  refpropm('V','T',T_hot_fluid_bulk_actual(i),'P',P,'water');
      Pr = (mu *Cp )/k;
      rho_b = refpropm('D','T',T_hot_fluid_bulk_actual(i),'P',P,'water');
      rho_w = refpropm('D','T',T_sheath_actual(i),'P',P,'water');
      Re = G * D_hy / mu;
      Nu = 0.0061 * Re^0.904 * Pr^0.684 * (rho_w/rho_b)^0.564;
      h = Nu * k /D_hy;
      T_sheath_actual_new = (q_prime(i)/h)+T_hot_fluid_bulk_actual(i);
      delta_T = abs(T_sheath_actual_new - T_sheath_actual(i));
      T_min_actual = min(T_sheath_actual(i),T_sheath_actual_new);
```

```
    T_sheath_actual(i) = T_min_actual +delta_T/2;
    end
    T_outer_sheath(i)= T_sheath_actual(i);
    if T_outer_sheath(i)< T_hot_fluid_bulk_actual(i)
      T_outer_sheath(i) = T_hot_fluid_bulk_actual(i);
    end
    h_hot_fluid(i)= h;
  end



  T_hot_fluid = T_hot_fluid_actual;
  T_cold_fluid = T_cold_fluid_actual;

  T_cold_fluid_bulk = T_cold_fluid_bulk_actual;
  T_hot_fluid_bulk = T_hot_fluid_bulk_actual;

  Ts_FT_i = T_hot_fluid_bulk - Qdot .* (R_conv_1);
  Ts_FT_o = T_hot_fluid_bulk - Qdot .* (R_conv_1 + R_cond_1);

  Ts_PT_i = T_cold_fluid_bulk - (heat_loss_m) .*(R_conv_2);
  Ts_PT_o = T_cold_fluid_bulk - (heat_loss_m) .*(R_conv_2 + R_cond_2);

  Ts_INS_i = Ts_PT_o;
  Ts_INS_o = T_cold_fluid_bulk - (heat_loss_m) .*(R_conv_2 + R_cond_2 + R_cond_INS);


  Ts_OUT_i = Ts_INS_o;
  Ts_OUT_o = T_cold_fluid_bulk - (heat_loss_m) .*(R_conv_2 + R_cond_2 + R_cond_INS +
R_cond_OUT);


  for i=1:n-1;
     if(Ts_OUT_o(i)<T_m(i))
       Ts_OUT_o(i) = T_m(i);
     end

  end

  trials = trials + 1;

end

Ts_FT_end_avg = (T_hot_fluid(n)+T_cold_fluid(n))./2;
Ts_FT_i_plot(n) = (Ts_FT_end_avg+T_hot_fluid(n))./2;
Ts_FT_o_plot(n) = (Ts_FT_end_avg+T_cold_fluid(n))./2;


T_INS_end_avg = (T_cold_fluid(n)+ T_m(n-1))./2;

T_PT_end_avg = (T_INS_end_avg + T_cold_fluid(n))./2;


for i = 1:n-2;
  Ts_FT_i_plot(i+1) = (Ts_FT_i(i) + Ts_FT_i(i+1))/2;
```

```
  Ts_FT_o_plot(i+1) = (Ts_FT_o(i) + Ts_FT_o(i+1))/2;
end

Ts_FT_i_plot(1) =  Ts_FT_i_plot(2)+ ((0 - L1(1))/(L1(1)/2 - L1(1)))*(Ts_FT_i(1)-Ts_FT_i_plot(2));
Ts_FT_o_plot(1) =  Ts_FT_o_plot(2)+ ((0 - L1(1))/(L1(1)/2 - L1(1)))*(Ts_FT_o(1)-Ts_FT_o_plot(2));



for i = 1:n-2;
  Ts_PT_i_plot(i+1) = (Ts_PT_i(i) + Ts_PT_i(i+1))/2;
  Ts_PT_o_plot(i+1) = (Ts_PT_o(i) + Ts_PT_o(i+1))/2;
end

Ts_PT_i_plot(1) =  Ts_PT_i_plot(2)+ ((0 - L1(1))/(L1(1)/2 - L1(1)))*(Ts_PT_i(1)-Ts_PT_i_plot(2));
Ts_PT_o_plot(1) =  Ts_PT_o_plot(2)+ ((0 - L1(1))/(L1(1)/2 - L1(1)))*(Ts_PT_o(1)-
Ts_PT_o_plot(2));


for i = 1:n-2;
  Ts_INS_i_plot(i+1) = (Ts_INS_i(i) + Ts_INS_i(i+1))/2;
  Ts_INS_o_plot(i+1) = (Ts_INS_o(i) + Ts_INS_o(i+1))/2;
end

Ts_INS_i_plot(1) =  Ts_INS_i_plot(2)+ ((0 - L1(1))/(L1(1)/2 - L1(1)))*(Ts_INS_i(1)-
Ts_INS_i_plot(2));
Ts_INS_o_plot(1) =  Ts_INS_o_plot(2)+ ((0 - L1(1))/(L1(1)/2 - L1(1)))*(Ts_INS_o(1)-
Ts_INS_o_plot(2));


for i = 1:n-2;
  Ts_OUT_i_plot(i+1) = (Ts_OUT_i(i) + Ts_OUT_i(i+1))/2;
  Ts_OUT_o_plot(i+1) = (Ts_OUT_o(i) + Ts_OUT_o(i+1))/2;
end

Ts_OUT_i_plot(1) =  Ts_OUT_i_plot(2)+ ((0 - L1(1))/(L1(1)/2 - L1(1)))*(Ts_OUT_i(1)-
Ts_OUT_i_plot(2));
Ts_OUT_o_plot(1) =  Ts_OUT_o_plot(2)+ ((0 - L1(1))/(L1(1)/2 - L1(1)))*(Ts_OUT_o(1)-
Ts_OUT_o_plot(2));



Ts_PT_i_plot(n) = Ts_PT_i_plot(n-1);
Ts_PT_o_plot(n) = Ts_PT_o_plot(n-1);


Ts_OUT_i_plot(n) = Ts_OUT_i_plot(n-1);
Ts_OUT_o_plot(n) = Ts_OUT_o_plot(n-1);

Ts_INS_i_plot(n) = Ts_INS_i_plot(n-1);
Ts_INS_o_plot(n) = Ts_INS_o_plot(n-1);


 for i = 1:n-2;
  T_outer_sheath_plot(i+1) = (T_outer_sheath(i) + T_outer_sheath(i+1))/2;
  if T_outer_sheath_plot(i+1)< T_hot_fluid_bulk_actual(i+1)
```

```
        T_outer_sheath_plot(i+1) = T_hot_fluid_bulk_actual(i+1);
    end
end

T_outer_sheath_plot(1) =  T_outer_sheath_plot(2)+ ((0 - L1(1))/(L1(1)/2 -
L1(1)))*(T_outer_sheath(1)-T_outer_sheath_plot(2));

T_outer_sheath_plot(n) =  T_outer_sheath_plot(n-1)+ ((5.772 - (5.772-L1(1)))/((5.772-L1(1)/2) -
(5.772-L1(1))))*(T_outer_sheath(n-1)-T_outer_sheath_plot(n-1));


for i = 1:n-2;
  qdot_plot(i+1) = (qdot(i) + qdot(i+1))/2;
end

qdot_plot(1) =  qdot_plot(2)+ ((0 - L1(1))/(L1(1)/2 - L1(1)))*(qdot(1)-qdot_plot(2));
qdot_plot(n) =  qdot_plot(n-1)+ ((5.772 - (5.772-L1(1)))/((5.772-L1(1)/2) - (5.772-
L1(1))))*(qdot(n-1)-qdot_plot(n-1));


 T_hot_fluid(n+1) = T_mixing;
T_cold_fluid(n+1) = T_mixing;


%Properties of hot fluid

for i=1:n-1;
  H_hot_fluid_w_actual(i) = refpropm('H','T',T_outer_sheath(i),'P',P,'water');
  H_hot_fluid_b_actual(i) = refpropm('H','T',T_hot_fluid_bulk(i),'P',P,'water');
  Cp_hot_fluid_actual(i) = (H_hot_fluid_w_actual(i) - H_hot_fluid_b_actual(i))/(T_outer_sheath(i)-
T_hot_fluid_bulk(i));
  k_hot_fluid_actual(i) = refpropm('L','T',T_hot_fluid_bulk(i),'P',P,'water');
  mu_hot_fluid_actual(i) =  refpropm('V','T',T_hot_fluid_bulk(i),'P',P,'water');
  Pr_hot_fluid_actual(i) = (mu_hot_fluid_actual(i) *Cp_hot_fluid_actual(i))/k_hot_fluid_actual(i);
  rho_hot_fluid_b_actual(i) = refpropm('D','T',T_hot_fluid_bulk(i),'P',P,'water');
  rho_hot_fluid_w_actual(i) = refpropm('D','T',T_outer_sheath(i),'P',P,'water');
  Re_hot_fluid_actual(i) = G * D_hy / mu_hot_fluid_actual(i);
  Nu_hot_fluid_actual(i) = 0.0061 * Re_hot_fluid_actual(i)^0.904 * Pr_hot_fluid_actual(i)^0.684 *
(rho_hot_fluid_w_actual(i)/rho_hot_fluid_b_actual(i))^0.564;
  h_hot_fluid_actual(i) = Nu_hot_fluid_actual(i) * k_hot_fluid_actual(i) /D_hy;
end

for i = 1:n-2;
  H_hot_fluid_w_actual_plot(i+1) = (H_hot_fluid_w_actual(i)+ H_hot_fluid_w_actual(i+1))./2;
  H_hot_fluid_b_actual_plot(i+1) = (H_hot_fluid_b_actual(i) + H_hot_fluid_b_actual(i+1))./2;
  Cp_hot_fluid_actual_plot(i+1) = (Cp_hot_fluid_actual(i)+ Cp_hot_fluid_actual(i+1))./2;
  k_hot_fluid_actual_plot(i+1) = (k_hot_fluid_actual(i) + k_hot_fluid_actual(i+1))./2;
  mu_hot_fluid_actual_plot(i+1) = (mu_hot_fluid_actual(i) + mu_hot_fluid_actual(i+1))./2;
  Pr_hot_fluid_actual_plot(i+1) = (Pr_hot_fluid_actual(i) + Pr_hot_fluid_actual(i+1))./2;
  rho_hot_fluid_b_actual_plot(i+1) = (rho_hot_fluid_b_actual(i) + rho_hot_fluid_b_actual(i+1))./2;
  rho_hot_fluid_w_actual_plot(i+1) = (rho_hot_fluid_w_actual(i) + rho_hot_fluid_w_actual(i+1))./2;
  Re_hot_fluid_actual_plot(i+1) = (Re_hot_fluid_actual(i)+ Re_hot_fluid_actual(i+1))./2;
  Nu_hot_fluid_actual_plot(i+1) = (Nu_hot_fluid_actual(i) + Nu_hot_fluid_actual(i+1))./2;
  h_hot_fluid_actual_plot(i+1) = (h_hot_fluid_actual(i) + h_hot_fluid_actual(i+1))./2;
```

```
end

   H_hot_fluid_w_actual_plot(1) = refpropm('H','T',T_outer_sheath_plot(1),'P',P,'water');
   H_hot_fluid_b_actual_plot(1) = refpropm('H','T',T_hot_fluid(1),'P',P,'water');
   Cp_hot_fluid_actual_plot(1) = (H_hot_fluid_w_actual_plot(1) -
H_hot_fluid_b_actual_plot(1))/(T_outer_sheath_plot(1)-T_hot_fluid(1));
   k_hot_fluid_actual_plot(1) = refpropm('L','T',T_hot_fluid(1),'P',P,'water');
   mu_hot_fluid_actual_plot(1) =  refpropm('V','T',T_hot_fluid(1),'P',P,'water');
   Pr_hot_fluid_actual_plot(1) = (mu_hot_fluid_actual_plot(1)
*Cp_hot_fluid_actual_plot(1))/k_hot_fluid_actual_plot(1);
   rho_hot_fluid_b_actual_plot(1) = refpropm('D','T',T_hot_fluid(1),'P',P,'water');
   rho_hot_fluid_w_actual_plot(1) = refpropm('D','T',T_outer_sheath_plot(1),'P',P,'water');
   Re_hot_fluid_actual_plot(1) = G * D_hy / mu_hot_fluid_actual_plot(1);
   Nu_hot_fluid_actual_plot(1) = 0.0061 * Re_hot_fluid_actual_plot(1)^0.904 *
Pr_hot_fluid_actual_plot(1)^0.684 *
(rho_hot_fluid_w_actual_plot(1)/rho_hot_fluid_b_actual_plot(1))^0.564;
   h_hot_fluid_actual_plot(1) = Nu_hot_fluid_actual_plot(1) * k_hot_fluid_actual_plot(1) /D_hy;

   H_hot_fluid_w_actual_plot(n) = refpropm('H','T',T_outer_sheath_plot(n),'P',P,'water');
   H_hot_fluid_b_actual_plot(n) = refpropm('H','T',T_hot_fluid(n),'P',P,'water');
   Cp_hot_fluid_actual_plot(n) = (H_hot_fluid_w_actual_plot(n) -
H_hot_fluid_b_actual_plot(n))/(T_outer_sheath_plot(n)-T_hot_fluid(n));
   k_hot_fluid_actual_plot(n) = refpropm('L','T',T_hot_fluid(n),'P',P,'water');
   mu_hot_fluid_actual_plot(n) =  refpropm('V','T',T_hot_fluid(n),'P',P,'water');
   Pr_hot_fluid_actual_plot(n) = (mu_hot_fluid_actual_plot(n)
*Cp_hot_fluid_actual_plot(n))/k_hot_fluid_actual_plot(n);
   rho_hot_fluid_b_actual_plot(n) = refpropm('D','T',T_hot_fluid(n),'P',P,'water');
   rho_hot_fluid_w_actual_plot(n) = refpropm('D','T',T_outer_sheath_plot(n),'P',P,'water');
   Re_hot_fluid_actual_plot(n) = G * D_hy / mu_hot_fluid_actual_plot(n);
   Nu_hot_fluid_actual_plot(n) = 0.0061 * Re_hot_fluid_actual_plot(n)^0.904 *
Pr_hot_fluid_actual_plot(n)^0.684 *
(rho_hot_fluid_w_actual_plot(n)/rho_hot_fluid_b_actual_plot(n))^0.564;
   h_hot_fluid_actual_plot(n) = Nu_hot_fluid_actual_plot(n) * k_hot_fluid_actual_plot(n) /D_hy;

%Properties of cold fluid

for i=1:n-1;
   H_cold_fluid_w_actual(i) = refpropm('H','T',Ts_FT_o(i),'P',P,'water');
   H_cold_fluid_b_actual(i) = refpropm('H','T',T_cold_fluid_bulk(i),'P',P,'water');
   Cp_cold_fluid_actual(i) = (H_cold_fluid_w_actual(i) - H_cold_fluid_b_actual(i))/(Ts_FT_o(i)-
T_cold_fluid_bulk(i));
   k_cold_fluid_actual(i) = refpropm('L','T',T_cold_fluid_bulk(i),'P',P,'water');
   mu_cold_fluid_actual(i) =  refpropm('V','T',T_cold_fluid_bulk(i),'P',P,'water');
   Pr_cold_fluid_actual(i) = (mu_cold_fluid_actual(i) *Cp_cold_fluid_actual(i))/k_cold_fluid_actual(i);
   rho_cold_fluid_b_actual(i) = refpropm('D','T',T_cold_fluid_bulk(i),'P',P,'water');
   rho_cold_fluid_w_actual(i) = refpropm('D','T',Ts_FT_o(i),'P',P,'water');
   Re_cold_fluid_actual(i) = G_annulus * D_hy_annulus / mu_cold_fluid_actual(i);
   Nu_cold_fluid_actual(i) = 0.0061 * Re_cold_fluid_actual(i)^0.904 * Pr_cold_fluid_actual(i)^0.684 *
(rho_cold_fluid_w_actual(i)/rho_cold_fluid_b_actual(i))^0.564;
   h_cold_fluid_actual(i) = Nu_cold_fluid_actual(i) * k_cold_fluid_actual(i) /D_hy_annulus;
end

for i = 1:n-2;
   H_cold_fluid_w_actual_plot(i+1) = (H_cold_fluid_w_actual(i)+ H_cold_fluid_w_actual(i+1))./2;
   H_cold_fluid_b_actual_plot(i+1) = (H_cold_fluid_b_actual(i) + H_cold_fluid_b_actual(i+1))./2;
```

```
   Cp_cold_fluid_actual_plot(i+1) = (Cp_cold_fluid_actual(i)+ Cp_cold_fluid_actual(i+1))./2;
   k_cold_fluid_actual_plot(i+1) = (k_cold_fluid_actual(i) + k_cold_fluid_actual(i+1))./2;
   mu_cold_fluid_actual_plot(i+1) = (mu_cold_fluid_actual(i) + mu_cold_fluid_actual(i+1))./2;
   Pr_cold_fluid_actual_plot(i+1) = (Pr_cold_fluid_actual(i) + Pr_cold_fluid_actual(i+1))./2;
   rho_cold_fluid_b_actual_plot(i+1) = (rho_cold_fluid_b_actual(i) + rho_cold_fluid_b_actual(i+1))./2;
   rho_cold_fluid_w_actual_plot(i+1) = (rho_cold_fluid_w_actual(i) +
rho_cold_fluid_w_actual(i+1))./2;
   Re_cold_fluid_actual_plot(i+1) = (Re_cold_fluid_actual(i)+ Re_cold_fluid_actual(i+1))./2;
   Nu_cold_fluid_actual_plot(i+1) = (Nu_cold_fluid_actual(i) + Nu_cold_fluid_actual(i+1))./2;
   h_cold_fluid_actual_plot(i+1) = (h_cold_fluid_actual(i) + h_cold_fluid_actual(i+1))./2;

end

   H_cold_fluid_w_actual_plot(1) = refpropm('H','T',Ts_FT_o_plot(1),'P',P,'water');
   H_cold_fluid_b_actual_plot(1) = refpropm('H','T',T_cold_fluid(1),'P',P,'water');
   Cp_cold_fluid_actual_plot(1) = (H_cold_fluid_w_actual_plot(1) -
H_cold_fluid_b_actual_plot(1))/(Ts_FT_o_plot(1)-T_cold_fluid(1));
   k_cold_fluid_actual_plot(1) = refpropm('L','T',T_cold_fluid(1),'P',P,'water');
   mu_cold_fluid_actual_plot(1) =  refpropm('V','T',T_cold_fluid(1),'P',P,'water');
   Pr_cold_fluid_actual_plot(1) = (mu_cold_fluid_actual_plot(1)
*Cp_cold_fluid_actual_plot(1))/k_cold_fluid_actual_plot(1);
*   rho_cold_fluid_b_actual_plot(1) = refpropm('D','T',T_cold_fluid(1),'P',P,'water');
   rho_cold_fluid_w_actual_plot(1) = refpropm('D','T',Ts_FT_o_plot(1),'P',P,'water');
   Re_cold_fluid_actual_plot(1) = G_annulus * D_hy_annulus / mu_cold_fluid_actual_plot(1);
   Nu_cold_fluid_actual_plot(1) = 0.0061 * Re_cold_fluid_actual_plot(1)^0.904 *
Pr_cold_fluid_actual_plot(1)^0.684 *
(rho_cold_fluid_w_actual_plot(1)/rho_cold_fluid_b_actual_plot(1))^0.564;
   h_cold_fluid_actual_plot(1) = Nu_cold_fluid_actual_plot(1) * k_cold_fluid_actual_plot(1)
/D_hy_annulus;

   H_cold_fluid_w_actual_plot(n) = refpropm('H','T',Ts_FT_o_plot(n),'P',P,'water');
   H_cold_fluid_b_actual_plot(n) = refpropm('H','T',T_cold_fluid(n),'P',P,'water');
   Cp_cold_fluid_actual_plot(n) = (H_cold_fluid_w_actual_plot(n) -
H_cold_fluid_b_actual_plot(n))/(Ts_FT_o_plot(n)-T_cold_fluid(n));
   k_cold_fluid_actual_plot(n) = refpropm('L','T',T_cold_fluid(n),'P',P,'water');
   mu_cold_fluid_actual_plot(n) =  refpropm('V','T',T_cold_fluid(n),'P',P,'water');
   Pr_cold_fluid_actual_plot(n) = (mu_cold_fluid_actual_plot(n)
*Cp_cold_fluid_actual_plot(n))/k_cold_fluid_actual_plot(n);
   rho_cold_fluid_b_actual_plot(n) = refpropm('D','T',T_cold_fluid(n),'P',P,'water');
   rho_cold_fluid_w_actual_plot(n) = refpropm('D','T',Ts_FT_o_plot(n),'P',P,'water');
   Re_cold_fluid_actual_plot(n) = G_annulus * D_hy_annulus / mu_cold_fluid_actual_plot(n);
   Nu_cold_fluid_actual_plot(n) = 0.0061 * Re_cold_fluid_actual_plot(n)^0.904 *
Pr_cold_fluid_actual_plot(n)^0.684 *
(rho_cold_fluid_w_actual_plot(n)/rho_cold_fluid_b_actual_plot(n))^0.564;
   h_cold_fluid_actual_plot(n) = Nu_cold_fluid_actual_plot(n) * k_cold_fluid_actual_plot(n)
/D_hy_annulus;



% Properties at bulk from NIST

for i=1:n+1;
   H_cold_bulk_prop(i) = refpropm('H','T',T_cold_fluid(i),'P',P,'water');
   Cp_cold_bulk_prop(i) = refpropm('C','T',T_cold_fluid(i),'P',P,'water');
   k_cold_bulk_prop(i) = refpropm('L','T',T_cold_fluid(i),'P',P,'water');
```

```
    mu_cold_bulk_prop(i) = refpropm('V','T',T_cold_fluid(i),'P',P,'water');
    rho_cold_bulk_prop(i) = refpropm('D','T',T_cold_fluid(i),'P',P,'water');
    Pr_cold_bulk_prop(i) = (mu_cold_bulk_prop(i)*Cp_cold_bulk_prop(i))/k_cold_bulk_prop(i);


    H_hot_bulk_prop(i) = refpropm('H','T',T_hot_fluid(i),'P',P,'water');
    Cp_hot_bulk_prop(i) = refpropm('C','T',T_hot_fluid(i),'P',P,'water');
    k_hot_bulk_prop(i) = refpropm('L','T',T_hot_fluid(i),'P',P,'water');
    mu_hot_bulk_prop(i) = refpropm('V','T',T_hot_fluid(i),'P',P,'water');
    rho_hot_bulk_prop(i) = refpropm('D','T',T_hot_fluid(i),'P',P,'water');
    Pr_hot_bulk_prop(i) = (mu_hot_bulk_prop(i)*Cp_hot_bulk_prop(i))/k_hot_bulk_prop(i);


end
```

APPENDIX B: VERIFICATION OF NUMERICAL MODEL

The temperature of the coolant in the hot side of the reference case REC was compared to the bulk fluid temperature of the HEC published by Grande for a channel power of 8.5 MW_{th}, mass flow rate of 4.37 kg/s, uniform heat flux and no heat loss to the moderator [**46**]. Figure B1 shows the two temperature profiles. The largest difference is approximately 5% at $x = 0\ m$. This is because the coolant in the REC is preheated in the cold side before it enters the fuelled region. The figure validates the MATLAB code shown in Appendix A.

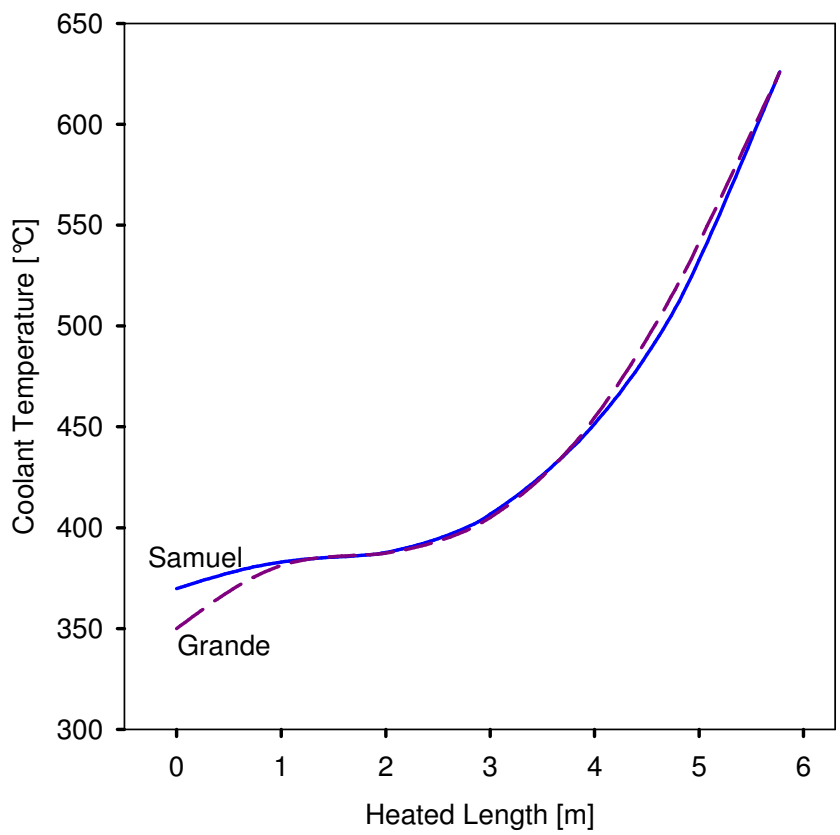

Figure B.1: Comparison of coolant temperature between profile for a total channel power of 8.5 MW_{th}, mass flow rate of 4.37 kg/s, uniform heat flux and no heat loss to the moderator

APPENDIX C: IMPACT OF INSULATORS – THERMOPHYSICAL PROPERTIES

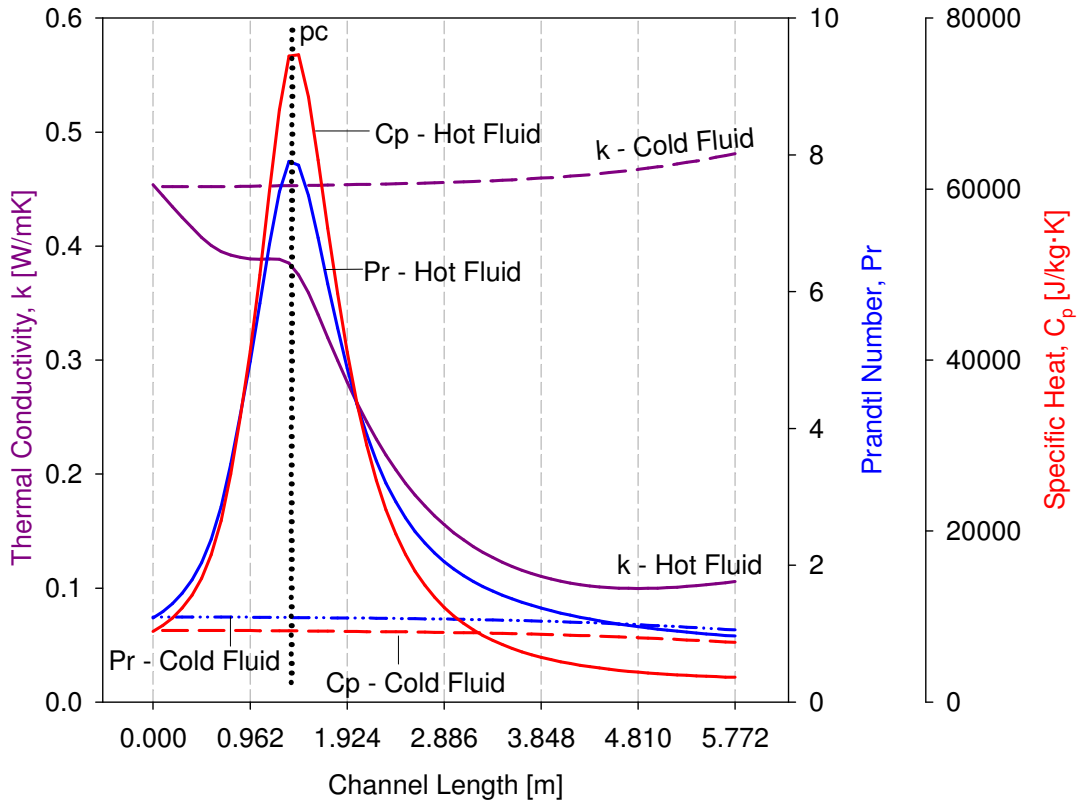

Figure C 1(a): Specific heat, thermal conductivity and Prandtl number profiles along a YSZ insulated fuel-channel for a channel power of 8.5 MW_{th}, inner-tube thickness of 2 mm, pressure tube thickness of 11 mm, inlet temperature of 350°C, mass flow rate of 4.37 kg/s and uniform heat flux

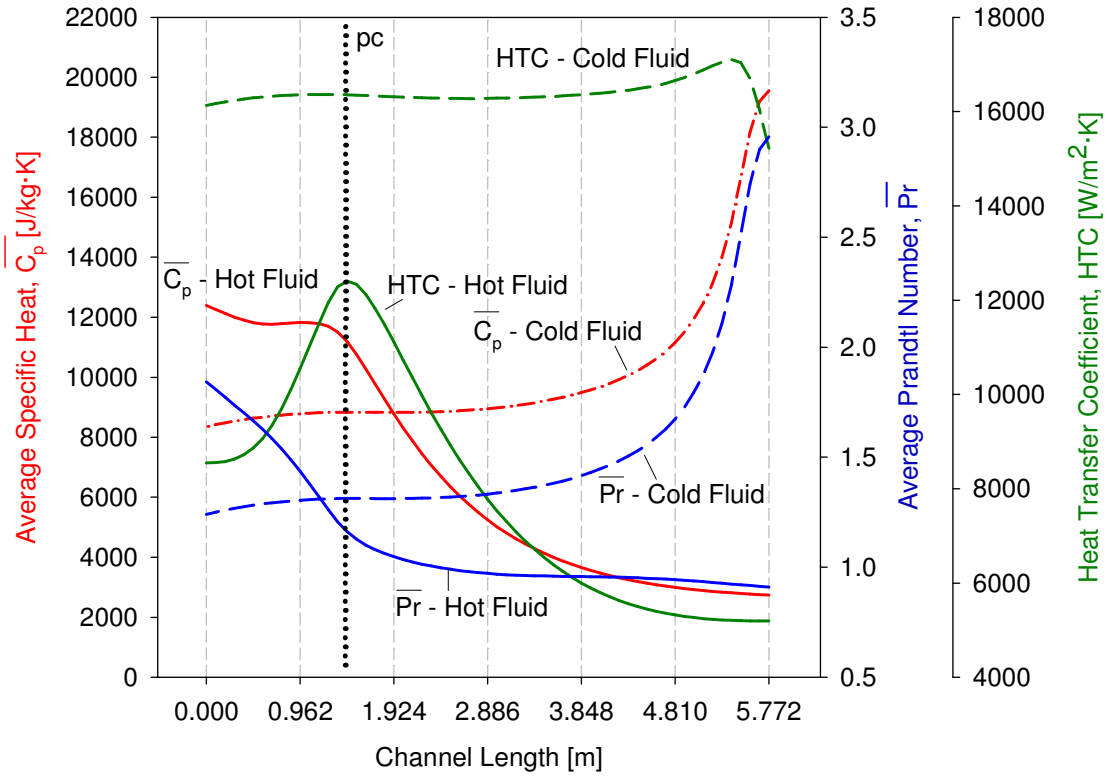

Figure C 1(b): Average specific heat, average Prandtl number and HTC profiles along a YSZ insulated fuel-channel for a channel power of 8.5 MW_{th}, inner-tube thickness of 2 mm, pressure tube thickness of 11 mm, inlet temperature of 350°C, mass flow rate of 4.37 kg/s and uniform heat flux

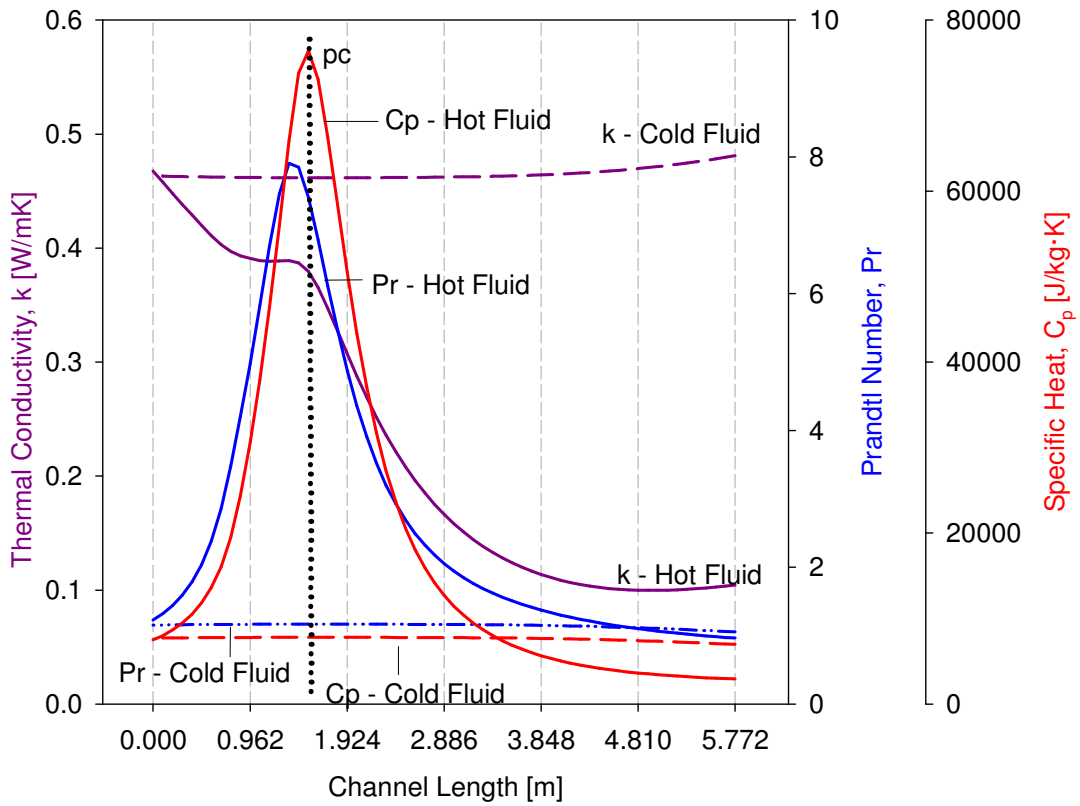

Figure C 2 (a): Specific heat, thermal conductivity and Prandtl number profiles along a ZrO_2 insulated channel for a channel power of 8.5 MW_{th}, inner-tube thickness of 2 mm, pressure tube thickness of 11 mm, insulation thickness of 7 mm, inlet temperature of 350°C, mass flow rate of 4.37 kg/s and uniform heat flux

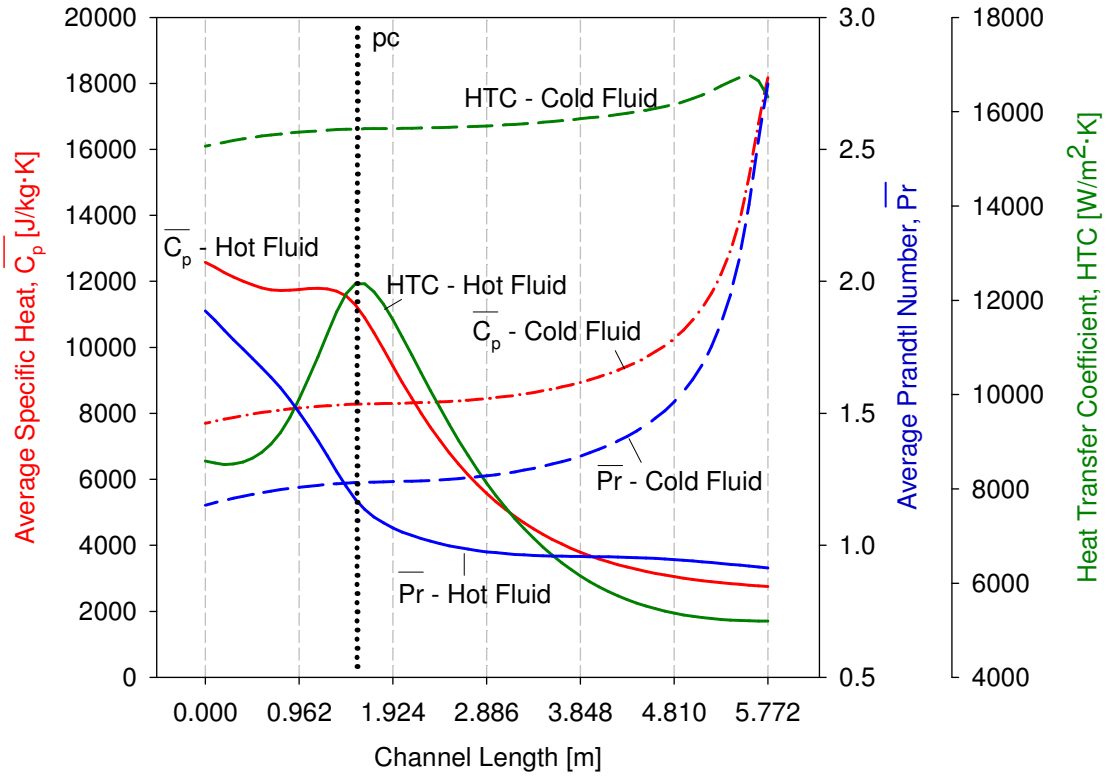

Figure C 2(b): Average specific heat, average Prandtl number and HTC profiles along a ZrO_2 insulated channel for a channel power of 8.5 MW_{th}, inner-tube thickness of 2 mm, pressure tube thickness of 11 mm, insulation thickness of 7 mm, inlet temperature of 350°C, mass flow rate of 4.37 kg/s and uniform heat flux

APPENDIX D: IMPACT OF NON-UNIFORM FLUX SHAPES – THERMOPHYSICAL PROPERTIES

Case 2: Typical Nominal Axial Power Profile

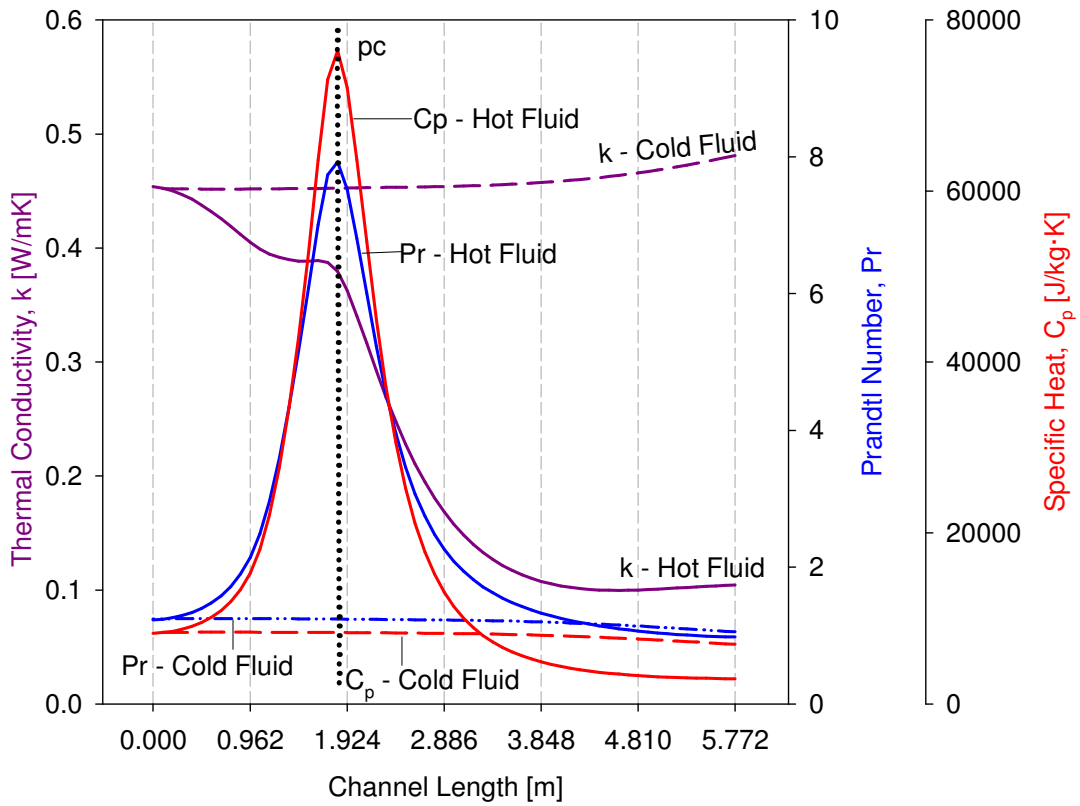

Figure D.1 (a): Case 2 - Specific heat, Prandtl number and thermal conductivity profiles along a 7 mm thick Porous YSZ insulated channel for a total channel power of 8.5 MW_{th}, inner-tube thickness of 2 mm, pressure tube thickness of 11 mm, inlet temperature of 350°C and mass flow rate of 4.37 kg/s

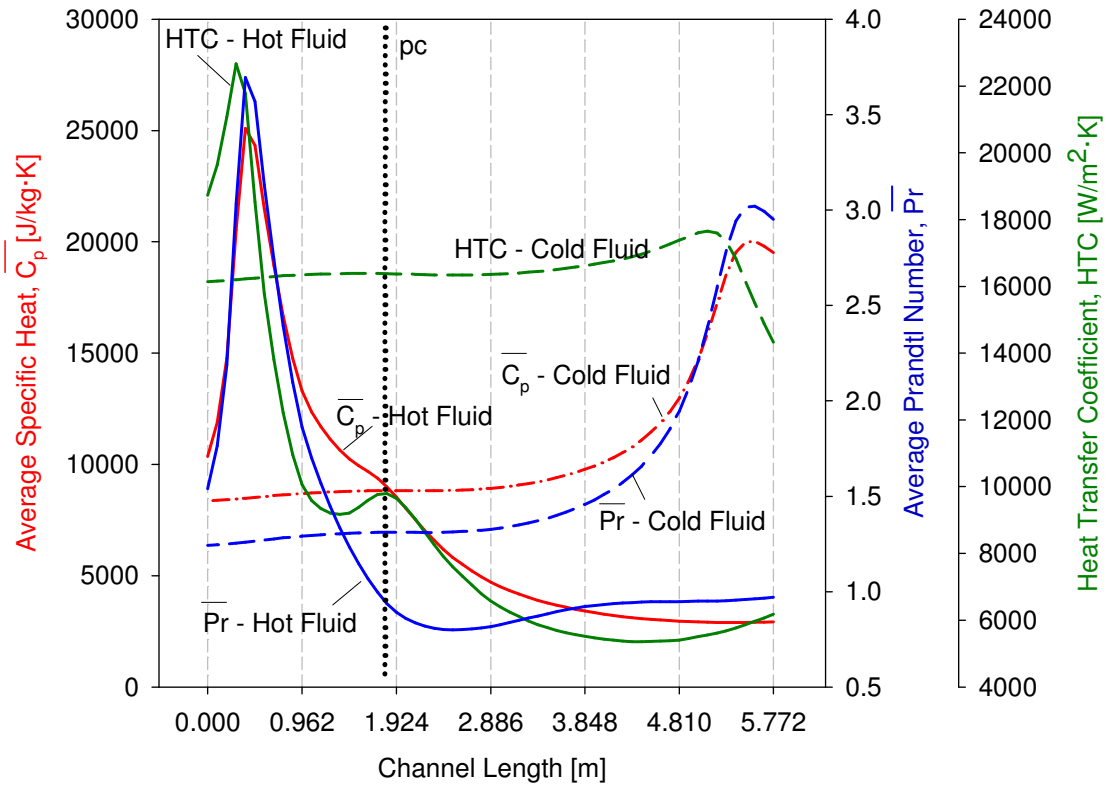

Figure D.2 (b): Case 2 - Average specific heat, average Prandtl number and HTC profiles along a 7 mm thick Porous YSZ insulated channel for a total channel power of 8.5 MW, inner-tube thickness of 2 mm, pressure tube thickness of 11 mm, inlet temperature of 350°C and mass flow rate of 4.37 kg/s

Case 3: Peaked Shape Axial Power Profile

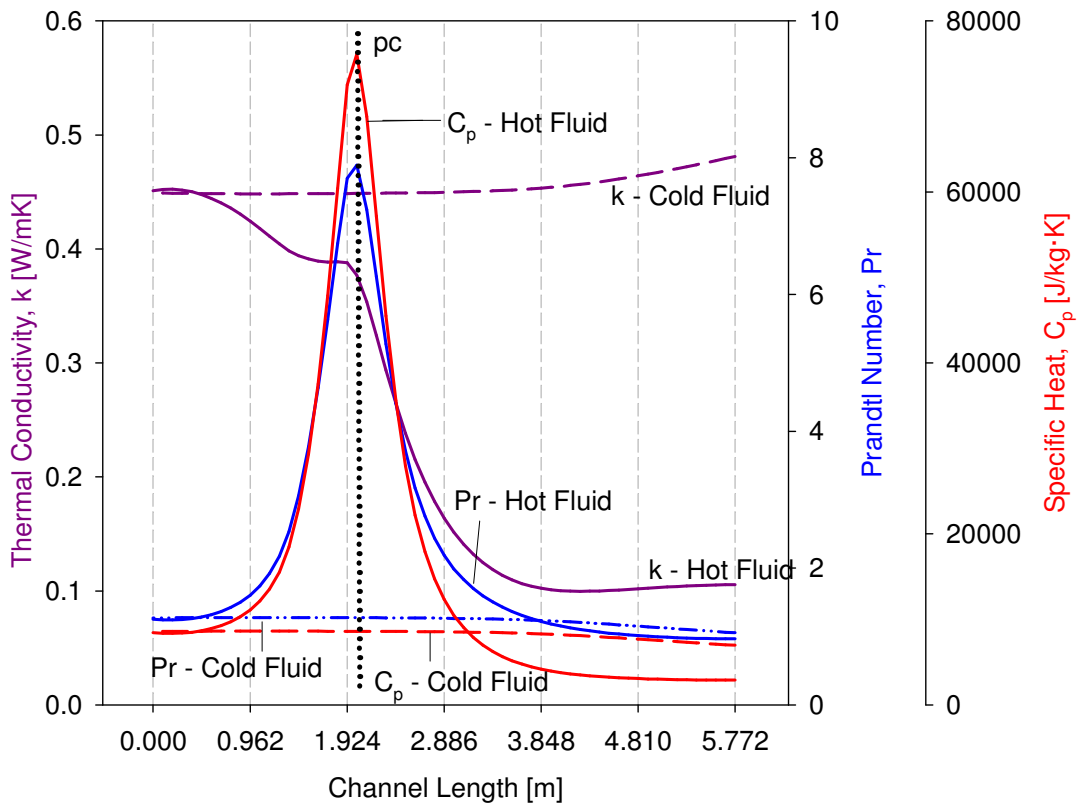

Figure D.2 (a): Case 3 - Specific heat, Prandtl number and thermal conductivity profiles along a 7 mm thick Porous YSZ insulated channel for a total channel power of 8.5 MW_{th}, inner-tube thickness of 2 mm, pressure tube thickness of 11 mm, inlet temperature of 350°C and mass flow rate of 4.37 kg/s

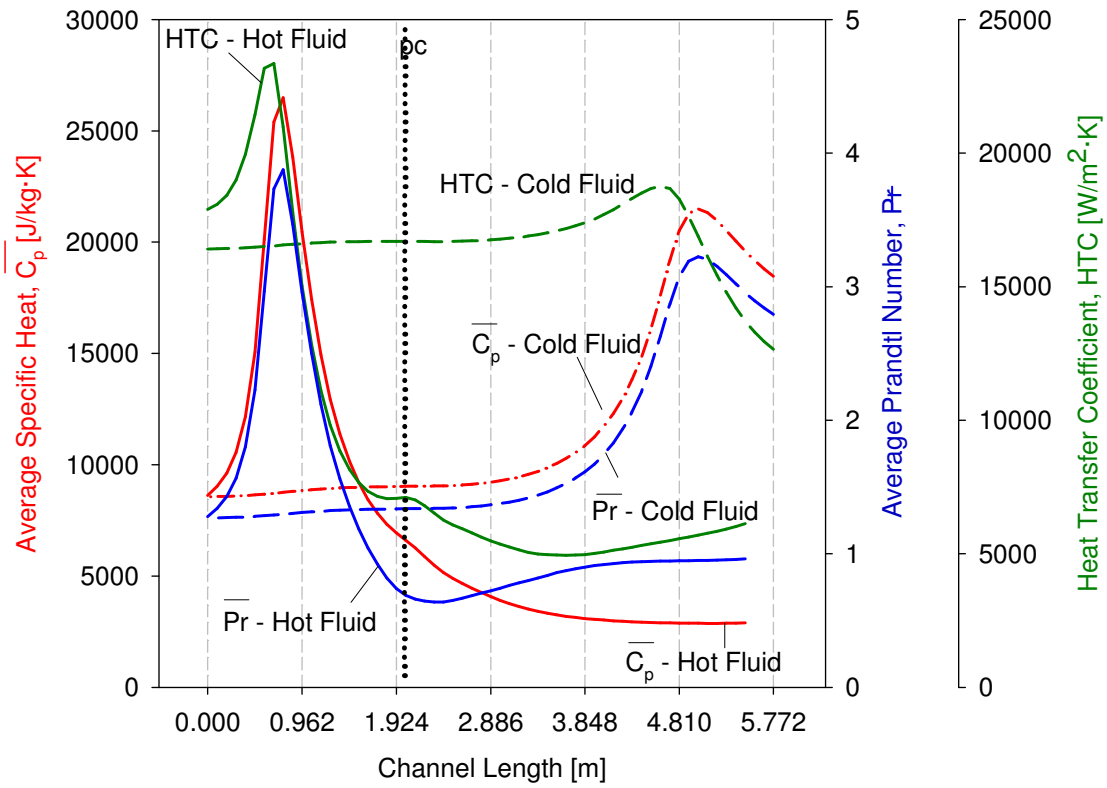

Figure D.2 (b): Case 3 - Average specific heat, average Prandtl number and HTC profiles along a 7 mm thick Porous YSZ insulated channel for a total channel power of 8.5 MW_{th}, inner-tube thickness of 2 mm, pressure tube thickness of 11 mm, inlet temperature of 350°C and mass flow rate of 4.37 kg/s

Case 4: Upstream-skewed Axial Power Profile

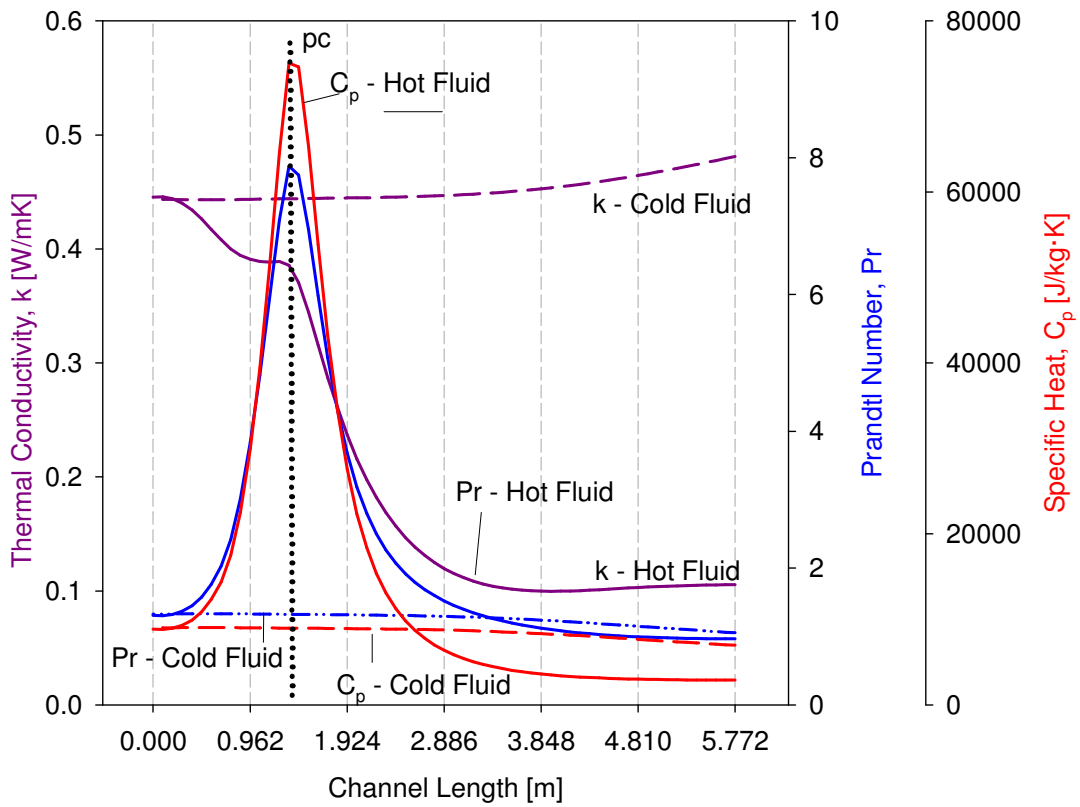

Figure D.3 (a): Case 4 - Specific heat, Prandtl number and thermal conductivity profiles along a 7 mm thick Porous YSZ insulated channel for a total channel power of 8.5 MW_{th}, inner-tube thickness of 2 mm, pressure tube thickness of 11 mm, inlet temperature of 350°C and mass flow rate of 4.37 kg/s

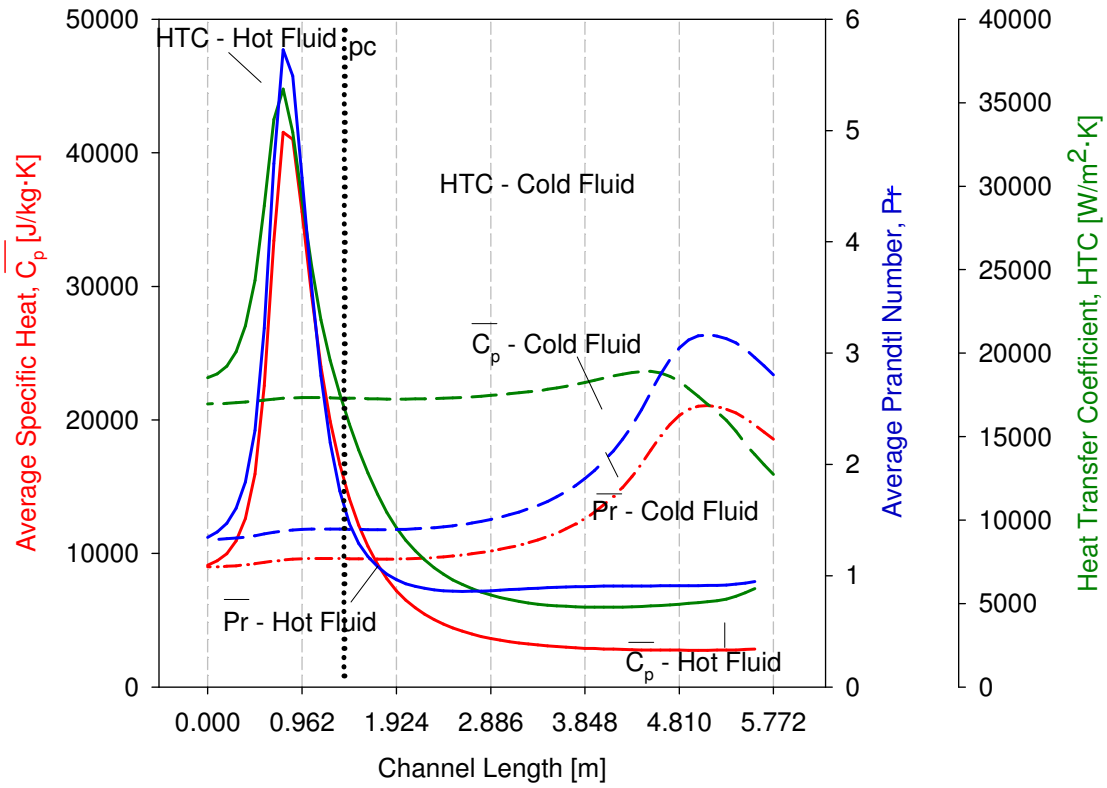

Figure D.3 (b): Case 4 - Average specific heat, average Prandtl number and HTC profiles along a 7 mm thick Porous YSZ insulated channel for a total channel power of 8.5 MW_{th}, inner-tube thickness of 2 mm, pressure tube thickness of 11 mm, inlet temperature of 350°C and mass flow rate of 4.37 kg/s

Case 5: Downstream-skewed Axial Power Profile

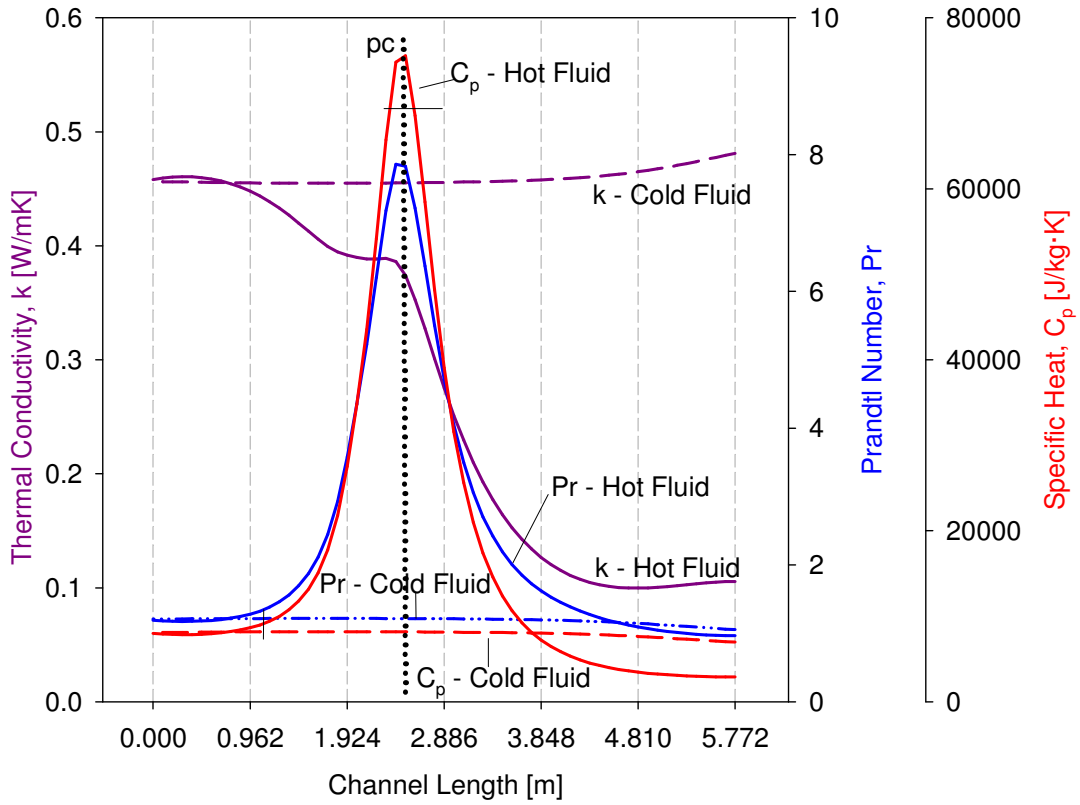

Figure D.4 (a): Case 5 - Specific heat, Prandtl number and thermal conductivity profiles along a 7 mm thick Porous YSZ insulated channel for a total channel power of 8.5 MW_{th}, inner-tube thickness of 2 mm, pressure tube thickness of 11 mm, inlet temperature of 350°C and mass flow rate of 4.37 kg/s

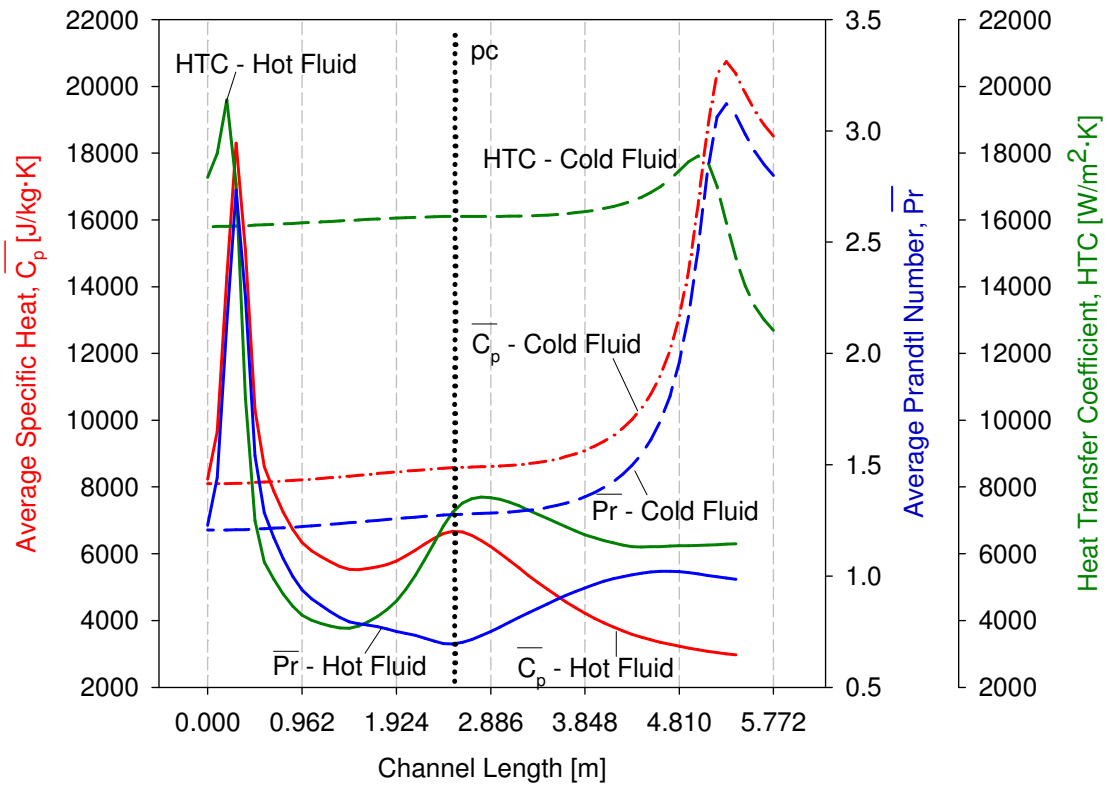

Figure D.4 (b): Case 5 - Average specific heat, average Prandtl number and HTC profiles along a 7 mm thick Porous YSZ insulated channel for a total channel power of 8.5 MW_{th}, inner-tube thickness of 2 mm, pressure tube thickness of 11 mm, inlet temperature of 350°C and mass flow rate of 4.37 kg/s

Case 6: Variable Axial Power Profile

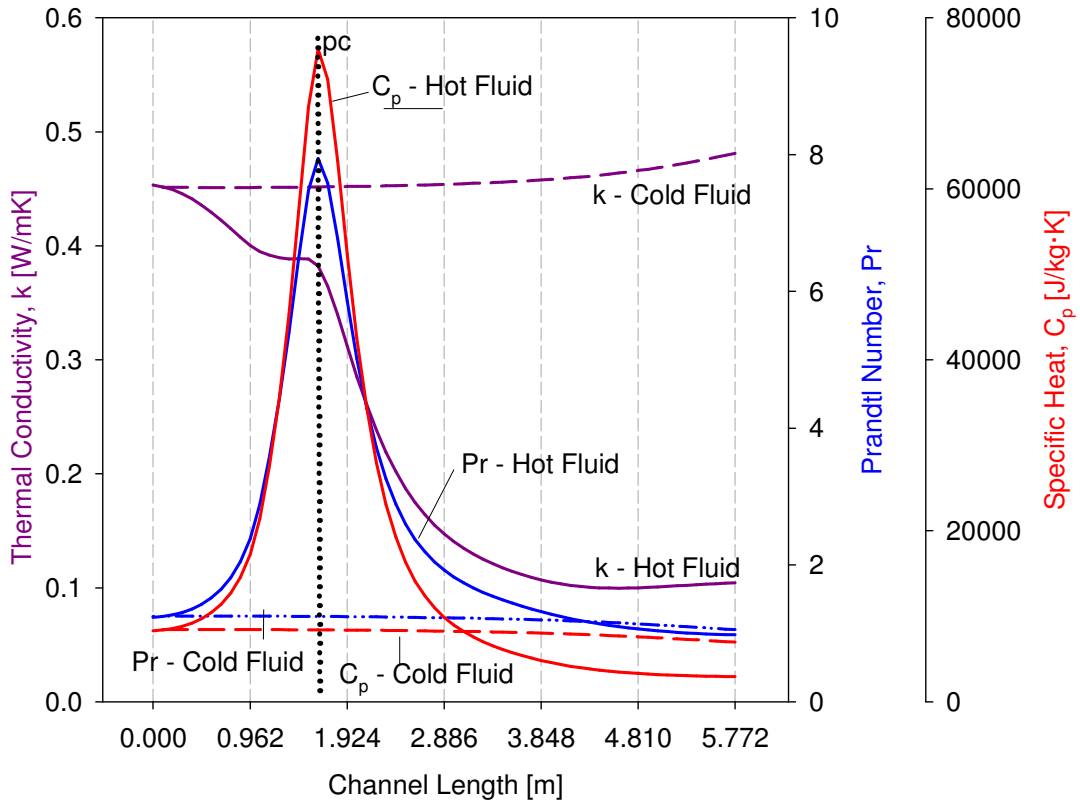

Figure D.5 (a): Case 6 - Specific heat, Prandtl number and thermal conductivity profiles along a 7 mm thick Porous YSZ insulated channel for a total channel power of 8.5 MW_{th}, inner-tube thickness of 2 mm, pressure tube thickness of 11 mm, inlet temperature of 350°C and mass flow rate of 4.37 kg/s

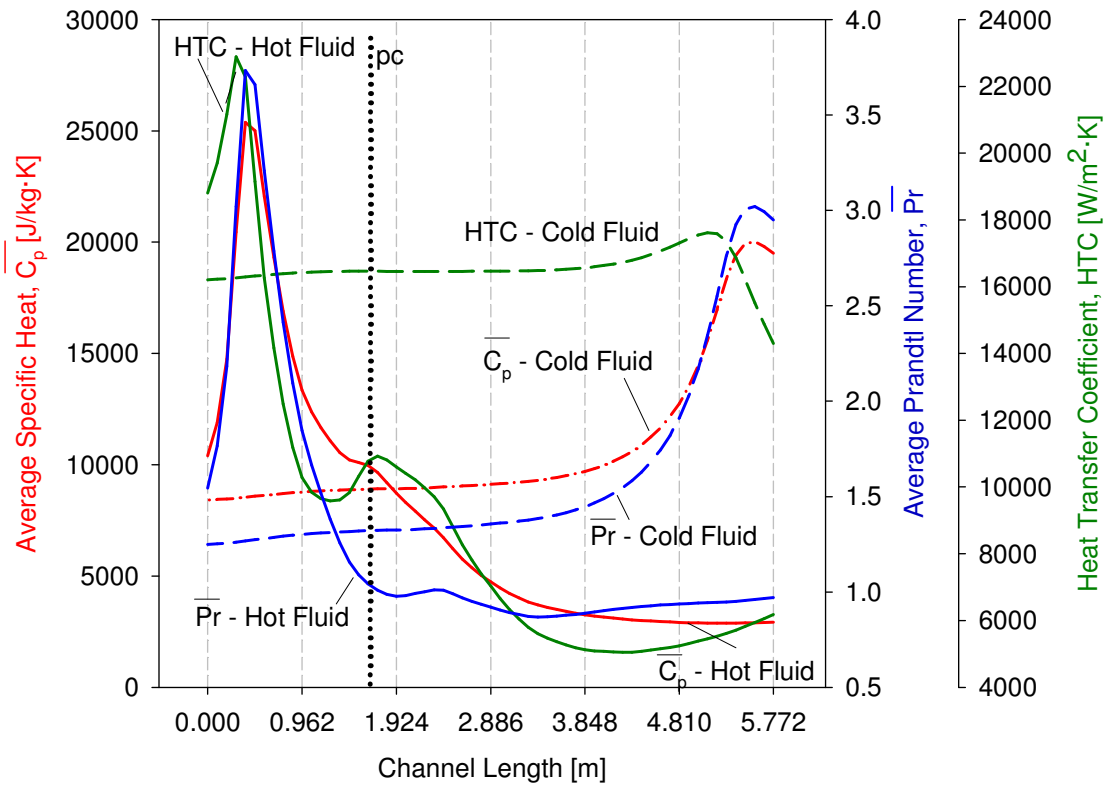

Figure D.5 (b): Case 6 - Average specific heat, average Prandtl number and HTC profiles along a 7 mm thick Porous YSZ insulated channel for a total channel power of 8.5 MW_{th}, inner-tube thickness of 2 mm, pressure tube thickness of 11 mm, inlet temperature of 350°C and mass flow rate of 4.37 kg/s

APPENDIX E: CONTRIBUTIONS TO KNOWLEDGE

Refereed Conference Proceedings

Samuel, J., Harvel, G., & Pioro., I. "Design Concept and Heat Transfer Analysis for a Double Pipe Channel for SCWR Type Reactors", Proceedings of the International Conference on Nuclear Engineering (ICONE-18), Xi'an, China, 2010, May 17-21.

Pioro, I., Mokry, S., Peiman, W., Saltanov, Eu., Thind, H., Grande, L., Samuel, J. and Harvel, G., 2010. Supercritical Water-Cooled Nuclear Reactors: Thermodynamic-Cycles Plant Layouts and Thermal Aspects of Pressure-Channel Design, Transactions of the European Nuclear Conference (ENC 2010), Barcelona, Spain, May 30 – June 2.

Samuel. J., Harvel, G., and Pioro, I., "Heat Loss Analysis of a Re-Entrant Fuel Channel for SCWR Type Reactors", Proceedings of the 5th International Symposium on Supercritical Water-Cooled Reactors (ISSCWR-5), Vancouver, Canada, 2011, Mar 13-16.

Samuel, J., Harvel, G., & Pioro., I. "Moderator Heat Loss Analysis of a Ceramic Insulated Re-Entrant SCWR Fuel-Channel", Proceedings of the International Conference on Nuclear Engineering (ICONE-19), Chiba, Japan, 2011, May 15-19.

Technical Reports

Peiman, W., Richards, G., Samuel, J., Grande, L., Harvel, G. and Pioro, I., 2010. Key Thermalhydraulic and Material Parameters for Fuel-Channel Design, Report for NSERC/NRCan/AECL Generation IV Energy Technologies Program (NNAPJ) entitled "Alternative Fuel-Channel Design for SCWR" with Atomic Energy of Canada Ltd., Version 1, UOIT, Oshawa, ON, Canada, December, 42 pages.

Pioro, I., Saltanov, Eu., Naidin, M., King, K., Farah, A., Peiman, W., Mokry, S., Grande, L., Thind, H., Samuel, J. and Harvel, G., 2010. Steam-Reheat Option in SCWRs and Experimental BWRs, Report for NSERC/NRCan/AECL Generation IV Energy Technologies Program (NNAPJ) entitled "Alternative Fuel-Channel Design for SCWR" with Atomic Energy of Canada Ltd., Version 1, UOIT, Oshawa, ON, Canada, March, 128 pages